
LINKING EVAPORATION AND VEGETATION CHARACTERISTICS:
A DATA-DRIVEN STUDY FROM PLOT TO GLOBAL SCALE
ANNE J. HOEK VAN DIJKE

Propositions

1. The vegetation's looks are deceiving while studying their control on evaporation. (this thesis)

2. Forest age and water stress data are as important as the NDVI for satellite-based forest evaporation monitoring. (this thesis)

3. Cohousing is beneficial to all of the Sustainable Development Goals.

4. For a PhD candidate, the quantity and quality of their publications are of equal importance.

5. Creative thinking starts inside the box.

6. Dutch should be the primary language in Dutch bachelor education.

Propositions belonging to the thesis, entitled

Linking evaporation and vegetation characteristics: a data-driven study from plot to global scale

Anne Hoek van Dijke
Wageningen, 10-06-2022

Linking evaporation and vegetation characteristics: a data-driven study from plot to global scale

Anne J. Hoek van Dijke

Thesis committee

Promotors
Prof. Dr M. Herold
Professor of Geo-information Science and Remote Sensing
Wageningen University & Research

Dr A.J. Teuling
Associate Professor, Hydrology and Quantitative Water Management
Wageningen University & Research

Co-promotors
Dr K. Mallick
Researcher, Remote Sensing and Natural Resources Modelling
Luxembourg Institute of Science and Technology, Belvaux, Luxembourg

Dr M. Machwitz
Researcher, Remote Sensing and Natural Resources Modelling
Luxembourg Institute of Science and Technology, Belvaux, Luxembourg

Other members:
Prof. Dr M. van Noordwijk, Wageningen University & Research
Dr C. van der Tol, University of Twente, Enschede
Dr A. Bastos, Max Planck Institute for Biogeochemistry, Jena, Germany
Dr M. de Kauwe, University of Bristol, United Kindom

This research was conducted under the auspices of the C.T. de Wit Graduate School of Production Ecology & Resource Conservation (PE&RC)

Linking evaporation and vegetation characteristics: a data-driven study from plot to global scale

Anne J. Hoek van Dijke

Thesis
submitted in fulfilment of the requirements for the degree of doctor
at Wageningen University
by the authority of the Rector Magnificus
Prof. Dr A.P.J. Mol,
in the presence of the
Thesis Committee appointed by the Academic Board
to be defended in public
on Friday 10 June 2022
at 4 p.m. in the Omnia Auditorium.

Anne J. Hoek van Dijke

Linking evaporation and vegetation characteristics:
a data-driven study from plot to global scale

166 pages.

PhD thesis, Wageningen University, Wageningen, the Netherlands (2022)
With references, with summaries in English and Dutch

ISBN 978-94-6447-191-5
DOI https://doi.org/10.18174/568097

Voor An, Agje, Jaap, en Jan

Summary

Evaporation and vegetation are closely linked. Vegetation impacts the evaporation by enhancing the water and energy availability, and by increasing the aerodynamic conductance. On the other hand, vegetation can decrease evaporation through stomatal closure. This thesis addresses the statistical correlation between evaporation and the vegetation green biomass and the effect of vegetation changes on evaporation. The first objective of this thesis is: 'to study the link between ground-based observations of evaporation and satellite remote sensing observations of vegetation'. Satellite observations of the vegetation green biomass, such as the leaf area index or vegetation indices, are integrated in most remote sensing based evaporation models. It is however unknown whether the link between remote sensing observations of the vegetation green biomass and evaporation are valid over different vegetation types, climate zones, and across spatial-temporal scales. Chapter 2, 3, and 4 study the link between remote sensing observations of vegetation and ground-based observations of evaporation. The second objective of this thesis is: 'to study the effect of drought and land-cover change on evaporation over large areas'. Global change, including an increasing number of droughts (chapter 4) and land-cover change (chapter 5) will have an impact on future evaporation and the water, energy, and carbon balance. A better understanding of the impact of vegetation on evaporation under global change is therefore crucial to study future global evaporation.

Chapter 2 studies the link between daily mean tree sap velocity and Landsat derived NDVI in a catchment in Luxembourg. The studied hypothesis is 'there is a positive correlation between the NDVI and sap velocity', because forests with a higher leaf biomass are expected to have a higher sap velocity. However, we found a positive correlation between sap velocity and NDVI only in April during the phase of vegetation green-up. During the rest of spring and summer, we found a significant negative correlation for half of the studied days. During a dry summer, sap velocity was uncorrelated with NDVI, but varied with water availability and soil type. Methods using the NDVI to predict or scale (evapo)transpiration should be carefully applied in temperate forest ecosystems.

Chapter 3 studies the link between the yearly mean satellite-derived LAI and the latent heat flux, sensible heat flux, and GPP for a range of vegetation types. The ecosystem fluxes were derived from FLUXNET data and the LAI data was available from MODIS.

In this chapter we show that the link between LAI and the latent and sensible heat fluxes depends on the vegetation type and aridity. Under arid conditions, the link between the LAI and water and energy fluxes was strong, but in energy-limited forests, there was no correlation between LAI and water and energy fluxes. In contrast to the water and energy fluxes, GPP was always positively correlated with LAI. For savanna and arid grassland, the LAI can be useful to model or extrapolate water fluxes, but for deciduous broadleaf forest and evergreen needleleaf forest, the LAI is of limited use.

Forest and grassland have a different drought coping strategy. Trees control their stomata to reduce water loss, while grasslands take the risk to lose their aboveground biomass. Both the stomatal control and the reduction in green biomass reduce the surface conductance (G_s) and evaporation. **Chapter 4** studies how different MODIS vegetation and drought indices reflect the reduction in G_s in forest and grassland. We show that for grassland, the different optical and thermal indices were sensitive to the reduction in G_s. For the forest sites, the optical indices were not sensitive to the reduction in G_s, but the thermal indices did reflect the reduction in G_s. The results were however not uniform across all forest and grassland sites. A different strategy is required in order to monitor the effects of drought on the water, energy, and carbon cycle in grassland and forest.

Chapter 5 studies the effect of large-scale tree restoration (totalling 900 million hectares) on evaporation, precipitation, streamflow, and water availability. Large-scale tree restoration increases local evaporation, and increases (downwind) precipitation through evaporation recycling. We show that the combined effects of increasing evaporation and increasing precipitation create complex patterns of decreasing (up to 38 %) or increasing (up to 6 %) water availability. The effect on large river basins is diverge: several rivers could lose 6 % of their streamflow, while for other rivers, the increased evaporation would be counterbalanced by enhanced evaporation recycling. Tree restoration significantly shifts terrestrial water fluxes and future tree restoration strategies should consider these effects.

Chapter 6 synthesises the results of the four core chapters. The main conclusions are: 1) a significant correlation between ground-based observations of evaporation and satellite remote sensing observations of vegetation is an exception rather than the rule. Water availability seems to play an important role in the slope, direction, and strength of the correlation. This has implications for remote sensing based evaporation monitoring. 2) Drought and land-cover change had an impact on evaporation, and these effects propagate further into the water, energy, and carbon balance. Lastly, the synthesis discusses recommendations for tree restoration and future remote sensing of evaporation.

Samenvatting

Binnen ecosystemen staan planten (hierna: vegetatie) en verdamping van water nauw in verband tot elkaar. Enerzijds versterkt vegetatie de verdamping, en anderzijds kan vegetatie ook de verdamping verminderen. Vegetatie versterkt de verdamping omdat het de beschikbaarheid van water en energie verhoogt, respectivelijk door de diepe wortels en vele bladeren. Ook heeft vegetatie invloed op het transport van water in de atmosfeer. Vegetatie kan de verdamping verminderen wanneer planten de huidmondjes sluiten, zoals bijvoorbeeld tijdens een droogte. Het is belangrijk om goed te begrijpen hoe vegetatie de verdamping beïnvloedt. Zo kunnen we voorspellen hoe grootschalige veranderingen van klimaat en landgebruik invloed zullen hebben op de toekomstige water-, energie- en koolstofbalans. In dit proefschrift behandelen we zowel het statistische verband als het oorzakelijke verband (hoe de één de ander beïnvloed) tussen verdamping en de groene biomassa van ecosystemen.

Dit proefschrift heeft twee hoofddoelen. Het eerste hoofddoel is om het statistische verband tussen verdamping en satellietobservaties van vegetatie beter te begrijpen. Satellietdata van de groene biomassa, zoals de ´bladoppervlakte-index´ (LAI) of de ´Normalized Difference Vegetation Index´ (NDVI), worden op grote schaal gebruikt om verdamping te kwantificeren. Het is echter onbekend of er een statistisch verband is tussen verdamping en satellietmetingen van de vegetatie, en in hoeverre dit verband op gaat voor verschillende vegetatietypen, klimaatzones en voor verschillende tijd- en ruimteschalen. Hoofdstuk 2, 3 en 4 behandelen het statistische verband tussen satellietobservaties van de groene biomassa en in situ-metingen van verdamping. Het tweede hoofddoel van dit proefschrift is het bestuderen van het effect van droogte en landgebruiksverandering op grootschalige verdamping. Een toename in droogtes (hoofdstuk 4) en landgebruiksverandering (hoofdstuk 5) hebben invloed op verdamping, en daarmee op de water-, energie- en koolstofbalans van de toekomst.

Hoofdstuk 2 behandelt het statistische verband tussen de gemiddelde sapstroomsnelheid in bomen en de NDVI (afkomstig van Landsat-satellietdata) in een stroomgebied in Luxemburg. De hypothese is dat er een positieve correlatie is tussen de NDVI en de sapstroomsnelheid, omdat we verwachten dat bomen met meer groene biomassa (en dus een hogere NDVI) een hogere sapstroomsnelheid hebben. De resultaten laten echter

alleen in April, wanneer de bomen in blad komen, een positieve correlatie zien tussen de sapstroomsnelheid en NDVI. Tijdens de rest van de lente en zomer was de correlatie significant negatief voor acht van de achtien studiedagen. Tijdens de droge zomer van 2015 vonden we geen statistisch verband tussen de sapstroomsnelheid en NDVI. In deze zomer varieerde de sapstroomsnelheid met waterbeschikbaarheid en bodemtype. Dit hoofdstuk laat zien dat we terughoudend moeten zijn met het gebruik van de NDVI in verdampingsmodellen voor bossen in gematigde gebieden.

Hoofdstuk 3 behandelt het verband tussen de gemiddelde satellietgemeten LAI op jaarbasis en de energie die wordt gebruikt voor verdamping (de latente warmteflux), opwarming (de sensibele warmteflux) of bruto primaire productiviteit (de koolstofopname door een ecosysteem ten behoeve van photosynthese) voor verschillende vegetatietypen. De bruto primaire productiviteit en de warmtefluxen zijn berekend uit FLUXNET-metingen en de LAI was bepaald uit MODIS-satellietdata. In dit hoofdstuk laten we zien dat het verband tussen LAI en de verdampings- en warmte-energie verschilt per vegetatietype en varieert met de droogte-index. Onder droge omstandigheden is het verband tussen de LAI en water- en energiestromen sterk, maar onder koudere omstandigheden is er geen verband tussen LAI en water- en energiestromen. In tegenstelling tot water- en energiestromen was de bruto primaire productiviteit altijd positief gecorreleerd met de LAI. Deze studie toont aan dat de LAI gebruikt kan worden voor het modelleren of extrapoleren van verdamping in het geval van savannes en droge graslanden, maar dat de LAI voor dit doel niet geschikt is in gematigde loof- en naaldbossen.

Bossen en graslanden hebben een verschillende strategie om om te gaan met droogte. Bomen reguleren de huidmondjes om verlies van water te verminderen. Gras doet dit in mindere mate, en loopt zo het risico dat de groene biomassa afsterft. Zowel de regulatie van de huidmondjes als de afname van groene biomassa verminderen de oppervlaktegeleiding van de vegetatie (G_s, een maat voor hoe makkelijk vocht wordt overgedragen van de vegetatie naar de atmosfeer), waardoor de verdamping afneemt. In **Hoofdstuk 4** bestuderen we of en hoe verschillende satelliet-indexen van de MODIS-sensoren de afname van G_s weerspiegelen. De resultaten laten zien dat voor graslanden de verschillende optische indexen (weerkaatsing van zonlicht) en thermische indexen (warmte-uitstraling) gevoelig zijn voor de afname van G_s. Voor de bestudeerde bossen waren de optische indexen niet gevoelig voor de afname in G_s, maar de thermische indexen waren dat wel. De resultaten waren echter niet uniform voor alle bos- en graslandgebieden. Deze studie laat zien dat we voor bossen en graslanden een verschillende strategie nodig hebben om het effect van droogte op de water-, energie- en koolstofbalans te monitoren.

In **Hoofdstuk 5** behandelen we het effect van het grootschalig en wereldwijde aanplanten van bomen op verdamping, neerslag, rivierafvoer, en waterbeschikbaarheid. Door een toename van bomen neemt de verdamping toe, en door het hercirculeren van vocht in de atmosfeer neemt de (benedenwindse) neerslag ook toe. Door het gecombineerde effect van

de toename van verdamping en de toename van neerslag ontstaan ingewikkelde patronen van afnemende (tot 38 %) en toenemende (tot 6 %) waterbeschikbaarheid. Het effect op stroomgebieden verschilt: voor sommige rivieren vermindert de jaarlijkse afvoer met 6 %, terwijl voor andere rivieren de afname nagenoeg nul is, omdat de toename van verdamping wordt gecompenseerd door een toename in de neerslag. Het grootschalig aanplanten van bomen heeft een effect op de verdamping, neerslag, en waterbeschikbaarheid op Aarde. Toekomstige herbebossingsprojecten zouden hier rekening mee moeten houden om ongewenste afname van waterbeschikbaarheid te beperken.

Hoofdstuk 6 vat de resultaten van de vier eerdere hoofdstukken samen. De belangrijkste conclusies zijn: 1. Een significante correlatie tussen in situ-metingen van verdamping en satelietobservaties van vegetatie is eerder uitzondering dan regel. Waterbeschikbaarheid speelt hierbij een belangrijke rol: het beïnvloedt de hoogte en de richting van de correlatiecoëfficiënt, en de significantie van de correlatie. Dit heeft gevolgen voor het kwantificeren van verdamping op basis van satellietmetingen. 2. Droogte en landgebruiksverandering hebben een belangrijke invloed op verdamping en deze effecten op verdamping werken door in andere onderdelen van de water-, energie- en koolstofbalans.

Contents

Chapter 1

Introduction

1.1 Evaporation and its drivers

1.1.1 Introduction to evaporation, a physical and biological process

Evaporation is one of the major components of the terrestrial water cycle and represents the water flux from the land surface into the atmosphere. In the atmosphere, the evaporated water condensates into water droplets and eventually precipitates on the Earth's surface as rain, snow, drizzle, or hail. On the Earth's surface, part of this water will infiltrate in the soil, be taken up by the vegetation, or be transported by rivers to the ocean, and it will eventually evaporate back into the atmosphere and close the hydrological cycle.

The evaporation from the land surface consists of four components: evaporation from water bodies such as lakes and rivers, evaporation of intercepted water, evaporation of soil water, and plant transpiration. Interception evaporation is the evaporation of water that was intercepted by the vegetation leaves, and transpiration is the evaporation of water through the stomata of vegetation. Transpiration is the largest of the four components and accounts for more than two-thirds of the total evaporation over land (Schlesinger and Jasechko, 2014). The total evaporation from an ecosystem is also called evapotranspiration, which emphasises that it includes the evaporation of water through the stomata of vegetation (Miralles et al., 2020).

Evaporation of water from water bodies, soil, and leaf surfaces is merely a physical process. Energy (usually solar radiation) heats up the water molecules in a liquid and makes them move faster (and faster) until the individual molecules escape as a gas into the atmosphere. Transpiration is both a physical process (the water molecules in the leaves move faster and eventually escape through the stomata into the atmosphere), as well as a biological process. Transpiration involves the uptake of water by the vegetation roots and release through the leaf stomata. The stomata can close and thereby decrease the water loss through transpiration.

1.1.2 Evaporation is important for the water, energy, and carbon cycle

Evaporation is a critical component in the water, energy, and carbon cycle and has an impact on the terrestrial water, energy, and carbon stores and fluxes (Fig. 1.1).

Evaporation in the energy cycle

The incoming solar radiation is absorbed or reflected by the Earth's surface, and the Earth's surface also emits radiation. The net balance between the incoming and outgoing radiation is called the net radiation, and that is the energy that is available to affect our living environment. The net radiation at the Earth's surface is used to evaporate water (the so-called latent heat flux), to heat up the land surface (the sensible heat flux), or to heat up the soil and vegetation (the ground heat flux) (Fig. 1.1a). The ground heat flux

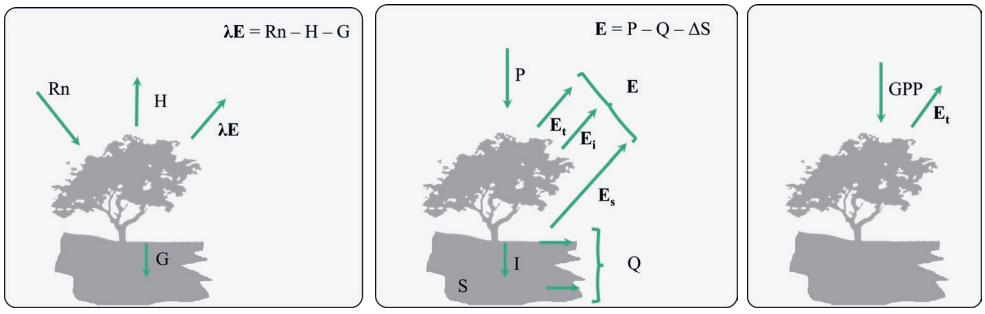

(**a**) E in the energy cycle (**b**) E in the water cycle (**c**) E in the carbon cycle

Figure 1.1: Evaporation (E) plays an important role in the energy, water, and carbon cycle. (a) In the energy cycle, the net radiation (Rn) is divided over the sensible heat flux (H), latent heat flux (λE), and ground heat flux (G). (b) In the water cycle, precipitation water (P) is divided over transpiration (E_t) and interception and soil evaporation (E_i and E_s) and, discharge (Q), and storage water in the soil and canopy (S). Note that $E = \lambda E/\lambda$ (evaporation, mass flux in m^{-3} = latent heat, energy flux in W m^{-2} / the latent heat of vaporization). (c) In the carbon cycle, the gross primary productivity (GPP), the amount of carbon fixed by the vegetation during photosynthesis, is closely linked to the transpiration of water (E_t).

is small as compared to the other two components and is often ignored in evaporation studies. Therefore, one can say that the energy that is not used for evaporation is used to heat up the Earth's surface. This explains why dry regions can get very hot, and why irrigation on a hot day decreases the air temperature.

Evaporation in the water cycle

Rainfall and other forms of precipitation that reach the Earth's terrestrial surface are partitioned between evaporation, surface runoff and streamflow, and soil or groundwater storage (Fig. 1.1b). The change in soil or groundwater storage is noticeable on smaller time scales (for example the soil water storage increases after a rainfall event), but is often ignored on longer time scales. The total amount of water that leaves an area as streamflow is the water that is available to humans for drinking water, irrigation, transportation over water, or hydroelectric energy. An increase in evaporation, during warm weather, or after forest planting, therefore decreases the fresh water availability and streamflow.

Evaporation in the carbon cycle

Transpiration and the fixation of carbon dioxide by the vegetation (the gross primary productivity) go hand in hand. When stomata open to take up carbon, water is released into the atmosphere (Fig. 1.1c). Forest planting, in order to increase the global carbon

stock, therefore impacts evaporation and water availability. Furthermore, stomatal closure on a dry day impacts both the evaporation and the carbon uptake by the vegetation.

1.1.3 The drivers of evaporation and variability in evaporation

In order to evaporate water, the following three things are required: water, energy for the phase change from liquid water to water vapour, and a vapour pressure gradient to remove the water vapour away from the evaporating surface. The water is supplied by precipitation or soil moisture, the energy is generally supplied by solar radiation, and the atmospheric vapour pressure deficit and wind speed drive the movement of water molecules into the atmosphere, and supply more dry air. There is generally not one driver of evaporation, and evaporation directly feed backs into a change in the temperature, vapour pressure gradient, and water availability, that will in turn change the evaporation flux.

If one would compare the evaporation in one region with another region, or one day with the next day, one would find a high spatial and temporal variability in evaporation. On large spatial and temporal scales, the climate plays a major role in this variability (Awada et al., 2013; Hasler and Avissar, 2007). Around 60 - 65 % of the variation in evaporation is explained by the mean yearly net radiation and mean yearly precipitation (Padrón et al., 2017; Williams et al., 2012). The leftover 35 - 40 % of the variability in evaporation is explained by other factors such as meteorological variables (wind speed, maximum air temperature, or relative humidity), topographic variables, such as slope and aspect, the soil water content and other soil characteristics, and vegetation (Awada et al., 2013; Mitchell et al., 2012; Williams et al., 2012). These factors mainly control small-scale variability in evaporation, for example from one day to another, and within a climate zone. The main focus of this thesis is the link between the vegetation on evaporation.

1.2 The link between vegetation and evaporation

1.2.1 In theory: how vegetation characteristics control evaporation

Vegetation interacts with solar radiation and the roots take up water from the deeper soil layers. Therefor vegetation impacts the availability of water and energy for evaporation. Furthermore, the vegetation can exert additional control on the evaporation flux through the stomata. When the stomata are open, water can freely move out of the vegetation, but when stomata close, the transpiration decreases also when enough water and energy are available. Below, five aspects of the vegetation (Fig. 1.2) are discussed that impact the vegetation control on evaporation:

- Albedo The albedo is the fraction of incoming solar radiation that is reflected back into space. The solar radiation that is not reflected back into space is available

at the Earth's surface for evaporation. The albedo of vegetation depends, among others, on the vegetation density and structure (Sellers, 1985). A forest, with a dense vegetation structure and high leaf area generally has a lower albedo than grassland and the total energy available for evaporation is therefore higher in forest. This effect is stronger in the snow-covered high-latitude areas, because snow-covered short vegetation has an even higher albedo than the short vegetation itself.

- Rooting depth Vegetation roots have excess to water that is stored deeper in the soil, while this water would have not been available for soil evaporation. Therefore vegetation increases the amount of water available for evaporation. Deep-rooted vegetation, such as pine forest, has access to deeper groundwater layers, compared to more shallow-rooted vegetation, such as grasses or crops (Canadell et al., 1996; Schenk and Jackson, 2002), which is important during the dry season or during a drought.

- Leaf area index (LAI) The leaf area index (LAI) is the leaf area per ground area (in m^2 m^{-2}). The LAI is a key vegetation property and important for the energy, water, and carbon balance. The LAI has a different impact on soil evaporation, interception evaporation, and transpiration. Soil evaporation decreases with increasing LAI, because the leaves shade the soil. In contrary, both the interception evaporation and transpiration increase with LAI, because the total surface for interception and transpiration of water increases with increasing LAI. Furthermore, the LAI impacts the available energy through the albedo, and the LAI impacts the surface aerodynamic properties and turbulent exchange of water (Granier et al., 2000; Wang et al., 2014).

- Aerodynamic roughness A combination of different vegetation properties, such as the leaf area and vegetation height, impact the aerodynamic roughness; the resistance to flow. A high roughness facilitates the turbulent exchange of energy and moisture, and therefore increases the aerodynamic conductance. Above a vegetation with a high roughness such as a forest, there is a high ventilation of the air and a more sustained supply of dry air from the overlying atmosphere, which maintains the vapour pressure gradient.

- Stomatal closure Vegetation closes their stomata when the conditions are unfavourable for photosynthesis (Jarvis, 1976). This is for example during the night, when there is no energy available, or when the soil moisture content is low, in order to reduce the water loss. The stomata do not completely close, but they reduce the size of the aperture to reduce water loss. Stomatal closure changes over the coarse of a day and is thus more dynamic than the other four vegetation characteristics described above.

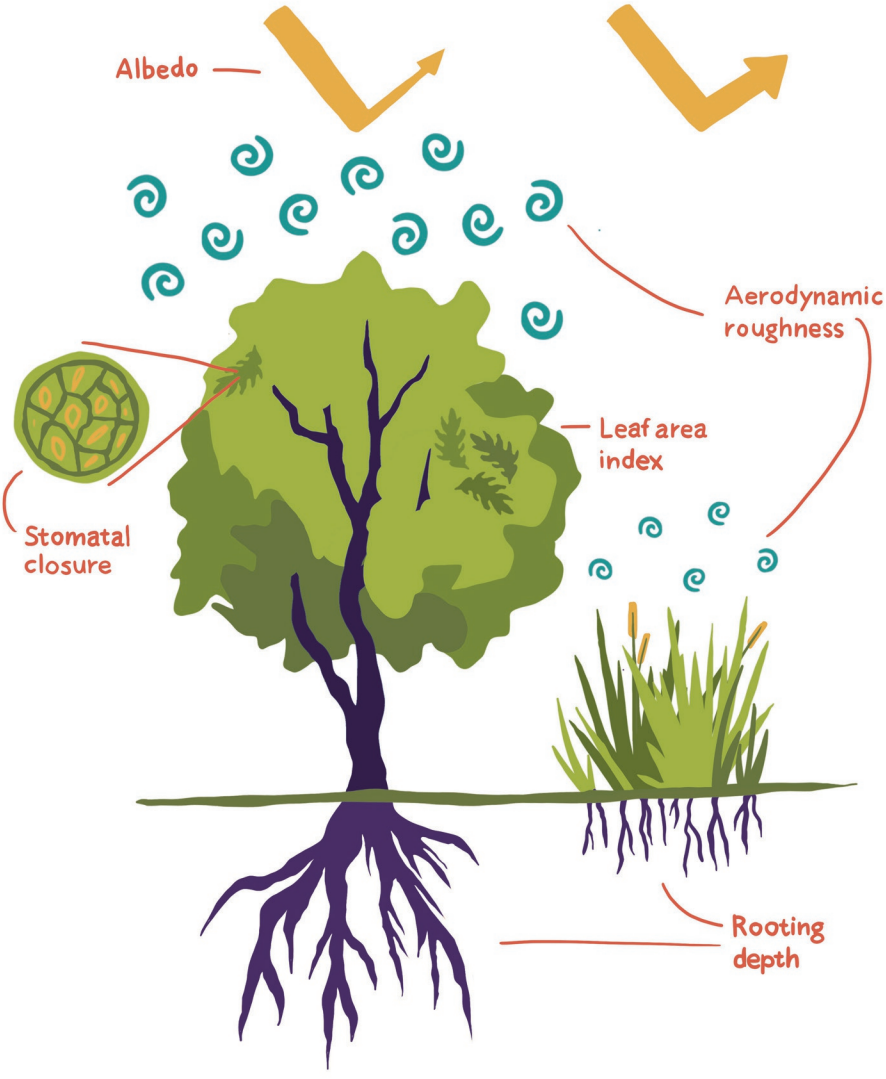

Figure 1.2: Vegetation characteristics that control evaporation. Trees have deeper roots, a higher leaf area index, a higher aerodynamic roughness, and a lower albedo than grasslands. Therefore, forest evaporation is generally higher than grassland evaporation.

1.2.2 In practise: How vegetation controls evaporation

It is very difficult, if not impossible, to study the effect of the albedo, rooting depth, or leaf area index on evaporation, and also the stomatal closure cannot be measured at the canopy scale. Therefore, studies that address the vegetation control of evaporation generally study 'vegetation' as a whole, through the vegetation type or the vegetation appearance, or focus solely on the stomatal regulation. Already in the eighteenth and nineteenth century, plant physiologists showed that vegetation impacts transpiration by regulating their stomatal aperture (Jarvis and McNaughton, 1986). In the 20th century, researchers derived the canopy scale stomatal regulation from measurements of the vapour pressure deficit and transpiration, or the inverted Penman-Monteith equation (Baldocchi et al., 1991; De Kauwe et al., 2017; Mallick et al., 2016; Monteith, 1965). These studies showed that the stomata are of main importance when the water supply becomes limiting and atmospheric demand is high, such as during the dry season, or during a drought (Blackman et al., 2019; Mallick et al., 2016; Meinzer et al., 1993). The impact of stomata on the evaporation depends on the spatial and temporal scale of the study, as well as on the vegetation type (Blackman et al., 2019; Jarvis and McNaughton, 1986; Mallick et al., 2016; Wolf et al., 2013).

In the early twentieth century, the so-called 'paired catchment studies' were one of the first studies to the effect of land-cover change on evaporation (Bates and Henry, 1928). These paired catchment studies compare two nearby river basins that have similar characteristics over a prolonged period, during which one of the river basins experiences land-cover change, while the other did not experience any change. These observational studies have, virtually without exception, concluded that tree planting increases annual evaporation and decreases streamflow (Bates and Henry, 1928; Bosch and Hewlett, 1982; Brown et al., 2005). More recently, Williams et al. (2012) studied evaporation from 167 flux tower sites and concluded that vegetation type plays a nearly-significant role on evaporation. Interestingly, they also concluded that grassland evaporation was higher than forest evaporation, which is in contrast to the paired catchment studies described above. This difference is referred to as the 'forest evapotranspiration paradox' (Teuling, 2018). Other studies reported that neither forest cover, nor the total vegetation cover reliably explained the spatial variability in the evaporation to precipitation ratio or that the contribution of vegetation cover was very low (Padrón et al., 2017; Yang et al., 2009). Generally, the vegetation control of evaporation differs per region and climate type, and there is no consensus on how important the vegetation or vegetation characteristics are.

1.2.3 In statistics: How vegetation controls evaporation

Above we describe how vegetation can control evaporation and how this is reflected in evaporation and vegetation data. According to these studies, a change in vegetation (characteristics) could have an effect on evaporation. A link between vegetation and

evaporation can however also be pure statistically, rather than causal. While a pure statistical correlations does not provide information about the relevance of vegetation for evaporation, it can be useful for example if one wants to use one component to measure the other. Several studies reported that the vegetation green biomass (measured from satellite remote sensing) explained 60 - 90 % of the spatial or temporal variability in evaporation (Nagler et al., 2005; Szilagyi, 2000), and Obrist et al. (2003) concluded that the LAI explained almost 90 % of the variability in daily evaporation in grassland. These high, but non-causal, correlations are confounded by the effect of water availability: both the green biomass of a canopy and evaporation increase with increasing water availability, especially in arid regions (Kergoat, 1998; Mallick et al., 2018).

1.3 Why study the link between evaporation and vegetation?

1.3.1 Using satellite observations of vegetation to estimate evaporation

Satellite data provides an opportunity to study the spatial and temporal variation in evaporation over large areas. Studies by Nagler et al. (2005) and Szilagyi (2000) found a strong correlation between ground-based measurements of evaporation and a satellite based vegetation index. This suggests that one could estimate or extrapolate evaporation using satelite based observations of the vegetation. Observations of the vegetation green biomass are integrated in most remote sensing based evaporation models, for example 1) models use vegetation indices and their empirical correlation with evaporation to estimate or scale evaporation, 2) surface energy balance models use vegetation indices to parameterize the aerodynamic roughness or the stomatal conductance, 3) models use the vegetation green biomass to calculate a spatio-temporal crop coefficient (e.g. Boegh et al., 2009; Chiesi et al., 2013; Kim et al., 2006; Mallick et al., 2009; Maselli et al., 2014; Su, 2002). Currently, it is however unclear if, and under what circumstances, vegetation green biomass represents evaporative processes. Therefore, there is a need to further investigate the link between satellite remote sensing observations of vegetation and ground-based measurements of evaporation for different vegetation types, different climate zones, and different spatial-temporal resolutions. Furthermore, in this century of major global changes, it is important to know whether these statistical correlations remain valid under global change.

1.3.2 Understanding the effect of global change on evaporation

Past and future climate change and land-cover change had, and will have, a great impact on evaporation and the water and energy balance. In the past thirty years, land-cover changes had affected almost a third of the global land area, especially forest area and agricultural area (Winkler et al., 2021). Furthermore, Zhu et al. (2016) showed that, between 1982 and 2009, the LAI increased for nearly half of the global vegetated area,

while the LAI decreased for 4 % of the vegetated areas. The increased atmospheric CO_2 concentration explained most of this greening, but also other factors played a role, such as nitrogen fertilization, climate change, and land-cover change. These changes will continue in the near future, for example through the continued deforestation in tropical regions in demand for agricultural land, and efforts to increase the tree cover elsewhere, to mitigate climate change.

Increasing global temperatures will impact the aridity and drought occurrence of the land surface. Under a warmer climate, evaporation will increase, there will be longer periods without precipitation, while having intense rainfall events. For most of the terrestrial surface, this will increase the aridity (Dai, 2011), and increase the frequency, duration, and intensity of droughts (Böhnisch et al., 2021). These changes in climate will shift vegetation types and change vegetation characteristics (Wu et al., 2015) and impact the vegetation control on evaporation through the stomata (Mallick et al., 2016).

Land-cover change and climate change will impact each other, as well as have an impact on vegetation characteristics and evaporation (Bonan, 2008). A better understanding of the vegetation control of evaporation under global change is crucial to study the future evaporation, as well as the effects on the global water and energy balance.

1.4 Observing evaporation and vegetation

The research in this thesis relies on evaporation and vegetation data acquired by various ground-based and satellite-based measurement techniques. Both ground-based and remote sensing measurement techniques have their own limitations and advantages, but a general advantage of satellite monitoring is the option to cover a large spatial area and to study spatial variability in both evaporation and vegetation characteristics. Furthermore, there is a high availability of free remote sensing data, and satellites monitor the Earth continuously which has a great potential for studying changes over time. Therefore, remote sensing data has become more popular in vegetation evaporation studies over the past decades (Fig. 1.3). The early satellites, launched in the sixties and seventies, had a spatial resolution of a few kilometers (Nimbus) or twice monthly revisit time (Landsat). Since then, the spatial and temporal resolution kept increasing, up to a ten meter resolution and twice weekly revisit time (Sentinel). Below, a few common monitoring techniques are discussed for evaporation and vegetation properties. For evaporation, the focus is on ground-based monitoring techniques, and for vegetation monitoring, the focus is on satellite-based monitoring techniques.

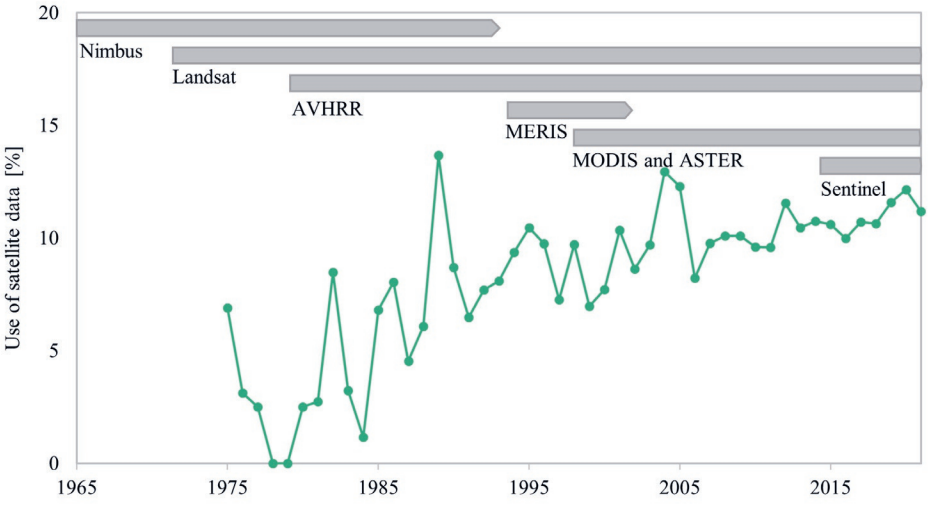

Figure 1.3: The use of remote sensing data increased over time. The percentage of studies in evaporation of vegetation that use remote sensing data has increased over the last decades. The figure includes a few commonly used satellite or sensor (series) in evaporation monitoring.

1.4.1 Observations of evaporation

Ecosystem evaporation and latent heat are very difficult to measure. Especially measuring variability over space, and measuring at the right spatial and temporal scale is extremely difficult. This paragraph shortly discusses some commonly used measurement methods, and addresses all data used in this thesis.

Water balance methods use the equation in fig. 1.1b to calculate evaporation. This equation is usually applied on a catchment scale, where lateral movement of water other than streamflow is absent, and on a yearly scale, when the change in storage is negligible. Lysiemeters are a measuring device to measure evaporation of a (semi-)natural vegetated surface. They are small or large, deep, vessels filled with soil and vegetation. Evaporation is derived from the difference between the incoming precipitation and outgoing water through the soil. Micro-meteorological methods calculate evaporation from meteorological measurements. This is for example through observations of the air temperature, vapour pressure deficit, and radiation, in combination with the Penman-Monteith equation (Monteith, 1965). The eddy correlation method is another micro-meteorological method where sensors measure the upward wind velocity and humidity and temperature. From these measurements one can derive the total upward or downward movement of water and energy (the latent heat and sensible heat). Tree transpiration can be derived from the sap velocity of single trees. Sensors measure the upward movement of the sap in a tree, and

based on this measurement of sap velocity, one can estimate whole tree transpiration. The ground-based evaporation observation methods all have their own uncertainties, but they generally work well on their own specific spatial and temporal scale. However, none of them can be used to study small- or large-scale spatial variation in evaporation.

Contrary to ground-based evaporation measurements, satellite remote sensing methods have the potential to calculate evaporation at all places and at all times. There are different of such monitoring methods, and a few of them are discussed. The so-called surface energy balance models use satellite observations of the infrared radiation emitted from the Earth's surface as a measure of the land surface temperature (Bastiaanssen et al., 1998; Su, 2002). The land surface temperature provides information on the partitioning of energy between the latent and sensible heat flux, and provides information on the water stress level. Other methods for example make use of the Penman-Monteith equation (Cleugh et al., 2007; Zhang et al., 2009), optionally in combination with the a surface energy balance model (Mallick et al., 2014), or use remote sensing data to scale ground-based measurements of evaporation to regional evaporation (Kim et al., 2006; Rahman et al., 2001). The major shortcoming of remote sensing evaporation techniques is that they only provide observations under non-cloudy conditions and that they cannot provide estimates at very high spatial and temporal resolution.

1.4.2 Satellite remote sensing of vegetation

Remote sensing data are commonly used to monitor the Earth's vegetation status. In this thesis, we selected the MODIS and Landsat satellite data among many other options (Fig. 1.3). These satellites have their own specific temporal revisit time and spatial resolution. MODIS provides data over the same location twice per day, and Landsat only twice per month, and one MODIS pixel pictures an area of $1 \times 1\,\text{km}$ while this is $30 \times 30\,\text{m}$ for Landsat. Satellites monitor the Earth's reflection or emission at different wavelengths, including wavelengths that we cannot observe by eye, such as the near-infrared and shortwave infrared. The different wavelengths reflect different vegetation characteristics, for example changes in the moisture content are reflected in the shortwave infrared, while changes in the surface temperature are reflected in the thermal infrared. The information from the different wavelengths can be used to observe the health or characteristics of the vegetation and fig. 1.4 shows a few examples of this.

In fig. 1.4a and 1.4b, a combination of the reflectance in red (wavelength: 665 nm) and near-infrared (wavelength: 842 nm) shows the green-up of the vegetation in the Attert region (Luxembourg) in Spring 2018. In fig. 1.4c and 1.4d, the reflectance in the red-near infrared transition zone (wavelength: 865 nm), combined with shortwave infrared (wavelength: 1610 nm) gives a good impression of the drying of the vegetation

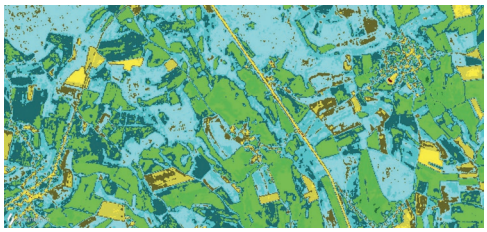

(**a**) Attert catchment on 8 April 2018

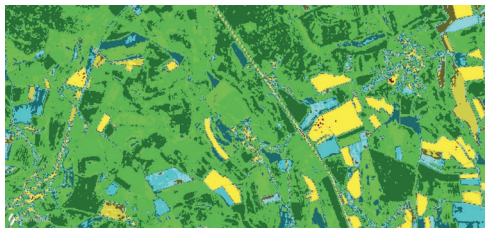

(**b**) Attert catchment on 8 May 2018

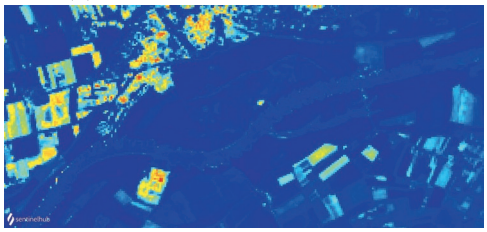

(**c**) Wageningen and Betuwe on 28 May 2018

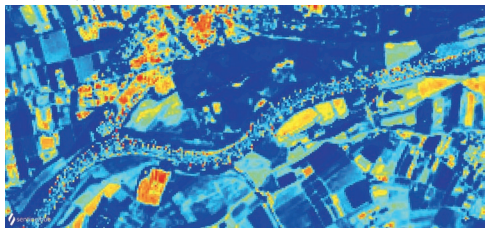

(**d**) Wageningen and Betuwe on 12 July 2018

(**e**) Attert catchment on 28 May 2018

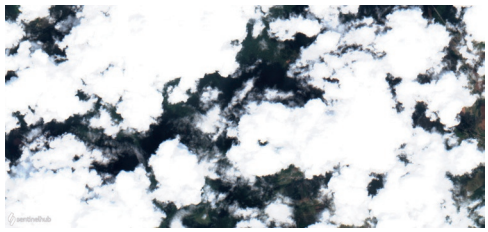

(**f**) Attert catchment on 12 July 2018

Figure 1.4: Satellite-based monitoring of the vegetation and moisture content. (a) and (b) show the green-up of the vegetation in the Attert catchment (Luxembourg), (c) and (d) show the effect of the summer drought in 2018 on the vegetation and water bodies in the Wageningen floodplains and Betuwe region (the Netherlands), and (e) and (f) show the cloudy skies on those same days as (c) and (d) but in the Attert catchment. The satellite figures are taken from the Sentinel 2A data and have a spatial resolution of 10 m (figure a, b, e, and f) and 20 m (c and d).

and water bodies during the summer drought 2018 in the Wageningen floodplains and Betuwe region (the Netherlands). On the exact same days, it was however difficult to study the drying in the Attert region, because of the cloud cover (Fig. 1.4e and 1.4f).

Vegetation indices combine information from several spectral bands to enhance the signal that one is interested in, while mitigating other factors, such as soil background effects or atmospheric distortion. Vegetation indices are commonly used to monitor land surface processes such as vegetation development or droughts. The most popular index for vegetation monitoring is the Normalized Difference Vegetation Index (NDVI): reflectance in the the red decreases with plant development, because the red light is absorbed by the

chlorophyll, while the reflectance in the near-infrared increases with plant development through scattering processes in the healthy leaves. A combination of these two is therefore a good measure of vegetation development and health. Many different indices exist to monitor the vegetation greenness, the moisture content, or vegetation water stress.

1.5 Research objectives and outline of this thesis

The introduction showed that there is a link between vegetation and evaporation. This link between vegetation and evaporation can be purely statistical, but this link can also be causal, which means that the vegetation controls the evaporation, and a vegetation change would impact the evaporation. In this thesis, both aspects of the link between vegetation and evaporation are discussed. First, we aim to improve the understanding of when and where we can use satellite remote sensing observations of vegetation for the monitoring of evaporation. Second, we aim to study evaporation in a changing world, with a focus on droughts and land-cover change. The two main research objectives of this thesis are:

- Research Objective 1 Study the link between ground-based observations of evaporation and satellite remote sensing observations of vegetation.
- Research Objective 2 Study the effect of drought and land-cover change on evaporation over large areas.

The chapters 2 to 5 constitute the core chapters of this thesis and these chapters are linked to the main research objectives of the thesis. Chapter 2, 3, and 4 contribute to research objective 1, while chapters 4 and 5 contribute to research objective 2 (Fig. 1.5).

Chapters 2 and 3 study the link between satellite remote sensing observations of vegetation green biomass and ground-based measurements of transpiration and evaporation. The two studies have a different spatial and temporal scale, and are conducted in a different study area, that differs in climate and vegetation characteristics. **Chapter 2** describes a study for oak and beech trees in the Attert catchment in Luxembourg. The study combines 30 m resolution NDVI data with sap velocity data. **Chapter 3** describes a study for 93 sites globally, distributed over five different vegetation types and a range of arid to humid climate zones. The study combines 500 m resolution estimation of the LAI with yearly mean flux tower estimations of evaporation. Next to evaporation, this study also includes fluxes of carbon and sensible heat. **Chapter 4** describes how the satellite-based monitoring of the vegetation drought differs between grasslands and forests.

Chapters 4 and 5 study evaporation and vegetation under global change. **Chapter 4** studies the vegetation response to the 2018 Central European drought. The study uses flux tower measurements of evaporation and stomatal conductance in combination with vegetation and drought satellite indices derived from MODIS data. The chapter aims to study how the different drought coping strategies of forest and grassland impact the

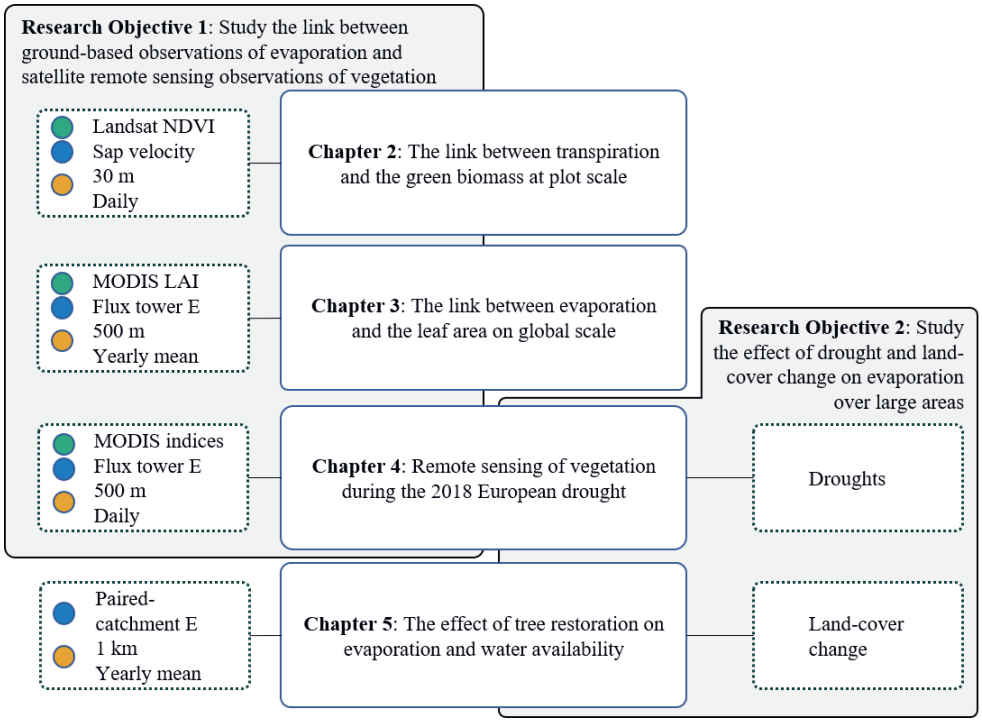

Figure 1.5: The outline of this thesis. The four core chapters of the thesis are linked to the two research objectives. In green the source of the satellite remote sensing data of vegetation, in blue the ground data of evaporation, and in yellow the spatial and temporal resolution of the study.

satellite based drought monitoring. **Chapter 5** describes a study to the effects of tree restoration on evaporation. The chapter describes how large-scale global tree restoration could impact evaporation and how this would impact precipitation, streamflow, and water availability.

Chapter 6 synthesises the main findings and results form the previous chapters. It reflects on the two main objectives. Subsequently the chapter provides a reflection and outlook on the link between vegetation and evaporation, and if and how one could use vegetation to monitor evaporation. Also it discusses the results in the context of global change, and discusses how changes in evaporation will propagate further into the water, energy, and carbon cycle.

I

Chapter 2

The link between transpiration and the green biomass at plot scale

This chapter is based on:
A. J. Hoek van Dijke, K. Mallick, A. J. Teuling, M. Schlerf, M. Machwitz, S. K. Hassler, T. Blume, and M. Herold (2019). "Does the Normalized Difference Vegetation Index explain spatial and temporal variability in sap velocity in temperate forest ecosystems?" *Hydrol. Earth Syst. Sci.* 23.4, 2077–2091. DOI: https://doi.org/10.5194/hess-23-2077-2019

Abstract

Understanding the link between vegetation characteristics and tree transpiration is a critical need to facilitate satellite-based transpiration estimation. Many studies use the Normalized Difference Vegetation Index (NDVI), a proxy for tree biophysical characteristics, to estimate evaporation. In this study, we investigated the link between sap velocity and 30 m resolution Landsat-derived NDVI for 20 days during 2 contrasting precipitation years in a temperate deciduous forest catchment. Sap velocity was measured in the Attert catchment in Luxembourg in 25 plots of 20×20 m covering three geologies with sensors installed in two to four trees per plot. The results show that, spatially, sap velocity and NDVI were significantly positively correlated in April, i.e. NDVI successfully captured the pattern of sap velocity during the phase of green-up. After green-up, a significant negative correlation was found during half of the studied days. During a dry period, sap velocity was uncorrelated with NDVI but influenced by geology and aspect. In summary, in our study area, the correlation between sap velocity and NDVI was not constant, but varied with phenology and water availability. The same behaviour was found for the Enhanced Vegetation Index (EVI). This suggests that methods using NDVI or EVI to predict small-scale variability in (evapo)transpiration should be carefully applied, and that NDVI and EVI cannot be used to scale sap velocity to stand-level transpiration in temperate forest ecosystems.

2.1 Introduction

Evaporation (E) is estimated globally as 60 % of the total precipitation (Oki and Kanae, 2006) and 80 % of total surface net radiation (Wild et al., 2013). This makes E the second largest component of the water and energy balance. Changes in E due to climate or land-use change have a major influence on the catchment water balance. Deforestation for example reduces E (Oliveira et al., 2018), leading to lower precipitation (Bagley et al., 2014) and higher streamflow (Dos Santos et al., 2018). Teuling et al. (2009) showed that changes in incoming radiation and water availability impact regional E and runoff. In order to predict these changes, a comprehensive understanding of "what controls E" is an important look forward.

The transpiration component of E, i.e. water loss through stomata E_t, is the largest contributor to total terrestrial E (Wang et al., 2014; Wei et al., 2017a), and therefore transpiration plays a major role in the global hydrological and biogeochemical cycle. Transpiration is controlled by complex interactions between climate (Awada et al., 2013; Hasler and Avissar, 2007), soil moisture content (Mitchell et al., 2012), topographic variables such as slope position and aspect (Mitchell et al., 2012), and vegetation characteristics (Williams et al., 2012). With respect to the vegetation biophysical characteristics, it has been shown that tree transpiration differs with leaf area index (LAI) (Granier et al., 2000; Wang et al., 2014), tree height (Ford et al., 2011; Waring and Landsberg, 2011), tree diameter (Chiu et al., 2016; Jung et al., 2011a), tree age (Baret et al., 2018), and phenological stage (Sobrado, 1994). With the advancements of remote sensing and free data availability, there have been many efforts to link E and E_t to satellite-derived vegetation indices (Carter and Liang, 2018). For example, studying large watersheds, Nagler et al. (2005) found a positive correlation between the Enhanced Vegetation Index (EVI) and Normalized Difference Vegetation Index (NDVI) and E in a riparian area, and Szilagyi (2000) found a positive correlation between NDVI and E in a mixed forest. Using the NDVI as a measure of vegetation biophysical properties has two major drawbacks: the saturation of NDVI at high biomass and the sensitivity to soil reflectance (Huete, 1988). Despite these drawbacks, NDVI is the most commonly used index for vegetation monitoring (Glenn et al., 2010).

The link between NDVI and E_t or E is used in different ways to either estimate E and E_t or to scale in situ water flux measurements to the landscape level. Five different ways are described below. First, the NDVI is used to calculate the fractional vegetation cover to estimate E_t or E in forests or mixed landuse types (Boegh et al., 2009; Chiesi et al., 2013; Maselli et al., 2014; Zhang et al., 2009). Second, NDVI is used to derive a spatio-temporal crop coefficient (the Kc-NDVI method) for grassland and agricultural fields (e.g. Kamble et al., 2013; Mutiibwa and Irmak, 2013; Reyes-González et al., 2018) or natural or mixed ecosystems (Hunink et al., 2017; Maselli et al., 2014). The Kc-NDVI method neglects the soil-moisture-driven controls on E_t or E, and this is one of the main drawbacks of

using this method in natural vegetation (Glenn et al., 2010). An additional water-stress term can be used with the Kc-NDVI equation to model dry ecosystem E or water-stressed conditions (Maselli et al., 2014; Park et al., 2017). Third, surface energy balance models use NDVI to parameterize aerodynamic roughness length and displacement height (Su, 2002), and models based on the Penman–Monteith equation use NDVI to parameterize surface conductance (Zhang et al., 2009). Fourth, the surface temperature-NDVI (Ts-VI) "triangle" method is used to derive a soil moisture stress scalar to constrain E. If pixels from different surface conditions are plotted in a Ts-NDVI scatterplot, they form a triangle pattern. The evaporative fraction and the Priestley–Taylor coefficient – the ratio potential evaporation over equilibrium evaporation – can be parameterized from that triangle, and are consequently used to calculate E (Jiang and Islam, 2001; Mallick et al., 2009; Zhu et al., 2017). Fifth, NDVI is used, e.g. as a proxy for stomatal conductance or absorbed photosynthetically active radiation, to scale in situ measured E to larger regions (Kim et al., 2006; Rahman et al., 2001). Thus, in many different approaches, NDVI plays a key role in estimating transpiration. The above-mentioned studies often derive the NDVI from MODIS or AVHRR data which have a spatial resolution of 250 m and 1 km (except for Kim et al. (2006), Rahman et al. (2001), Reyes-González et al. (2018), and Su (2002), who used airborne data or high-resolution satellite data; Landsat or IKONOS). The NDVI is often compared with E derived from different flux towers with a footprint length of $100 - 1000$ m (Kim et al., 2006), or a water balance model. Therefore, these studies encompass large spatial areas, with a larger variation in vegetation cover and sometimes multiple land-use types. Despite that the availability of high spatial resolution satellite products is increasing rapidly (e.g. Sentinel series), there is a lack of studies that investigate the link between satellite-derived NDVI and the water balance on the scale of forest patches or smaller. At the same time, there is a trend towards hyper-resolution land surface modelling and monitoring (Bierkens et al., 2015), where for example 30 m Landsat-derived NDVI data are used as a proxy for land cover in a continental land-surface model (Chaney et al., 2016). For many processes or parameters it is, however, unknown whether they can be applied at such high resolutions. Therefore, in this study we aim to understand whether the relation between NDVI and transpiration is also valid on the scale of forest patches by using 30 m resolution NDVI data.

Investigating the link between transpiration and NDVI requires high-resolution satellite data as well as a dense network of in situ transpiration observations. In the Attert catchment, a dense network of sensor clusters with – among others – sap velocity sensors allows for a detailed study of the link between tree transpiration and NDVI. For this catchment Hassler et al. (2018) showed that variability in sap velocity is mainly controlled by tree characteristics, such as tree diameter and tree height and site characteristics, such as geology and aspect. The aim of our study is to investigate the link between transpiration and NDVI using measurements of sap velocity combined with 30 m resolution NDVI data. Hassler et al. (2018) showed that small-scale variability in sap velocity was related to tree

structural characteristics, and therefore we expect sap velocity and NDVI to be correlated. We hypothesize this correlation to be positive, because we expect that forest stands with a higher leaf biomass (higher NDVI) will have a larger sap velocity.

Under water-stressed conditions, stomatal closure reduces tree transpiration to limit the risks of hydraulic failure. Among others, leaf area and leaf shedding play a role in mitigating these risks. To study the effect of water stress on the link between transpiration and NDVI, two growing seasons with above- and below-average precipitation are compared.

2.2 Material and methods

2.2.1 Site description

The study was carried out in the Attert catchment in midwestern Luxembourg. This area was chosen because of its small-scale diversity in geology and soil hydrological conditions. The 288 km^2 sized catchment lies on the border of the Ardennes Massif and the Paris Basin. The three distinct geologies in the catchment are schists, sandstone, and marls (Fig. 2.1). Soils vary between sand and silty clay loam (Müller et al., 2014). The land use is characterized by coniferous and deciduous forest on the hillslopes in the sandstone area, and grassland or agriculture in the valleys in the marl area and on the plateaus in the schist area. The elevation of the studied sensor clusters ranges from $217 - 473$ m above sea level. The average monthly temperature ranges from 0 °C (January) to 18 °C (July), the average yearly precipitation is 850 mm, and the mean annual evaporation is 570 mm (Müller et al., 2014).

Within the CAOS research unit, a monitoring network was set up in the Attert catchment including 29 sensor clusters in a forest (of which 25 are used in this study) in order to provide a new framework for hydrological models for catchments at the lower meso-scale (Zehe et al., 2014). A sensor cluster covers 20×20 m, and in each sensor cluster, soil moisture content (θ), meteorological characteristics, and sap velocity were measured. More information about these measurements can be found in Hassler et al. (2018) and Renner et al. (2016).

Soil moisture content was measured in three soil profiles in each cluster site using Decagon 5TE sensors at three depths (10, 30, and 50 cm). For this study, the average θ at 30 cm depth was calculated for the catchment. Wind speed and relative humidity were measured above grass at a weather station from the CAOS research unit (Fig. 2.1). Mean daily air temperature (T_a) was available from the Roodt weather station, and global radiation (R_g) was available from the Useldange weather station. Daily potential evaporation (E_p) was calculated for the catchment using the FAO Penman–Monteith equation (Allen et al., 1998).

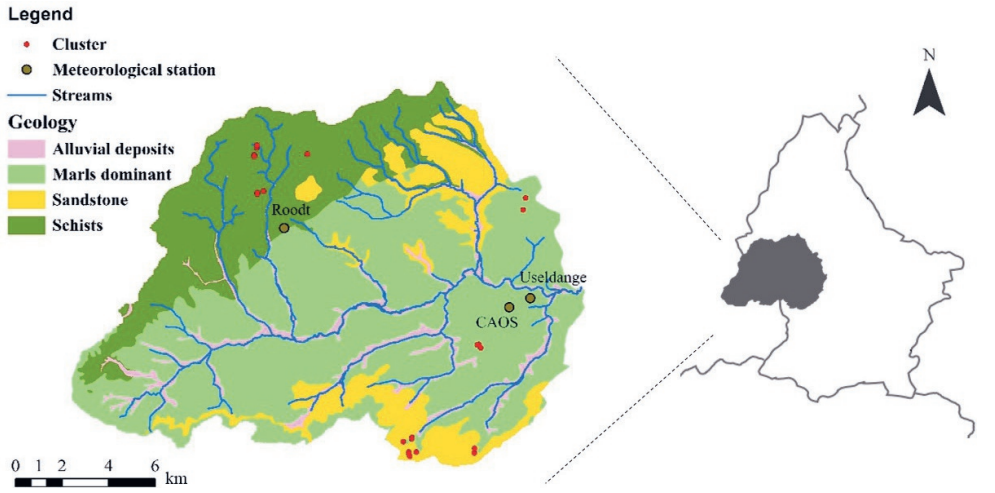

Figure 2.1: The geology of the Attert catchment and its location in Luxembourg. Sandstone in the catchment is a combination of Buntsandstein sandstone in the north and Lower Jurassic sandstone in the south. Also shown are the main streams, sensor clusters, meteorological stations Roodt and Useldange, and the location of the CAOS sensor cluster where wind speed and relative humidity measurements were taken from.

2.2.2 Meteorological conditions

In this study, 2 meteorologically contrasting years were analysed: 2014, a growing season with above-average precipitation, and 2015, a growing season with below-average precipitation. For the months May and June, meteorological conditions were not significantly different between 2014 and 2015, but for July and August, mean daily temperature, vapour pressure deficit (D), global radiation, and E_p were higher in 2015. E_p was 46 % (July) and 107 % (August) higher in 2015 compared to the same months in 2014 (Fig. 2.2). Total precipitation from April to August was 489 mm in 2014 and 249 mm in 2015, compared to an average of 374 mm for the years 2011 to 2017. September 2015 was wet, with a total precipitation of 160 mm. The high E_p and below-average precipitation in 2015 resulted in a cumulative precipitation deficit of 113 mm at the end of August (Fig. 2.3). Consequently, θ was low in the summer of 2015 (Fig. 2.2).

2.2.3 Data

Sap velocity

Sap velocity is used as a measure of tree transpiration (e.g. Smith and Allen, 1996). In summary, in this method, heat is applied to the water in the xylem of the tree trunk, and this heat is carried upwards with the water. Temperature sensors monitor the time it takes before the heat pulse reaches the sensor. This time is related to the velocity of the

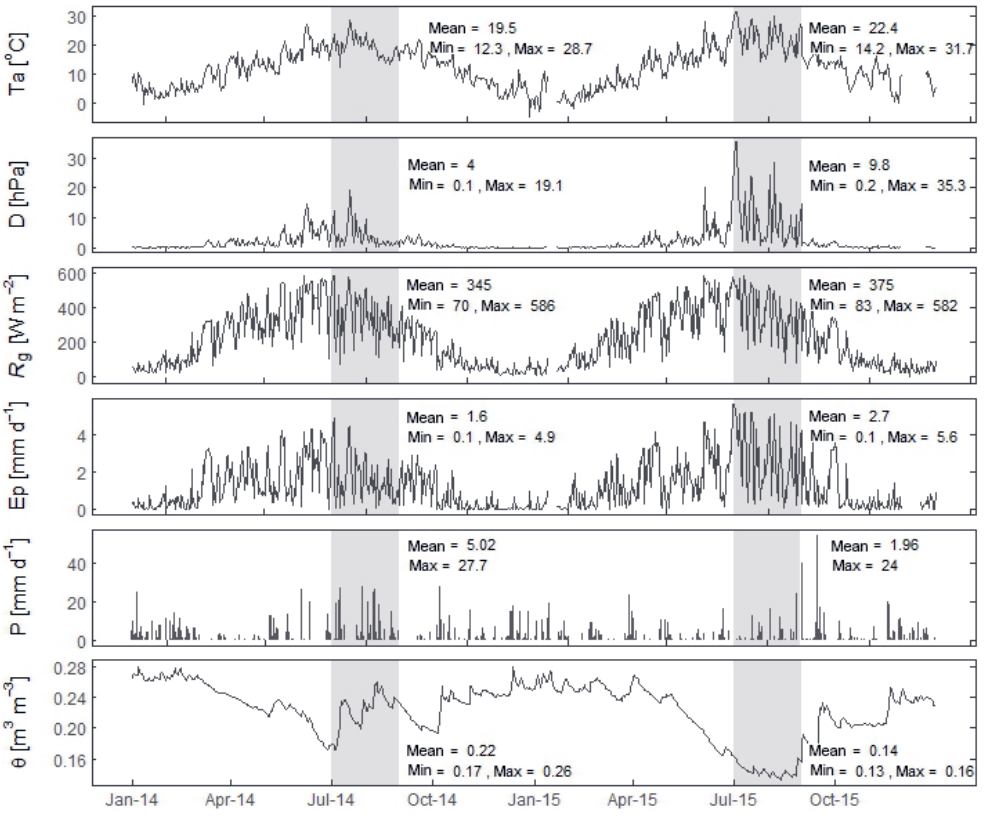

Figure 2.2: Meteorological conditions in 2014 and 2015. Daily average temperature (T_a), vapour pressure deficit (D), global radiation (R_g), potential evaporation (E_p), precipitation (P), and soil moisture content (θ). The min, mean, and max values are calculated for July and August in both years, indicated by the grey box.

water in the xylem. More information about sap velocity measurements can be found in Smith and Allen (1996).

At each sensor cluster (all located in deciduous forest stands), four trees roughly representative of the sensor cluster were selected for the sap velocity measurements. The main deciduous tree species in the area are beech (*Fagus sylvatica L.*) and oak (*Quercus robur* L. and *Quercus petraea* (Matt.) Liebl.); less abundant are hornbeam (*Carpinus betulus* L.), maple (*Acer pseudoplatanus* L.), and alder (*Alnus glutinosa* (L.) Gaertn.). Table 2.1 shows the presence of the different species in this study. Sap velocity was measured at the north-facing side of the stems using sap flow sensors manufactured by East 30 Sensors in Washington, US. From the measured temperatures, sap velocities were calculated based on the equation of Campbell et al. (1991), which is recommended by the manufacturer.

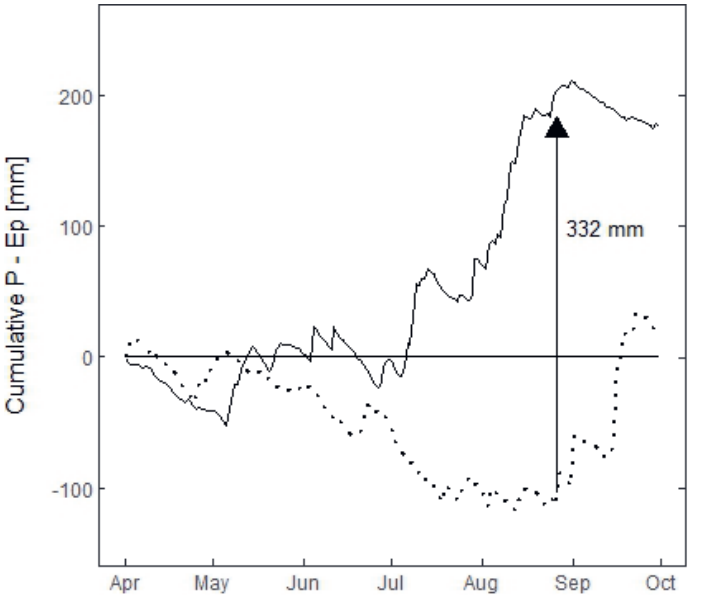

Figure 2.3: Cumulative precipitation surplus ($P - E_p$) from April to October for 2014 (solid line) and 2015 (dashed line). The difference in precipitation surplus between the 2 years was largest at the end of August, as indicated by the arrow.

Afterwards, a wounding correction was performed following Burgess et al. (2001). Sap velocity differs with horizontal depth in a tree, and this radial variability is one of the main sources of uncertainty in sap velocity measurements (Hernandez-Santana et al., 2015). To account for the radial velocity profile, the sensors measure at three depths: 5, 18, and 30 mm. Following Hassler et al. (2018), for each tree, the sensor with the highest mean daily sap velocity was selected. Trees with less than 80 % available data from June to August, or with a prolonged period of negative sap velocity, were excluded from the analysis. This resulted in a data set with 73 trees at 25 sensor clusters (Table 2.1). For each cluster, the mean daily sap velocity (from 08:00 to 20:00 LT – local time) was calculated. To match the spatial scale of the sap velocity data to the NDVI data with a 30 m resolution, mean daily sap velocity was calculated for each cluster.

Sap velocity measurements can be scaled up to whole tree transpiration from the total sapwood area for each tree (Smith and Allen, 1996), but these data were not available within our study area. Alternatively, a species- and site-specific allometric equation between tree diameter at breast height and sapwood area can be used to calculate tree total sap flow, but this conversion introduces uncertainties (Ford et al., 2004; Gebauer et al., 2012). Therefore, we used sap velocity directly in our study.

Table 2.1: Sensor cluster characteristics.

Geology	No. of sensor clusters	No. of studied trees	No. of beech / Oak / other	Elevation (min - max)	No. of stems per cluster (min - max)	mean cluster DBH (min - max)
Sandstone	9	29	21/7/1	217 – 284	9 – 54	2 – 44
Marl	5	13	2/8/3	283 – 351	16 – 34	5 – 17
Schist	11	31	23/5/3	428 – 473	20 – 346	4 – 37

NDVI and EVI

The vegetation indices were calculated from Landsat-7 (ETM+ sensor) and Landsat-8 (OLI sensor) surface reflectance data were obtained from EarthExplorer of the US Geological Survey. Both sensors acquire images with a spatial resolution of 30 m and, combined, they have a temporal resolution of 8 days. The overpass time of the satellites is 10:27GMT. Clouds and cloud shadows were removed from the images using the cloud quality information delivered with the data product, and this automatic procedure was followed by a visual check to remove cloudy pixels. After the cloud removal, surface reflectance values were extracted for each cluster centre using bilinear interpolation, where the four closest raster cells are interpolated. Images were removed when surface reflectance information was available for less than five clusters or for only one geology type. This resulted in a total availability of 20 Landsat images, 11 for the growing season of 2014 and 9 for the growing season of 2015. The NDVI and EVI were calculated as follows:

$$NDVI = \frac{\rho_{NIR} - \rho_{Red}}{\rho_{NIR} + \rho_{Red}} \tag{2.1}$$

$$EVI = \frac{\rho_{NIR} - \rho_{Red}}{\rho_{NIR} + 6 \times \rho_{Red} - 7.5 \times \rho_{Blue} + 1} \times 2.5 \tag{2.2}$$

where ρ is the surface reflectance in the near-infrared (NIR), red, and blue parts of the electromagnetic spectrum.

Tree and sensor cluster characteristics

To study the effect of static vegetation and environmental characteristics on sap velocity and NDVI, correlations with tree and environmental characteristics were calculated (Hassler et al., 2018). For every cluster, the total number of stems was counted, and the DBH was measured for each tree with a circumference of more than 4 cm (Table 2.1). The tree height was estimated for every tree where sap velocity was measured, and for each cluster site, aspect was noted. Elevation and geology are derived from a digital elevation model and a geological map.

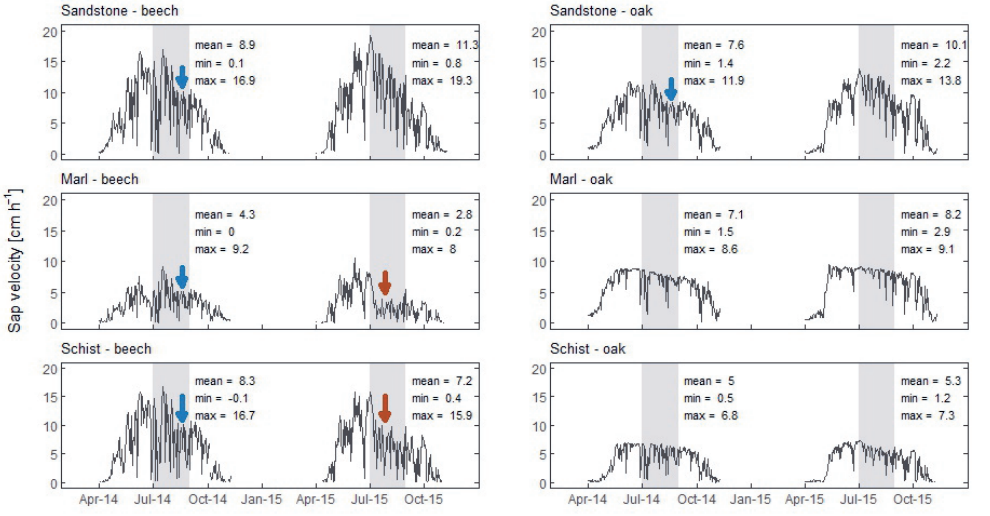

Figure 2.4: Mean daily sap velocity for beech and oak trees in the three different geologies. The drop in sap velocity in August 2014 (blue arrow) is related to a lower incoming radiation, while the drop in August 2015 (red arrow) is not related to a lower incoming radiation, but falls into a period of below-average precipitation and low soil moisture content. The min, mean, and max values are calculated for July and August in both years, indicated by the grey box.

2.3 Results

2.3.1 Temporal and spatial variability in sap velocity and NDVI

The seasonality in sap velocity is clearly visible, with a steep increase in April and a decrease in October (Fig. 2.4). Mean daily sap velocity for July and August was highest for beech trees in the sandstone area (8.9 cm h^{-1} in 2014 and 11.3 cm h^{-1} in 2015) and lowest for beech trees in the marl area (4.3 cm h^{-1} in 2014 and 2.8 cm h^{-1} in 2015). In July 2014, sap velocity was low for part of the trees, which corresponds to a low R_g. Also from July to August 2015, the period with little rainfall, sap velocity was low for part of the trees located in the marl and schist area. The reduced sap velocity in 2015 did not correlate with a low R_g. Redundancy analysis showed that in 2014, 78 % of the variability in daily sap velocity was explained by R_g and T_a. In 2015, R_g, T_a, and θ together explained 65 % of the variability in sap daily velocity.

The phenological cycle is clearly visible in the temporal dynamics of NDVI with a rapid green-up in April (Fig. 2.5). In April, the mean Landsat-derived NDVI over the clusters was 0.62 ($\pm$0.05), as compared to 0.82 ($\pm$0.05) during the fully developed stage of the vegetation. On 12 August 2015, the NDVI of all clusters was low, which did not appear in

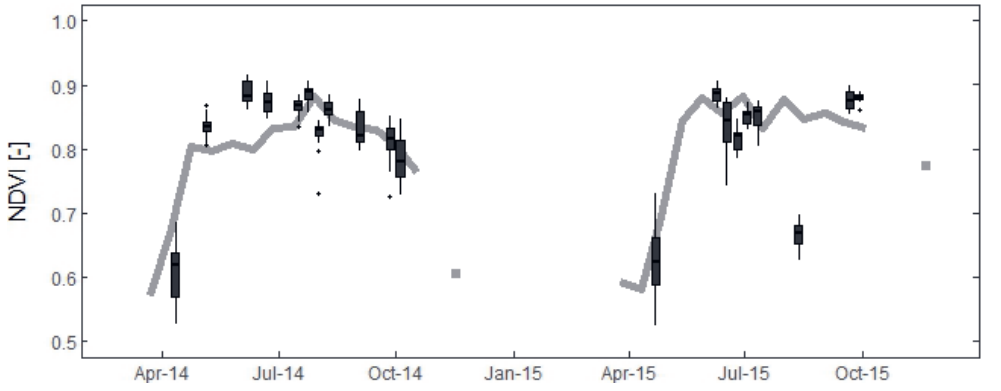

Figure 2.5: Observed NDVI dynamics during the growing seasons of 2014 and 2015. The grey line and dots represent the mean NDVI over the forested clusters derived from the MOD13Q1 product of MODIS. It provides a better overview of the seasonal course. The 20 boxplots (in black) show the variability in Landsat-derived NDVI over the studied clusters for each studied day.

the MODIS NDVI product. These pixels were not removed by the cloud removal procedure, but haze is visible in the image, which possibly influenced the cluster pixels. Unfortunately no other cloudless images were available for the second half of July and August in 2015, the driest months of the summer.

2.3.2 Correlation between sap velocity and NDVI

Analysing all sensor clusters together for all 20 days, a moderate positive correlation was found between sap velocity and NDVI ($p < 0.001$, Pearson's $r = 0.47$) (Fig. 2.6a). Considering temporal correlation, both sap velocity and NDVI had low values at the start and end of the growing season and high values in summer. This means that sap velocity and NDVI were positively correlated for 22 of the 25 clusters ($p < 0.05$) (Fig. 2.6b-e). Considering the months May to September only, when the canopy was in full leaf, there was no (significant) correlation between sap velocity and NDVI for 22 of the 25 clusters.

Scatterplots of spatial variability in sap velocity and NDVI show three different patterns: (1) a significant linear positive correlation (Fig. 2.7a and d: Pearson's r between 0.50 and 0.60), (2) a significant linear steep negative correlation (Fig. 2.7b and e: Pearson's r is between -0.51 and -0.70), and (3) no significant correlation (Fig. 2.7c and f). The positive correlation coefficient between sap velocity and NDVI was found in April in both years. This was the beginning of the growing season, and sap velocity and NDVI values were below average. For 5 of the studied days during the growing season of 2014 and early

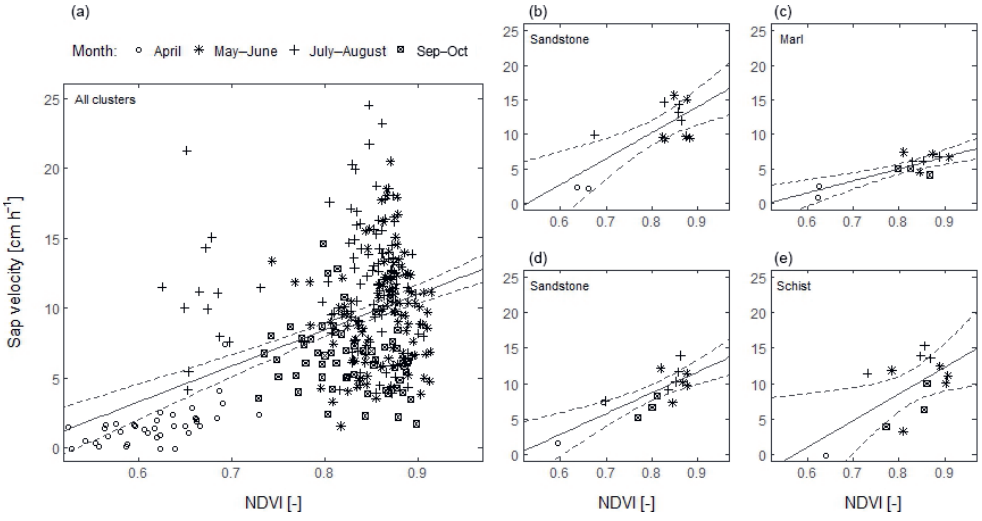

Figure 2.6: Temporal correlation between sap velocity and NDVI for all 20 studied days in 2014 and 2015. (a) For all sensor clusters together, sap velocity and NDVI were positively correlated ($p \leq 0.001$, $R^2_{adj} = 0.22$). (b–e) The correlation for four different clusters in different geologies. For each shown cluster, the correlation is significant ($p \leq 0.05$). For 1 of the 25 clusters, the correlation is not significant, and for 2 clusters the correlation is significant only at $p \leq 0.1$. The dashed line represents the 95 % confidence interval.

June and September 2015, sap velocity and NDVI were negatively correlated. For 5 days in 2014 and 6 days in 2015, sap velocity and NDVI were uncorrelated.

2.3.3 Correlation between sap velocity and NDVI in relation to soil moisture content θ

Figure 2.8a shows the dynamic changes in the correlation coefficient between sap velocity and NDVI. In both years, the correlation coefficient was positive at the beginning of the growing season (April) and negative or close to zero during the rest of the year. In the year 2014, no trend was visible in the variability of the correlation coefficient. In 2015, the correlation coefficient was initially positive and became negative in May. As the growing season progressed and θ dropped (to a minimum of $\theta = 0.13$ m^3 m^{-3} in mid-August), the correlation became weaker and insignificant. At the end of September, when θ increased following high precipitation, the correlation between sap velocity and NDVI was again negative. Studying all days together, sap velocity and NDVI were positively correlated during the period of highest θ (in April, $\theta > 0.22$ m^3 m^{-3}) (Fig. 2.8b). Contrastingly, at high θ during September 2015 ($\theta > 0.20$ m^3 m^{-3}, sap velocity and NDVI were negatively correlated. The correlation coefficient was close to zero when θ was lowest. At intermediate θ, the correlation coefficient was mostly negative.

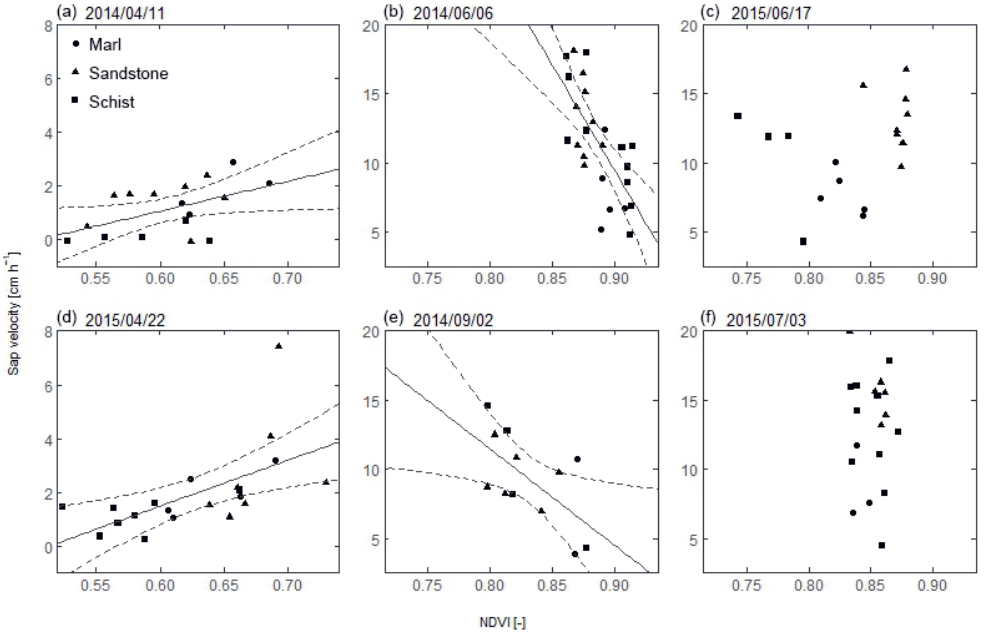

Figure 2.7: Relationship between sap velocity and NDVI for 6 days. Each dot represents one sensor cluster in the sandstone, schist, and marl area. The dashed line represents the 95% confidence interval. (a, d) April 2014 and 2015, during the period of green-up. At the (b) start and (e) end of the growing season in 2014. (c, f) At the beginning of the dry summer of 2015.

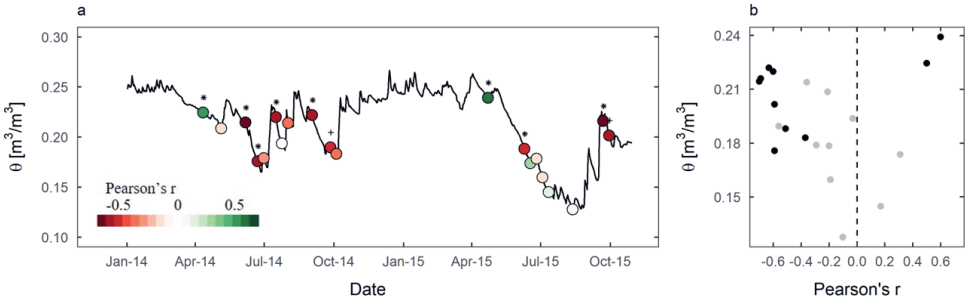

Figure 2.8: Relationship between sap velocity and NDVI and observed soil moisture content (θ). (a) The average soil moisture content at 30 cm depth over the sensor clusters. The colours indicate the spatial correlation coefficient (Pearson's r) between sap velocity and NDVI for the 20 studied days. Symbols indicate whether the correlation is significant at $p \leq 0.05$ ($*$) or at $p < 0.1$ ($+$). (b) The soil moisture content and Pearson's correlation coefficient for the 20 studied days. Black dots indicate that $p \leq 0.1$.

2.3.4 Effect of static vegetation and environmental characteristics on sap velocity and NDVI

The effects of static vegetation and environmental characteristics on sap velocity and NDVI were calculated. This was also done to check whether dependency on one of these characteristics could explain the negative correlation between sap velocity and NDVI. Assessing individual trees, sap velocity was related to tree DBH and tree height, but at cluster level, sap velocity was not or moderately dependent on these characteristics (Table 2.1). The number of stems and mean tree DBH per sensor cluster did not correlate with sap velocity. For some days, sap velocity was higher in clusters with higher trees. For most studied days, sap velocity for beech trees was higher than for oak trees, but this difference was usually not significant. Altitude and sap velocity were negatively correlated in April for both years. Geology and aspect explained part of the variability in sap velocity, especially during summer 2015, when sandstone clusters had a higher sap velocity than schist and marl clusters, and north-facing slopes had a higher sap velocity than south-facing slopes. The different cluster characteristics were not independent and, therefore, a relation between two variables could also have been the result of a causal relation with another variable.

Cluster-averaged tree characteristics were usually not related to NDVI, and their direction of influence was not consistent. Also, the change in NDVI with altitude was not consistent over the year, but in April of both years, the correlation was negative. In both years, schist clusters had the lowest NDVI in April ($p < 0.1$ in 2014). From June till August 2015, sandstone clusters had the highest NDVI, except for 9 and 25 June. Variability in species and aspect were correlated with variability in NDVI only for a few days.

2.4 Discussion

2.4.1 Sap velocity and scaling to tree transpiration

In the present study, mean sap velocity was calculated for the two to four trees in each sensor cluster. This is only a small selection of the total number of trees per cluster, which varied from 9 to 346, with a median of 34 trees per cluster. The trees selected for sap velocity measurements are roughly representative of the cluster with respect to species and DBH. But velocity of the sap depends on tree DBH, height, species, and tree age (Gebauer et al., 2012; Ryan et al., 2006), and therefore, making a true representative selection remains challenging. We looked for a relationship between tree sap velocity and a canopy trait, NDVI. Please note that two scaling steps are required to scale sap velocity up to the canopy level: a first step to scale from sap velocity to whole tree transpiration and a second step from tree to stand transpiration. In this study, measurements of sap velocity were preferred over whole tree or stand transpiration, because scaling introduces uncertainties, especially when sapwood area is not known (Ford et al., 2004; Gebauer et al.,

2012). An empirical scaling formula can be used to calculate whole tree transpiration from (1) sap flow, (2) tree DBH, and (3) a species- and site-specific parameter. On an individual tree level, trees with a larger DBH had a higher sap velocity, which is also known from other studies (Jung et al., 2011a). Calculating whole tree transpiration from sap velocity would have thus increased the mutual differences among clusters, but usually would have not changed the order of values and direction of correlation with NDVI. The species-specific parameter in the scaling formula would have increased the differences in transpiration between beech and oak trees. This is because beech trees in this study had, on average, a larger sap velocity and, despite the lower DBH, a higher average sapwood area.

2.4.2 Temporal and spatial variability in sap velocity and NDVI

The moments of vegetation green-up and leaf senescence are reflected in both sap velocity and NDVI as they increase in April and decrease in October. Comparing the summer (July and August) of 2014 and 2015, the higher potential evaporation in 2015 resulted in a higher sap velocity for beech and oak trees in the sandstone area compared to 2014. For the beech trees in the marl and schist area however, mean sap velocity was lower in summer 2015. This drop in sap velocity in 2015 could not be attributed to a reduction in atmospheric demand or available energy (Fig. 2.9), and was likely the result of stomatal closure in response to water stress. No drought-related reduction was observed in NDVI, and also no lagged effect. This indicates that trees were conservative with water and closed their stomata to prevent transpirational water loss. Under the relatively mild stress during the summer of 2015 no change in tree canopy structure (leaf area index, leaf angle distribution) and thus no change in structural indices like NDVI can be expected as structural vegetation changes become visible only after a prolonged dry period (Eklundh, 1998).

Considering the spatial variability, Hassler et al. (2018) found that in the Attert catchment, tree characteristics (species, DBH, and tree height) explained 22 % of the variability in sap velocity. Interestingly, our study showed that cluster mean tree characteristics did not explain variability in cluster mean sap velocity during most of the growing season (Table 2.2). This is likely because of the smaller variability in sap velocity and tree characteristics on the cluster level as compared to individual trees.

Part of the trees showed a water-stress-induced drop in sap velocity in 2015. The statistical analysis revealed that during this period, geology and aspect significantly explained part of this spatial variability in sap velocity (Table 2.2). The higher sap velocity on north-facing slopes could indicate the effect of a higher water availability compared to south-facing slopes. In the sandstone area, trees maintained high sap velocity during the dry period, but sap velocity was reduced in the schist and marl area. Also, this effect of geology is likely related to water availability. Pfister et al. (2017) and Wrede et al. (2015) showed

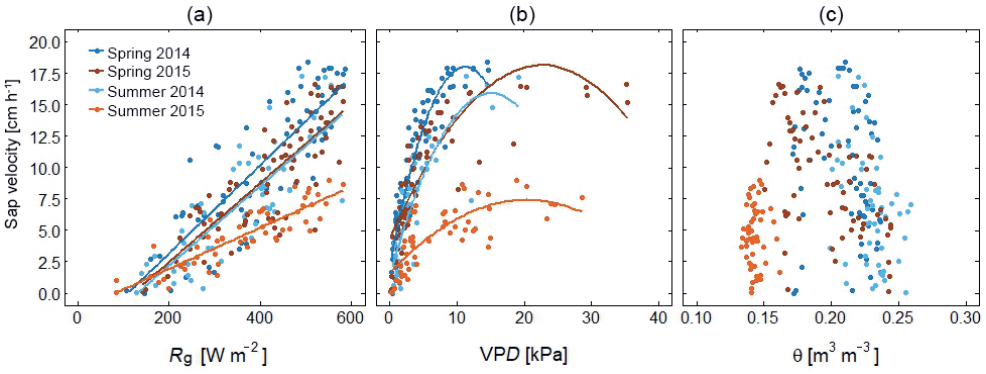

Figure 2.9: Relationship between sap velocity and meteorological conditions for spring and summer 2014 and 2015 for a beech tree in the schist area. The relationship between mean daily sap velocity and (a) global radiation (R_g), (b) vapour pressure deficit (D), and (c) soil moisture content (θ). The regression line is shown in the plot. In summer 2015, sap velocity is low, despite high R_g and D.

that in the Attert catchment, sandstone has a high storage capacity, because of the deep permeable soils, while the storage capacity is low in the marl and schist area. Furthermore, trees in the sandstone area were on average taller and had a larger DBH. These trees might have been able to access water from deeper layers because of a more developed root system.

2.4.3 Correlation between sap velocity and NDVI

Temporally, sap velocity and NDVI were positively correlated, because both follow a similar seasonal cycle with lower values in April and October than in summer. Considering only the full leaf period (May–September), sap velocity and NDVI were not correlated. Variability in sap velocity during the full leaf period was to a large extent explained by daily variations in R_g and T_a, and these meteorological controls of transpiration are not reflected in the NDVI. Nor is the NDVI affected by daily variations in R_g and T_a.

Considering spatial correlation, three different patterns were found: positive, negative, and no correlation. The different patterns are discussed below. During April in both years, sap velocity and NDVI were positively correlated. This was before complete leaf-out and the spatial variability in NDVI was high. In April, elevation of the clusters significantly explained part of the variability in both sap velocity – Pearson's $r = -0.56$ (2014) and $r = -0.45$ (2015) – and NDVI – Pearson's $r = -0.78$ (2015). Onset of greenness varies with elevation and associated temperature differences (Elmore et al., 2012; Kang et al., 2003) and at the moment of image acquisition, the clusters were in different stages of phenological development. This was reflected in both NDVI and sap velocity, and likely explains the positive correlation between them.

Table 2.2: Seven (semi-)static sensor cluster characteristics and whether they are significantly correlated ($p \leq 0.05$) with spatial variability in mean sap velocity (α) and NDVI (β). Parentheses indicate a significance level of $p \leq 0.1$. The results are based on Pearson's correlation for numerical data and one-way ANOVA for species, geology, and aspect. The mean sensor cluster DBH is the mean DBH of all trees in the sensor cluster, while the mean tree height is the mean of the sap velocity trees only. Species classes are beech, oak, or a mixture. The number of stems, DBH, and tree height are not independent. Mean tree height, aspect, and altitude are related to geology. Italic indicates that the correlation between sap velocity and NDVI was positive for this day, while bold indicates a negative correlation.

Year	Date	Number of stems	Mean tree DBH	Mean tree height	Species	Altitude	Geology	Aspect
2014	*11-04*			α		α	α (β)	(α)
	05-05	β			(α)			(β)
	06-06					(β)	α (β)	(α)
	22-06	(α) β	β	β		β	β	α
	16-07			α (β)			(α)	(α)
	24-07		β				(α)	(α)
	01-08			(α)		β	α β	α
	09-08			(β)				(α)
	02-09				(α) β		β	(α) β
	26-09						β	
	04-10							β
2015	*22-04*	(α) β	β	β		α β	(α) β	
	09-06	β	β	β	(α)	β	α β	α
	17-06	(β)		β	(α)	β	α β	α
	25-06			(β)	α		α	α
	03-07				(α)		α	α
	11-07	β		α β		(α) β	α β	α
	12-08			α		α	α	(α) (β)
	21-09			(α)				(β)
	29-09			(α)				(α)

The negative correlation between sap velocity and NDVI – a higher sap velocity for lower leaf biomass – was found during most of the studied period, though it was sometimes weak and not significant. There is no clear explanation for this unexpected result, but four probable reasons are foreseen that could have influenced the correlation. First, for NDVI it is well known that it saturates at high LAI (Huete, 1988), which makes the index insensitive to vegetation biophysical and biochemical properties (Gamon et al., 1995). NDVI saturation was found for LAI greater than ~ 4 in a beech forest (Wang et al., 2005) and LAI greater than $\sim 5 - 6.5$ for a mixed beech, oak, and Scots pine forest (Davi et al.,

2006). For the sensor clusters in this study, measured LAI in 2012 was on average 4.9 ± 0.4 for the beginning of May (sandstone and marl clusters) and 6.4 ± 0.8 for mid- August (schist clusters) (unpublished data, described in Sun and Schulz, 2017). Therefore the clusters are likely at saturation, which could introduce noise into the data. The negative correlation however seems to be robust even at high values of NDVI. Second, because we studied small-scale variability, the spatial variability in NDVI was low (standard deviation ranges from 0.01 in summer to 0.05 in April). Both could explain the absence of a positive correlation, but they do not explain the negative correlation. Third, sap velocity is not per se transpiration (as explained in Sect. 2.4.1), but a conversion of sap velocity to tree transpiration is not expected to influence the sign of the correlation. Lastly, a correlation with static tree and site characteristics was investigated, but this was also not found to explain the negative correlation.

On half of the studied days, no correlation was found between sap velocity and NDVI, which could be due to noise in the data caused by the saturation of the NDVI signal. Absence of a correlation could also indicate that optical vegetation characteristics are uncoupled from E, i.e. that no significant control of stomata and vegetation structure on E was apparent in the Attert catchment. The temporal change in Pearson's r during the growing season of 2015 – a negative correlation during the beginning (June) and end (September) of the growing season, but no correlation during the drier period – points to an effect of short-term water stress, which is discussed in Sect. 2.4.4.

2.4.4 Comparing the dry and wet growing seasons

Summer 2015 experienced below-average precipitation, but was not exceptionally dry. Nevertheless, sap velocity dropped during this dry period. In 2014, when ample soil water was available, temporal variability in sap velocity was strongly coupled with R_g, D, and T_a. During the period of low soil moisture content in 2015 sap velocity was, next to R_g, D, and T_a, also coupled with soil moisture content. The water stress occurred only for a short time period, and therefore no change in NDVI was apparent. Given that the spatial pattern in sap velocity changed from the wet to dry periods, while NDVI did not change, the correlation between sap velocity and NDVI was different in the two summer seasons. During the wet summer of 2014, we found a weak to moderate negative correlation, and during the dry summer of 2015, sap velocity and NDVI were uncorrelated. During the dry summer of 2015, water availability (through geology and aspect) likely explained spatial variability in sap velocity, and this soil moisture control of E was not reflected in NDVI.

2.4.5 Using NDVI to estimate evaporation

We hypothesized finding a positive correlation between sap velocity and NDVI, but spatially, this was the case only in April. This means that NDVI successfully captured the

pattern of sap velocity during the phase of green-up when water was not limited. After green-up, the positive correlation changed into a negative correlation or no correlation. The inconsistent correlation between sap velocity and NDVI would also translate into an inconsistent correlation between transpiration and NDVI, after applying a scaling equation. Various methods however use NDVI to estimate $E_{(t)}$, among others, in evergreen, boreal, and deciduous forests, and assume the two to be positively correlated (Glenn et al., 2010, provide a review). Of these methods, the Kc-NDVI method is used most frequently, and it is shown that including NDVI as a spatio-temporal crop coefficient improves $E_{(t)}$ prediction compared to the conventional use of a crop coefficient in forests (Hunink et al., 2017; Maselli et al., 2014). Other studies however found a weak correlation between NDVI and flux tower transpiration and reported that EVI provides better results in salt cedar and cottonwood dominated stands (Nagler et al., 2005) and boreal forest (Rahman et al., 2001), because the EVI does not saturate as quickly at high LAI (Huete, 1988). Therefore we also explored the correlation between sap velocity and the EVI. The results, although in absolute terms different and "less significant", tell a similar story to NDVI – a positive correlation in April, a negative but not always significant correlation during the rest of the year, and no correlation during the dry summer of 2015.

Compared to our study, earlier studies that found a positive correlation between $E_{(t)}$ and NDVI encompassed large spatial areas and sometimes multiple land-use types. This raises the question whether the link between $E_{(t)}$ and NDVI holds on a small spatial scale. Methods that use NDVI to estimate E, including land-surface models, should be carefully applied when studying small-scale variability in E.

NDVI lags behind sap velocity in relation to drought and cannot be used to predict transpiration under dry conditions. A water-stress factor has been introduced by several studies to overcome this problem, but this stress factor is not always spatially explicit (e.g. Maselli et al., 2014). Our study showed that, in the studied catchment, a spatially explicit stress factor is required for accurate transpiration prediction under drying conditions, because neither NDVI nor meteorological conditions capture the spatial variability in E controlled by geologically induced differences in water availability.

2.4.6 Using NDVI to scale transpiration

The scaling of water flux measurements across scales is a main challenge in ecohydrology (Asbjornsen et al., 2011; Hatton and Wu, 1995). Scaling in situ measurements over a larger area, for example flux tower or sap velocity measurements, is traditionally done by scaling over in situ measured biometric parameters such as DBH, basal area, or sapwood area (Čermák et al., 2004). Obtaining these characteristics from satellite images is less resource demanding, can be applied over larger areas, and provides the opportunity to study both spatial and temporal patterns simultaneously. Satellite derived scaling parameters have another advantage over the conventional ones: (semi-)static characteristics are unreliable

under the changing conditions that we face for the future, with among others more intense droughts (Cleverly et al., 2016; IPCC, 2012).

This study shows that, in a temperate forest with high LAI and low variability in NDVI and EVI, these indices cannot be used to estimate transpiration or scale sap flux measurements to the stand level. The benefits that satellite-derived scaling parameters provide makes it worth exploring other possibilities using remote data to characterize vegetation and $E_{(t)}$. Reyes-Acosta and Lubczynski (2013) for example used high-resolution images to identify single trees to scale sap flow data to the stand level. Future research could focus on where and under which conditions tree characteristics control or describe .$E_{(t)}$ and whether this relation holds when scaling up to remote-sensing-derived data on different scales.

2.5 Conclusions

The aim of this study was to investigate the link between sap velocity and satellite-derived NDVI in a temperate forest catchment. We focussed on small-scale variability, in both space and time. A positive correlation between sap velocity and NDVI was expected. Data analysis for 2 consecutive years led us to the following conclusions.

a Temporally, a correlation between sap velocity and NDVI was only found when the entire growing season was considered. Spatially, a positive correlation was found in April, when spatial variability in sap velocity and NDVI was large and reflected an altitude-dependent difference in green-up. This means that NDVI did capture the spatial pattern in leaf-out which also affected sap velocity. During the rest of the growing season, a negative correlation was found between sap velocity and NDVI. This negative correlation was significant during half of the studied days. The likely saturation of the NDVI signal in combination with the small spatial variability in NDVI could explain the absence of a positive correlation, but does not explain this negative correlation.

b In 2015, during the dry summer period, the spatial correlation between sap velocity and NDVI changed. Variability in sap velocity could not be captured by NDVI. Instead, sap velocity was controlled by geology and aspect, likely through their effect on water availability. This shows that a stress factor, used to estimate transpiration during dry periods, cannot always be based on meteorology only, but should include information that reflects the water availability.

c The time-variable and inconsistent spatial correlation between sap velocity and NDVI would also translate into an inconsistent correlation between transpiration and NDVI. From this we conclude that NDVI alone cannot describe small-scale temporal and spatial variability in sap velocity and transpiration in a temperate forest ecosystem. Only for temporal scales that cover the whole phenological cycle was NDVI a significant predictor of transpiration processes. The EVI, which is less

sensitive to saturation effects, was also unsuitable as a predictor of transpiration under the studied conditions. Therefore, we suggest that the use of vegetation indices to predict transpiration should be limited to ecosystems and scales where the correlation was confirmed.

Chapter 3

The link between evaporation and the leaf area on global scale

This chapter is based on:

A. J. Hoek van Dijke, K. Mallick, M. Schlerf, M. Machwitz, M. Herold, and A. J. Teuling (2020). "Examining the link between vegetation leaf area and land–atmosphere exchange of water, energy, and carbon fluxes using FLUXNET data". *Biogeosciences* 17.17, 4443–4457. DOI: https://doi.org/10.5194/bg-17-4443-2020

Abstract

Vegetation regulates the exchange of water, energy, and carbon fluxes between the land and the atmosphere. This regulation of surface fluxes differs with vegetation type and climate, but the effect of vegetation on surface fluxes is not well understood. A better knowledge of how and when vegetation influences surface fluxes could improve climate models and the extrapolation of ground-based water, energy, and carbon fluxes. We aim to study the link between vegetation and surface fluxes by combining the yearly average MODIS leaf area index (LAI) with flux tower measurements of water (latent heat), energy (sensible heat), and carbon (gross primary productivity and net ecosystem exchange). We show that the correlation of the LAI with water and energy fluxes depends on the vegetation type and aridity. Under water-limited conditions, the link between the LAI and the water and energy fluxes is strong, which is in line with a strong stomatal or vegetation control found in earlier studies. In energy-limited forest we found no link between the LAI and water and energy fluxes. In contrast to water and energy fluxes, we found a strong spatial correlation between the LAI and gross primary productivity that was independent of vegetation type and aridity. This study provides insight into the link between vegetation and surface fluxes. It indicates that for modelling or extrapolating surface fluxes, the LAI can be useful in savanna and grassland, but it is only of limited use in deciduous broadleaf forest and evergreen needleleaf forest to model variability in water and energy fluxes.

3.1 Introduction

Vegetation and water, energy, and carbon fluxes are tightly coupled. Large-scale vegetation patterns are driven by the long-term memory of water and energy availability (Cramer et al., 2001; Köppen, 1936; Prentice et al., 1992). Recent climate change has led to shifts in the spatial distribution of vegetation as well as shifts in the timing of the growing season (Fei et al., 2017; Jeong et al., 2011; Rosenzweig et al., 2008). Additionally, vegetation plays a crucial role in the exchange of water, energy, and carbon between the land surface and the atmosphere, mainly through its effects on evaporation, turbulence, the redistribution of water, and surface heating (Esau and Lyons, 2002; Jia et al., 2014; Shao et al., 2015). Large-scale reforestation and afforestation has increased evaporation over most of Europe (Teuling et al., 2019), and large-scale deforestation has increased the air temperature in tropical regions and decreased air temperature in boreal regions (Perugini et al., 2017). This two-way interaction between vegetation and terrestrial surface fluxes has been known for a long time (e.g. Bates and Henry, 1928; Woodwell et al., 1978), but it is still a very relevant research topic today (Evaristo and McDonnell, 2019; Forkel et al., 2019; Kirchner et al., 2020; Lu et al., 2019; Teuling and Hoek van Dijke, 2020) given the importance of understanding the impacts of climate change on vegetation as well as the effects of land cover change on climate.

Plants regulate the exchange of water, energy, and carbon with the atmosphere through their stomata. The stomatal regulation of these fluxes depends on available energy, the transpiration demand, and the available soil moisture in the root zone. When both the available energy and soil moisture are abundant, stomata open and water and carbon can freely move in and out: the stomatal control on surface fluxes is low. When the available energy is high but soil moisture is limiting, stomata tend to close and exert a large control on water and carbon fluxes (Mallick et al., 2016; O'Toole and Cruz, 1980). Zooming out from the stomatal to canopy scale, there are several other ways in which vegetation influences surface fluxes. Soil and crown mutual shadowing and deep ground water uptake by vegetation influence the latent heat flux, whereas soil moisture influences ecosystem respiration and, in turn, carbon exchange (Chen et al., 2019; Schmitt et al., 2010). The vegetation control of ecosystem fluxes has been shown by different data or modelling studies and depends on the climate and vegetation type (Wagle et al., 2015; Williams et al., 2012; Xu et al., 2013). Williams and Torn (2015) found a strong vegetation control on surface heat flux partitioning in both arid and humid grassland, cropland, and forest, but Padrón et al. (2017) concluded that, globally, vegetation control on evaporation was low or even absent in the equatorial regions. Chen et al. (2019) showed that temperature, precipitation, and vegetation leaf area explained 91% of the mean annual variability in vegetation carbon uptake for wetland sites. Mallick et al. (2018) showed that vegetation control on evaporation was stronger in arid ecosystems compared with the mesic ecosystems. Similar results were found for dry and wet Amazonian forest (Costa et al., 2010; Mallick et al.,

2016) and dry and wet grassland (De Kauwe et al., 2017). Ferguson et al. (2012) studied land– atmosphere coupling of fluxes, which includes the effect of vegetation as well as other factors such as soil wetness, soil texture, and surface temperature. From remote sensing data and model output, they concluded that transitional zones between arid and humid climates (shrublands, grasslands, and savannas) tend to have a strong land–atmosphere coupling, whereas land–atmosphere coupling is weak in the energy-limited regions.

Vegetation is coupled to the atmosphere through its leaves. The leaf area index (LAI) is an important vegetation characteristic and is indicative of the total amount of foliage that intercepts light and assimilates carbon. Furthermore, both rainfall interception and canopy conductance increase with the LAI (Gómez et al., 2001; Van Heerwaarden and Teuling, 2014). Therefore, a high LAI is related to high vegetation carbon uptake and high canopy evaporation of water (Duursma et al., 2009; Lindroth et al., 2008). The highest mean yearly LAI is found in tropical and temperate forests, whereas a low LAI is found in cold and in arid climate zones (Fig. 3.1; Asner et al., 2003; Iio et al., 2014). This global LAI pattern closely resembles large-scale patterns in estimates of water, energy, and carbon exchange (Jung et al., 2011b; Miralles et al., 2011). With the increasing availability of remotely sensed LAI data, the LAI – in addition to its usage in many remote sensing applications (e.g. Si et al., 2012; Zheng and Moskal, 2009) – has become a frequently used variable to represent vegetation in land surface models(Lawrence and Chase, 2010; Sellers et al., 1997; Williams et al., 2016, amongst many others) or to estimate or extrapolate regional or global water and carbon fluxes (Beer et al., 2007; Turner et al., 2003; Xie et al., 2019; Yan et al., 2012). The algorithms to retrieve the LAI from remotely sensed data have improved over the past few decades, thereby increasing the accuracy of LAI products (Shabanov et al., 2005; Yan et al., 2016). Nevertheless, it is important to be aware of the product uncertainties, especially over dense forest, where saturated reflectance and canopy clumping can only provide limited information for LAI retrievals (Shabanov et al., 2005; Xu et al., 2018), and at high latitudes, where the solar zenith angle is low (Fang et al., 2019).

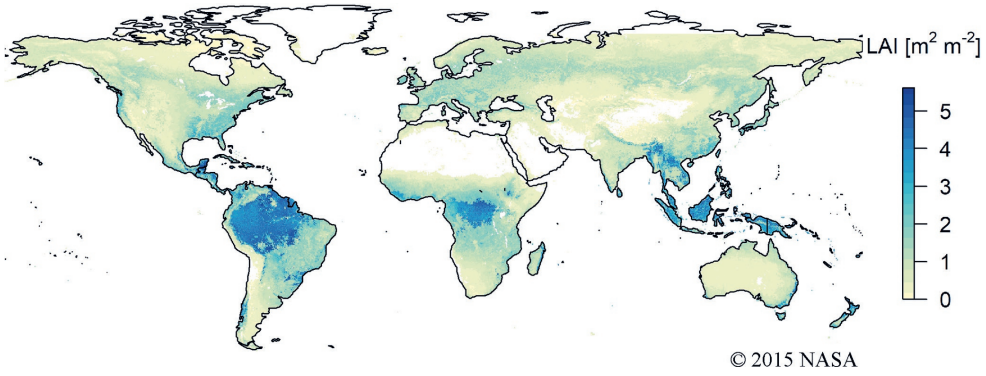

Figure 3.1: Global distribution of vegetation leaf area index (LAI). The mean LAI, at 5 km resolution, is derived from the MODIS data product MCD15A3H.006 (Myneni et al., 2015).

The interaction between the vegetation LAI and surface fluxes on the larger scale is not yet well understood, and vegetation is not well represented in many land–atmosphere and climate models (Williams et al., 2016). A small-scale study in temperate deciduous forest, for instance, revealed that the correlation between sap flow and the normalized difference vegetation index (NDVI) can change from positive to negative depending on the season and soil moisture availability (Hoek van Dijke et al., 2019). A detailed knowledge of how and when the vegetation LAI is linked to the surface fluxes is required to improve global climate modelling and extrapolation of water and carbon fluxes from canopy to ecosystems. The high availability of remote sensing LAI products, recent developments in cloud-based platforms for geospatial analysis (Mutanga and Kumar, 2019), and the availability of publicly available eddy covariance data from FLUXNET (Baldocchi et al., 2001) allows for an analysis of the link between vegetation characteristics and surface fluxes. Thus, the objective of our study is to gain insight into the link between the vegetation LAI and surface fluxes for different vegetation types along an aridity gradient. We address the following research questions:

1. What is the link between LAI and respective water, energy, and carbon fluxes in different vegetation types?

2. How is the interaction between LAI and respective water, energy, and carbon fluxes governed by climatological aridity?

We hypothesize that the link between the LAI and surface fluxes is strong in semi-arid and arid climates, owing to the strong stomatal control, whereas the link is weak in humid climates.

In our study we focus on five metrics of water, energy, and carbon fluxes measured by flux towers. Latent heat (LE), a measure for the evaporation of water, and sensible heat

(H), represent the exchange of water and energy between the Earth's surface and the atmosphere. LE and H are linked through the evaporative fraction (EF). The EF is the ratio of latent heat to the sum of LE and H and is a useful measure of the partitioning of total available energy between the evaporation of water and surface heating. Net ecosystem exchange (NEE) is the net exchange of carbon between the land and the atmosphere, which is directly measured by flux towers. Gross primary productivity (GPP) is derived from the NEE and is the gross uptake of atmospheric carbon by the vegetation.

3.2 Data and methodology

3.2.1 Data

This study includes five vegetation types: savanna (SAV), grassland (GRA), deciduous broadleaf forest (DBF), evergreen broadleaf forest (EBF), and evergreen needleleaf forest (ENF). The SAV sites include the two classes "savanna" and "woody savanna". These vegetation types follow the International Geosphere-Biosphere Programme (IGBP) classification (Loveland et al., 2000). These five vegetation types were selected because of the availability of a high number of flux tower sites. For some "site-years" (a term used to refer to the yearly averaged values for every site), the LAI flux or meteorological measurements were not available. These site-years were included in each of the analyses for which the required metrics were available.

Within the FLUXNET2015 dataset (Baldocchi et al., 2001), we selected all Tier 1 sites (open and free for scientific purposes; Pastorello et al., 2020) within the five studied vegetation types. We completed the dataset with two sites from the OzFlux network to increase the number of sites in the EBF class (Liddell, 2013a; Liddell, 2013b). Two forest sites were excluded from the analyses because they were affected by a beetle outbreak that resulted in high tree mortality, and one heavily managed grassland site was excluded from the analysis. For each site, only years with good-quality data were selected; this was carried out following the quality selection procedure explained below. This site selection procedure, in combination with the quality check, resulted in a dataset of 545 site-years spread over 93 sites (Fig. 3.2, Table 3.1).

Figure 3.2: Location and vegetation type of the 93 included flux tower sites.

3.2.2 Data averaging and aggregation

We studied the yearly averaged LAI and surface fluxes for different vegetation types. For most vegetation types, the LAI and surface fluxes showed seasonal variability, with high values during the growing season and lower or zero LAI and surface fluxes during the cold or dry season. The non-growing season might not be relevant for finding the link between the LAI and surface fluxes, but selecting growing season values alone led to difficulties. The vegetation types differ with respect to the timing, number, and length of the growing seasons, and procedures such as time-series analysis did not successfully select the growing seasons. To be consistent in the methodology, yearly averaged fluxes were used for all flux tower sites. Using yearly averaged values for every site (site-years) has a few implications: (1) we study both spatial (site-to-site) variability and temporal (year-to-year) variability simultaneously, and (2) the averaged flux and meteorological measurements might not represent similar conditions. The latter occurs, for example, when a site-year receives plenty of precipitation in December, increasing the site-year's aridity index, while this precipitation mainly impacts the next site-year's fluxes or LAI values. To test the effect of using site-year data, we also studied spatial and temporal variability separately. For these analyses, the data were aggregated in three ways: (1) site-year data with one average value per site per year; (2) multi-year data with one multi-year average LAI and flux value per site, which were used to study the spatial correlation; and (3) yearly average data for a few sites, which were used to study the temporal correlation. Sites were included in the multi-year data if at least 3 years of data were available. The three aggregation methods led to similar conclusions for water and energy but slightly different results for carbon, as is shown in the paper.

3.2.3 Flux measurements

Within the FLUXNET2015 database, LE, H, NEE, and GPP measurements are gap-filled using the MDS (marginal distribution sampling) method (Reichstein et al., 2005), and LE

Table 3.1: A list of all included site-years for the 93 sites. For each site, the yearly average leaf area index (LAI) and aridity index (AI) are calculated for all years included in the dataset. Studied vegetation types include the following: savanna (SAV), woody savanna (woody SAV; savanna and woody savanna sites are combined into one class, "savanna"), grassland (GRA) deciduous broadleaf forest (DBF), evergreen broadleaf forest (EBF), and evergreen needleleaf forest (ENF).

FLUXNET-ID	Country	Years included	mean LAI	mean AI	Vegetation	DOI
AT-Neu	Austria	2002-2012	2.31	1.78	GRA	10.18140/FLX/1440121
AU-Ade	Australia	2008	1.19	0.96	Woody SAV	10.18140/FLX/1440193
AU-Cow	Australia	2009-2018	5.78	3.83	EBF	102.100.100/14244
AU-Cpr	Australia	2011-2013	0.47	0.29	SAV	10.18140/FLX/1440195
AU-Ctr	Australia	2010-2018	5.39	3.80	EBF	102.100.100/14242
AU-Cum	Australia	2013-2014	1.34	0.49	EBF	10.18140/FLX/1440196
AU-DaP	Australia	2008, 2010	1.71	1.11	GRA	10.18140/FLX/1440123
AU-DaS	Australia	2008-2010, 2012-2014	1.34	0.87	SAV	10.18140/FLX/1440122
AU-Dry	Australia	2012, 2014	1.26	0.52	Woody SAV	10.18140/FLX/1440197
AU-Emr	Australia	2012, 2013	0.76	0.51	GRA	10.18140/FLX/1440198
AU-Gin	Australia	2014	0.96	0.34	Woody SAV	10.18140/FLX/1440199
AU-GWW	Australia	2013	0.37	-	SAV	10.18140/FLX/1440200
AU-How	Australia	2003, 2008, 2010-2014	1.83	1.09	Woody SAV	10.18140/FLX/1440125
AU-Rig	Australia	2011-2012, 2014	1.56	0.47	GRA	10.18140/FLX/1440202
AU-Rob	Australia	2014	5.82	1.43	EBF	10.18140/FLX/1440203
AU-Stp	Australia	2010, 2012, 2014	0.52	0.53	GRA	10.18140/FLX/1440204
AU-Tum	Australia	2002-2003, 2005-2009, 2011, 2013-2014	4.62	0.97	EBF	10.18140/FLX/1440126
AU-Whr	Australia	2012-2014	1.12	0.34	EBF	10.18140/FLX/1440206
AU-Wom	Australia	2011-2012	5.10	1.07	EBF	10.18140/FLX/1440207
AU-Ync	Australia	2013	0.45	0.58	GRA	10.18140/FLX/1440208
BR-Sa3	Brazil	2001-2003	5.94	0.96	EBF	10.18140/FLX/1440033
CA-Man	Canada	1995, 2001	1.07	0.64	ENF	10.18140/FLX/1440035
CA-NS1	Canada	2003-2004	1.10	-	ENF	10.18140/FLX/1440036
CA-NS3	Canada	2002-2004	0.75	-	ENF	10.18140/FLX/1440038
CA-NS5	Canada	2004	1.10	0.48	ENF	10.18140/FLX/1440040
CA-NS6	Canada	2002-2004	0.76	0.49	ENF	10.18140/FLX/1440041
CA-NS7	Canada	2003-2004	0.32	0.66	ENF	10.18140/FLX/1440042
CA-Qfo	Canada	2004-2009	0.87	1.82	ENF	10.18140/FLX/1440045
CA-SF1	Canada	2004-2005	1.34	1.08	ENF	10.18140/FLX/1440046
CA-SF2	Canada	2003-2004	1.06	0.73	ENF	10.18140/FLX/1440047
CA-SF3	Canada	2003-2005	0.66	0.98	ENF	10.18140/FLX/1440048
CH-DAV	Switzerland	1997, 1999-2004, 2006-2014	0.94	1.46	ENF	10.18140/FLX/1440132
CH-Fru	Switzerland	2007-2008, 2011-2014	1.88	2.67	GRA	10.18140/FLX/1440133
CH-Oe1	Switzerland	2005-2008	1.27	2.41	GRA	10.18140/FLX/1440135
CN-Cng	China	2008-2009	0.41	0.75	GRA	10.18140/FLX/1440209
CN-Dan	China	2004-2005	0.11	1.14	GRA	10.18140/FLX/1440138
CN-Din	China	2003, 2005	3.30	1.49	EBF	10.18140/FLX/1440139
CN-Du2	China	2007-2008	0.45	0.52	GRA	10.18140/FLX/1440140
CN-HaM	China	2003-2004	0.41	1.21	GRA	10.18140/FLX/1440190
CN-Qia	China	2003-2005	2.95	1.30	ENF	10.18140/FLX/1440141
CN-Sw2	China	2011	0.25	0.32	GRA	10.18140/FLX/1440212
DE-Gri	Germany	2004-2010, 2012-2014	2.40	1.93	GRA	10.18140/FLX/1440147
DE-Hai	Germany	2000-2009, 2011-2012	2.65	1.60	DBF	10.18140/FLX/1440148
DE-Lkb	Germany	2011-2012	0.84	2.53	ENF	10.18140/FLX/1440214
DE-Obe	Germany	2009-2014	2.47	1.96	ENF	10.18140/FLX/1440151
DE-RuR	Germany	2012-2014	2.58	1.97	GRA	10.18140/FLX/1440215
DE-Tha	Germany	1997-2014	2.59	1.53	ENF	10.18140/FLX/1440152
DK-Sor	Denmark	1997-2004, 2006-2010, 2012	2.30	1.93	DBF	10.18140/FLX/1440155
FI-Hyy	Finland	1997-1999, 2001-2014	1.79	1.44	ENF	10.18140/FLX/1440158
FI-Sod	Finland	2003-2011, 2013-2014	0.56	2.27	ENF	10.18140/FLX/1440160
FR-Fon	France	2006-2013	2.67	1.10	DBF	10.18140/FLX/1440161
FR-LBr	France	1998, 2001-2008	1.61	0.88	ENF	10.18140/FLX/1440163
FR-Pue	France	2001-2010, 2013-2014	2.02	1.20	EBF	10.18140/FLX/1440164
GF-Guy	French Guiana	2004, 2006-2014	5.24	1.89	EBF	10.18140/FLX/1440165
IT-CA1	Italy	2012, 2014	1.23	-	DBF	10.18140/FLX/1440230
IT-CA3	Italy	2012, 2013	1.16	1.03	DBF	10.18140/FLX/1440232
IT-Col	Italy	2007, 2009, 2011, 2014	2.32	1.53	DBF	10.18140/FLX/1440167
IT_Cp2	Italy	2013	3.84	0.93	EBF	10.18140/FLX/1440233
IT_Cpz	Italy	2003, 2006, 2007	3.12	0.89	EBF	10.18140/FLX/1440168
IT_Isp	Italy	2013, 2014	1.66	2.41	DBF	10.18140/FLX/1440234
IT_Lav	Italy	2003-2013	2.55	1.74	ENF	10.18140/FLX/1440169
IT_MBO	Italy	2003-2013	1.16	2.41	GRA	10.18140/FLX/1440170
IT_PT1	Italy	2003	0.81	0.77	DBF	10.18140/FLX/1440172
IT_Ren	Italy	2003, 2005-2013	1.53	1.60	ENF	10.18140/FLX/1440173
IT_Ro1	Italy	2002-2006	-	0.91	DBF	10.18140/FLX/1440174
IT_Ro2	Italy	2002-2007, 2012	1.99	0.83	DBF	10.18140/FLX/1440175
IT_SR2	Italy	2013	2.12	1.38	ENF	10.18140/FLX/1440236
IT_SRo	Italy	1999-2004, 2006-2007, 2009, 2012	2.05	0.70	ENF	10.18140/FLX/1440176
IT_Tor	Italy	2010-2014	0.98	2.54	GRA	10.18140/FLX/1440237
NL_Hor	Netherlands	2004-2005, 2007-2008, 2010	1.81	2.01	GRA	10.18140/FLX/1440177
NL_Loo	Netherlands	1996-1997, 2000-2013	2.09	1.20	ENF	10.18140/FLX/1440178
RU_Fyo	Russia	1999-2014	2.09	1.19	ENF	10.18140/FLX/1440183
SD_Dem	Sudan	2008	0.34	0.12	SAV	10.18140/FLX/1440186
SN_Dhr	Senegal	2012	0.61	0.27	SAV	10.18140/FLX/1440246

Table 3.1 continued

US_AR1	United States	2010-2011	0.57	0.68	GRA	10.18140/FLX/1440103
US_AR2	United States	2010-2011	0.54	0.59	GRA	10.18140/FLX/1440104
US_Blo	United States	2000-2006	1.94	1.26	ENF	10.18140/FLX/1440068
US_Ha1	United States	1992, 1994-2001, 2004, 2006, 2009, 2011	2.58	1.91	DBF	10.18140/FLX/1440071
US_Me2	United States	2002, 2004-2005, 2007, 2009-2010, 2012-2014	1.97	0.65	ENF	10.18140/FLX/1440079
US_Me6	United States	2014	0.82	-	ENF	10.18140/FLX/1440099
US_MMS	United States	1999-2014	2.71	1.28	DBF	10.18140/FLX/1440083
US_NR1	United States	1999-2014	1.32	1.02	ENF	10.18140/FLX/1440087
US_Prr	United States	2011	-	0.92	ENF	10.18140/FLX/1440113
US_SRG	United States	2009-2014	0.41	0.42	GRA	10.18140/FLX/1440114
US_SRM	United States	2004-2014	0.35	0.31	Woody SAV	10.18140/FLX/1440090
US_Ton	United States	2002-2006, 2008-2014	1.02	0.50	Woody SAV	10.18140/FLX/1440092
US_UMB	United States	2000-2014	2.14	0.95	DBF	10.18140/FLX/1440093
US_UMd	United States	2008-2013	1.90	1.09	DBF	10.18140/FLX/1440101
US_Var	United States	2001-2004, 2006-2014	1.07	0.70	GRA	10.18140/FLX/1440094
US_WCr	United States	2000-2003, 2005, 2011, 2013-2014	2.00	1.40	DBF	10.18140/FLX/1440095
US_Wkg	United States	2005-2014	0.28	0.35	GRA	10.18140/FLX/1440096
ZA_Kru	South Africa	2002, 2010	1.08	0.38	SAV	10.18140/FLX/1440188
ZM_Mon	Zambia	2008	1.62	0.49	DBF	10.18140/FLX/1440189

and H are corrected by an energy balance closure correction factor. The MDS method uses the correlation of fluxes with the driver variables (incoming radiation, temperature, and vapour pressure deficit) to estimate flux values during gap periods. The energy balance closure corrects LE and H for the total incoming radiation, assuming that the Bowen ratio (the ratio of the sensible heat flux to the latent heat flux) is correct. A similar energy balance closure correction was applied to the LE and H measurements of the OzFlux sites. Monthly averaged flux values were discarded if the percentage of measured and good-quality gap-fill data was below 50 %. Yearly average fluxes were calculated if measurements for each month were available. The evaporative fraction (EF), the ratio between LE and the total energy available at Earth's surface, was calculated using Eq. 3.1 as follows:

$$EF = \frac{LE}{LE + H} \tag{3.1}$$

where LE is the latent heat flux and H is the sensible heat flux.

3.2.4 Meteorological measurements

Meteorological measurements are delivered with the flux tower data. Precipitation data are downscaled from the ERAInterim reanalysis data (Vuichard and Papale, 2015). Net radiation and air temperature are measured at the flux tower and gap-filled using the MDS method (Reichstein et al., 2005). Yearly potential evaporation (E_p) was calculated from mean daily air temperature and net radiation using the Priestley–Taylor formulation (Priestley and Taylor, 1972). The Priestley–Taylor equation is a modification of the Penman equation and requires less measurements. The aridity index (AI), an indicator of dryness, was calculated according to Eq. 3.2:

$$AI = \frac{P}{E_p} \tag{3.2}$$

where P is precipitation and E_p is the potential evaporation. An aridity value of one indicates that, on a yearly scale, precipitation equals potential evaporation, whereas values below one indicate site-years that received less precipitation than their potential evaporation.

3.2.5 Leaf area index

The leaf area index (LAI) is the ratio of green leaf area to ground area (unitless). We used the LAI derived from the MODIS data product MCD15A3H.006 (Myneni et al., 2015). This algorithm derives 4 d composite LAI values at a 500 m spatial resolution from the Terra and Aqua satellites and is available for 2003 onwards.Within this 4 d period, the best pixel is selected from the MODIS sensors located on the Terra and Aqua satellite for the calculation of the LAI. The LAI calculation algorithm uses a lookup table that was generated using a 3D radiative transfer equation (Myneni et al., 2015). Heinsch et al. (2006) compared the MODIS data product with ground measurements at FLUXNET sites and concluded that 62.5 % of the MODIS LAI was well estimated but that MODIS LAI overestimated ground-measured LAI for the other sites. Despite this overestimation, MODIS LAI was used because it has a long record length, good (and free) data availability, good spatial coverage, and high temporal resolution. The overestimation and saturation of the signal at high LAI could introduce noise in the LAI data. However, we do not expect this noise to change the conclusions of our analysis. The resolution of the LAI data product is 500 m, compared with a typical flux tower footprint length of 100 to 1000 m (Kim et al., 2006). The exact size and location of the footprint of flux towers, however, varies with factors such as wind direction and wind speed, surface roughness, and flux measurement height (Barcza et al., 2009; Kim et al., 2006). For our analyses, we selected the one nearest LAI pixel for each flux tower. Data were filtered to remove clouds, using the product's delivered quality label. To smoothen outliers, the moving mean LAI was calculated for three consecutive data points. Monthly mean values were calculated if a maximum of one data point was missing. The site-year average LAI was calculated when no monthly data were missing.

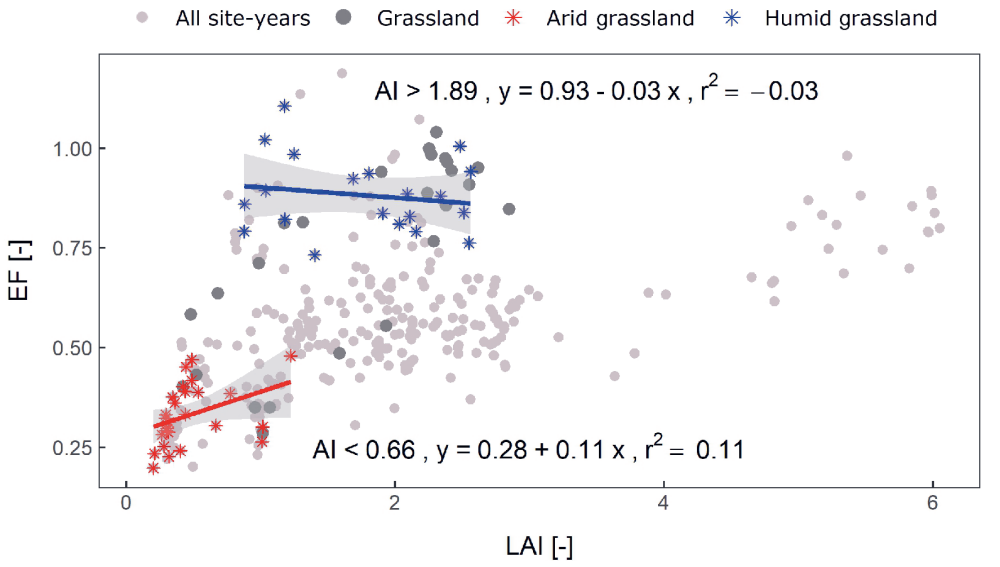

Figure 3.3: Illustration of the applied methodology. The correlation coefficient between leaf area index (LAI) and evaporative fraction (EF) is calculated for 30 site-years for grassland over a moving window of aridity index. In the illustration, the correlation has a significant positive slope at $p = 0.056$ for the 30 most arid grassland sites, whereas the slope is nearly flat and is not significant ($p = 0.49$) for the 30 most humid grassland sites

3.2.6 Methodology

To study the link between the LAI and surface fluxes, we performed a linear regression between the LAI and the surface fluxes. We calculated the correlation coefficient for (1) site-year data, (2) multi-year average data (spatial variability), and (3) yearly data for a few specific sites (temporal variability). Afterwards, to study if the link between the LAI and fluxes changed with aridity, all site-years within one vegetation type were ranked by aridity, from most arid to most humid. For each consecutive 30 site-years in this ranking, we performed a linear regression between the LAI and the fluxes. For some site-years, part of the data was missing that was needed to calculate the regression. Within each window of 30 site-years, the slope of the regression was calculated if at least 15 complete site-years were available (Fig. 3.3).

3.3 Results

3.3.1 The link between LAI and the respective water, energy, and carbon fluxes

LAI and LE were positively correlated in SAV, GRA, and EBF (Fig. 3.4, Table 3.2). The slope of the correlation between the different vegetation types is different; the slope was steepest for SAV (slope = $46.1\,\mathrm{W\,m^{-2}}$): a twofold increase in the LAI ($1-2$) was associated with an almost twofold increase in LE ($51-97\,\mathrm{W\,m^{-2}}$), compared with a flatter slope in GRA ($9.8\,\mathrm{W\,m^{-2}}$) and EBF ($13.0\,\mathrm{W\,m^{-2}}$). In ENF and DBF, the LAI and LE were not significantly correlated. LAI and H were negatively correlated in SAV, GRA, and EBF, whereas there was no significant correlation in ENF and DBF. The LAI and the EF were positively correlated in SAV, GRA, and EBF, whereas no correlation was found in ENF and DBF. A positive slope indicates that, for a higher LAI, a higher fraction of the available energy is used for the evaporation of water, compared with surface heating. The slope between the LAI and EF was steeper in SAV and GRA (slope = 0.27 for both) than in EBF (slope = 0.08). A positive correlation between LAI and GPP was found in all vegetation types ($r = 0.47-0.97$), with a very strong correlation coefficient for SAV ($r = 0.97$). The correlation followed a steep slope for SAV (slope = $3.37\,\mathrm{gC\,m^{-2}\ d^{-1}}$) and GRA (slope = $2.17\,\mathrm{gC\,m^{-2}\ d^{-1}}$) a similar slope in EBF (slope = $1.71\,\mathrm{gC\,m^{-2}\ d^{-1}}$) and ENF (slope = $1.81\,\mathrm{gC\,m^{-2}\ d^{-1}}$), and a less steep slope in DBF (slope = $0.76\,\mathrm{gC\,m^{-2}\ d^{-1}}$). The correlation between the LAI and NEE was negative in SAV, EBF, and ENF. This indicates that the net carbon uptake increases with the LAI. Among the different fluxes, GPP showed the strongest correlation with the LAI for all vegetation types. Comparing the different vegetation types, the correlation between the LAI and fluxes was strongest in SAV.

Using multi-year average data reduced the number of data points to only $5-16$ sites per vegetation type. Nevertheless, the spatial correlation (site-to-site variability) between the LAI and surface fluxes is very similar to the spatio-temporal correlation (Fig. 3.5, Table 3.2). For SAV, GRA, and ENF, the slope and strength of the correlation were similar when compared with the site-year data. For the EBF, for the site-year data, the correlation with LE and EF was only significant at $p \leq 0.1$, and the correlation was not significant for H and NEE.

Temporal (year-to-year) variability in LAI and surface fluxes was smaller than spatial (site-to-site) variability (Figure 3.6). For both SAV sites, and one of the two GRA, EBF, and DBF sites, LAI and LE were positively correlated in time. For H, one EBF site showed a significant negative correlation with LAI, and for EF, and one of the two SAV, GRA, EBF, and DBF sites showed a positive correlation with LAI ($p \leq 0.1$ or $p \leq 0.05$). For GPP and NEE, one of the SAV, GRA, EBF, and ENF sites showed a positive correlation, and for NEE. Overall, the temporal correlations between LAI and surface fluxes was of

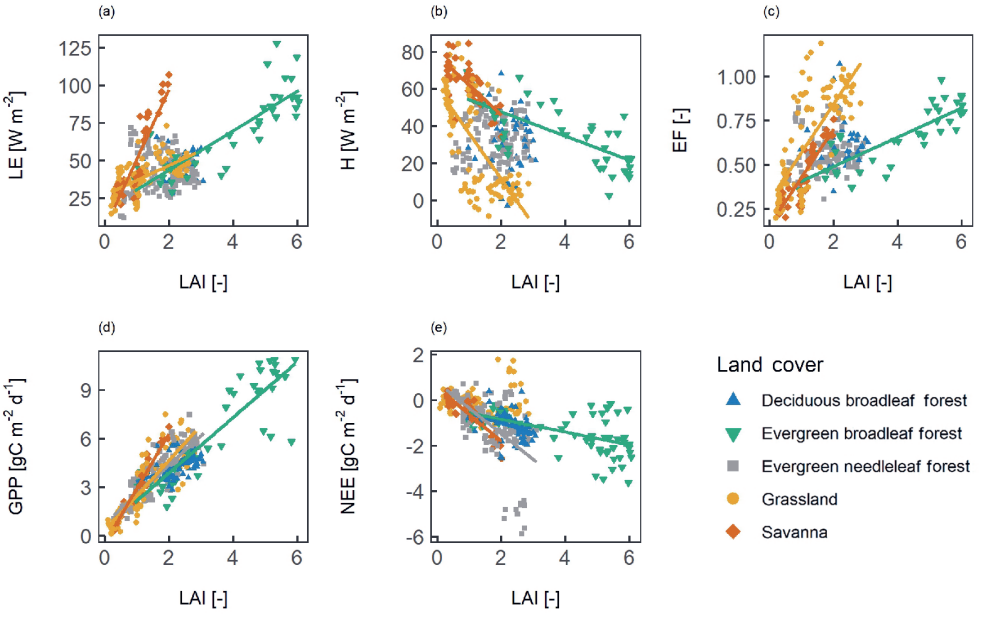

Figure 3.4: The spatio-temporal correlation between surface fluxes and leaf area index (LAI). Panels show (a) the latent heat flux (LE), (b) the sensible heat flux (H), (c) the evaporative fraction (EF), (d) gross primary productivity (GPP), and (e) net ecosystem exchange (NEE). A line indicates a significant correlation at $p < 0.05$.

similar direction as the spatio-temporal and spatial correlations. For more than half of the sites in Figure 3.6, however, year-to-year variability in LAI and surface fluxes was low and variability in fluxes was not significantly correlated with variability in the LAI.

3.3.2 The effect of climatological aridity on the link between LAI and surface fluxes

Figure 3.7 shows the steepness and significance of the correlation between the LAI and surface fluxes for different aridity values. In dry vegetation types or regions, the correlation between the LAI and fluxes was significant and had a steeper slope, whereas in the more humid vegetation types or regions, the slope was relatively horizontal and the correlation was often not significant. In SAV, GRA, and EBF, the correlation between the LAI and LE was significant for the whole range of aridity values. In arid GRA, the correlation had a steeper slope compared with humid GRA. With respect to the LAI versus H and LAI versus EF, the slope was steep and significant for SAV. For GRA, the correlation was strong and significant in the arid regions and insignificant in the humid regions. For EBF, the slope and the significance of the correlation did not change with aridity. For LAI and GPP, the slope and the significance of the correlation did not change with aridity

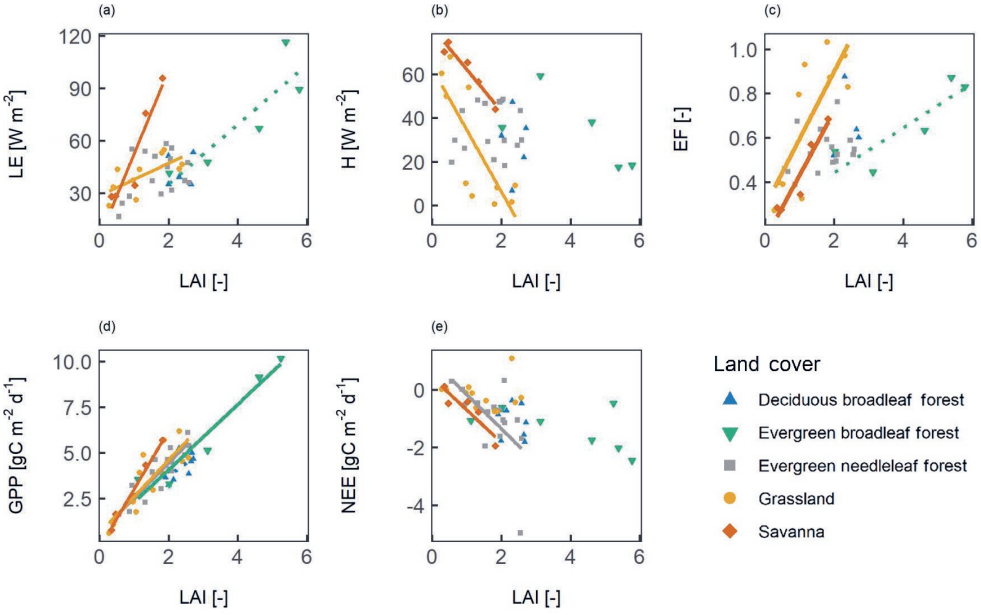

Figure 3.5: The spatial correlation between surface fluxes and the leaf area index (LAI). Panels show (a) the latent heat flux (LE), (b) the sensible heat flux (H), (c) the evaporative fraction (EF), (d) gross primary productivity (GPP), and (e) net ecosystem exchange (NEE). All sites are included that have at least 3 years of LAI and flux data available. A line indicates a significant correlation at $p < 0.05$, and a dashed line indicates a significant correlation at $p < 0.1$.

Table 3.2: Strength and significance of the correlation between the LAI and surface fluxes for site-year and multi-year average data. The correlation coefficients are shown for significant correlations at $* \; p \leq 0.05$ or at $** \; p \leq 0.1$. "–" indicates that the correlation was not significant.

	Site-years					Multi-year average				
	LE	H	EF	GPP	NEE	LE	H	EF	GPP	NEE
Savanna	0.88∗	−0.72∗	0.89∗	0.97∗	−0.89∗	0.94∗	−0.96∗	0.95∗	0.99∗	−0.90∗
Grassland	0.65∗	−0.71∗	0.74∗	0.86∗	-	0.68∗	−0.80∗	0.79∗	0.84∗	-
Evergreen Broadleaf Forest	0.84∗	−0.69∗	0.83∗	0.88∗	−0.51∗	0.87 ∗∗	-	0.87 ∗∗	0.96∗	-
Evergreen Needleleaf Forest	-	-	-	0.84∗	−0.58∗	-	-	-	0.89∗	−0.57∗
Deciduous Broadleaf Forest	-	-	-	0.47∗	−0.33∗	-	-	-	0.65 ∗∗	-

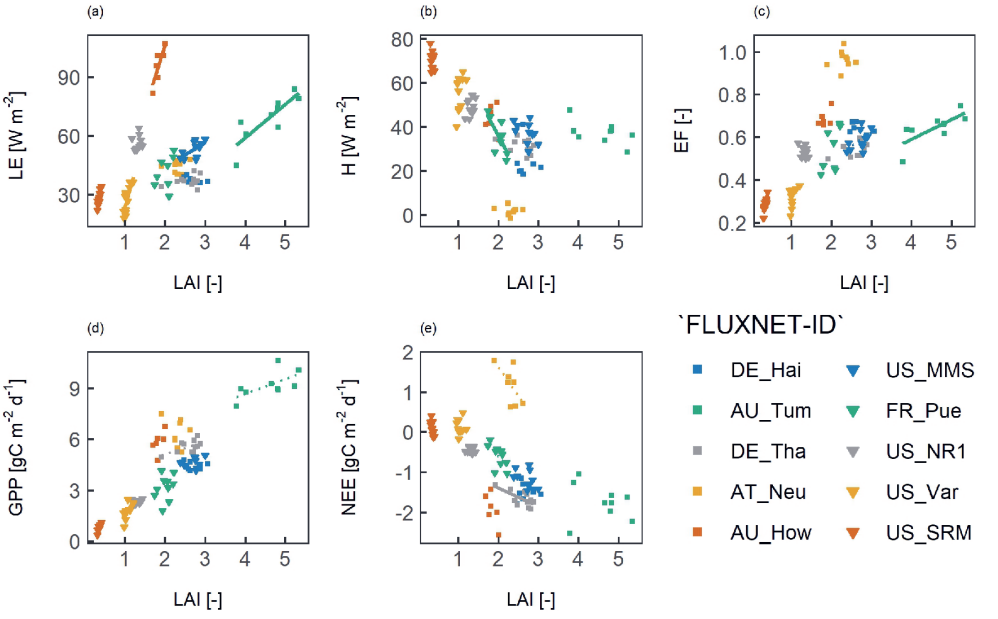

Figure 3.6: An illustration of the temporal correlation between the yearly average surface fluxes and the leaf area index (LAI). For each land cover type, two sites were selected that had the highest number of available data. The colours of the symbols indicate the land cover type as shown in Figs. 3.4 and 3.5. Panels show (a) the latent heat flux (LE), (b) the sensible heat flux (H), (c) the evaporative fraction (EF), (d) gross primary productivity (GPP), and (e) net ecosystem exchange (NEE). A line indicates a significant correlation at $p < 0.05$, and a dashed line indicates a significant correlation at $p < 0.1$.

for SAV, GRA, EBF, and ENF. For DBF, the correlation between the LAI and GPP was negative at higher aridity, but these results were strongly influenced by one site with an above average LAI for all site-years. For the LAI versus NEE, a steep slope with a negative correlation was found in arid SAV and humid ENF. In other humid regions, the correlation was less steep.

To study how the correlations varied with climatic drivers of surface fluxes, we calculated the correlation coefficient of the fluxes versus precipitation (P) and incoming shortwave radiation (R_g) (Fig. 3.8). In SAV, GRA, and EBF, the water fluxes showed a strong correlation with P, indicating that water availability partly explained the spatio-temporal variability in surface fluxes. In ENF and DBF, there was a weak or non-existing correlation between LE and P, but there was a strong correlation with R_g. This indicates that available radiation was the primary driver of water and energy fluxes at these sites.

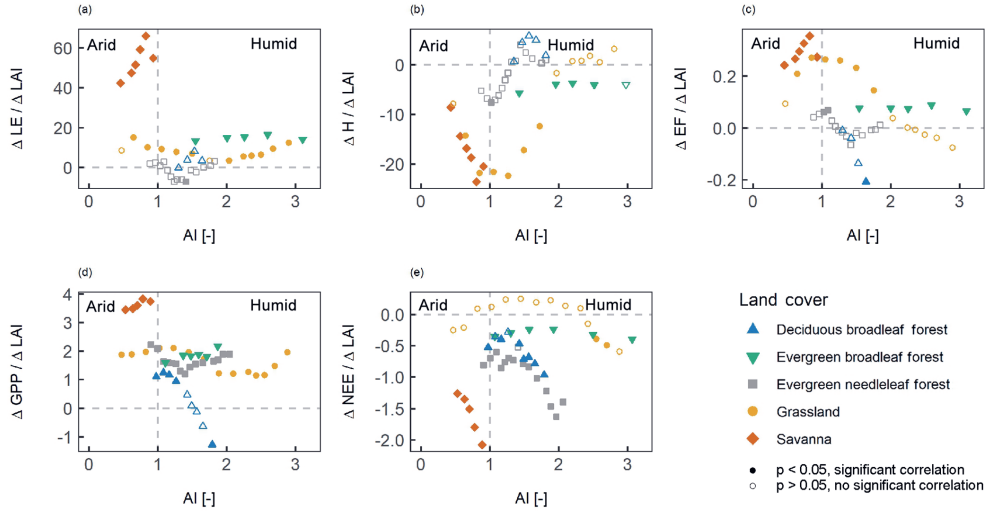

Figure 3.7: The effect of aridity on the relation between surface fluxes and the leaf area index (LAI). The slope of the correlation between the LAI and surface fluxes is shown for different aridity values for (a) the latent heat flux (LE), (b) the sensible heat flux (H), (c) the evaporative fraction (EF), (d) gross primary productivity (GPP), and (e) net ecosystem exchange (NEE). Each dot indicates the slope value for the 30 closest aridity values. The filled symbols indicate that the correlation was significant at $p < 0.05$, whereas the hollow symbols indicate a non-significant correlation.

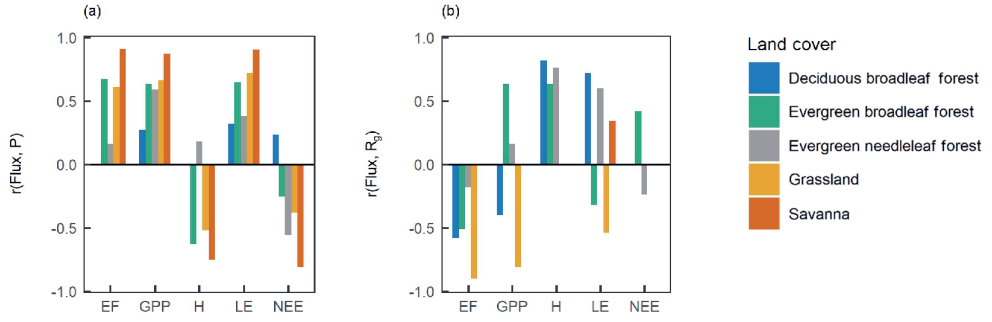

Figure 3.8: Water and energy control on surface fluxes. The correlation coefficient (r) of site-year surface fluxes versus (a) the mean yearly precipitation (P) and (b) incoming shortwave radiation (R_g). Each bar indicates a significant correlation at $p < 0.05$.

3.4 Discussion

The EBF site-years span a wide range of LAI values (LAI of 0.9–6.1) and aridity conditions (AI of 0.3–9.3), and both are a potential limitation of our analysis for the EBF vegetation type. The uncertainty of the LAI retrieval in dense vegetation is higher than in other vegetation types due to saturation of the remotely sensed signal. The large range of climatic conditions indicates that our EBF site-years range from arid, water-limited conditions to humid conditions. Despite this high variability in site-years, the sites fell within one vegetation type.

The correlation between the LAI and respective water and energy fluxes (LE, H, and EF) varied with vegetation type and aridity. For the spatio-temporal and spatial variability, we found (1) strong (positive or negative) correlations and (partly) steep slopes for SAV and GRA, (2) a significant correlation but less steep slope for EBF, and (3) no significant correlations for ENF and DBF. With respect to the temporal variability, this pattern was similar for LE, but almost no significant correlations were found between the LAI and the respective H and EF for SAV and GRA. Evaporation is the sum of transpiration, soil evaporation, and interception evaporation, and the magnitude of each component depends on the LAI. Transpiration increases with LAI at the cost of soil evaporation when there is sufficient moisture available (Gu et al., 2018; Wang et al., 2014). In arid climates, the transpiration component is higher than in wetter climates (Gu et al., 2018), and the link between transpiration and the LAI is particularly strong in these arid climates (Sun et al., 2019). When soil moisture is deficient and vegetation encounters a high evaporative demand, stomatal control is stronger (Mallick et al., 2016). This accelerates a strong stomatal coupling between the LAI and LE and could explain the strong correlation between the LAI and the respective LE, H, and EF that was found in SAV and arid GRA. Soil water deficiency and high evaporative demand leads to a high increase in LE, for a small increase in LAI, which could explain the steep(er) slope in arid GRA and SAV vegetation.

In forests, soil evaporation is low, whereas interception evaporation is high. The elevated interception evaporation is due to the large leaf area (both green leaves included in the LAI and brown leaves after leaf senescence) with a high canopy water storage capacity and a high turbulence, enhancing fast evaporation (De Jong and Jetten, 2007). In EBF, interception evaporation contributes to up to 30 % of the total evaporation (Gu et al., 2018; Wei et al., 2017b). This could explain the strong correlation between the LAI and the respective water and energy fluxes in EBF. A high interception evaporation was, however, also reported for temperate and boreal forest (Miralles et al., 2011); however, for the latter forest types, we found no correlation between the LAI and water and energy fluxes. The ENF and DBF sites were found in humid regions, and fluxes were primarily energy-limited. At these energy-limited sites, the LAI played a weak or nonexistent role in controlling surface fluxes. This indicates a weak or non-existent vegetation control on surface water

and energy fluxes at energy-limited sites. This is in line with a low land–atmosphere coupling at energy-limited sites (Ferguson et al., 2012).

In contrast to the results for water and energy fluxes, the spatio-temporal and spatial correlation between GPP and LAI was strong across all vegetation types and (almost) all aridity gradients. A strong link between the LAI and carbon uptake on a yearly timescale over all vegetation types is expected, as plants try to optimize carbon gain and would generally not display leaves with a negative carbon balance. A strong link between the LAI and the mean yearly GPP was also shown by Hashimoto et al. (2012). However, other studies found a weak link between the LAI and GPP on annual timescales (Law et al., 2002). In contrast to the spatial variability, year-to-year variability in GPP was only correlated with LAI at some sites. Water availability is an important driver of temporal variability in GPP (Kutsch et al., 2008; Williams and Albertson, 2004), and GPP is strongly reduced under drought conditions (Vicca et al., 2016). The effect of drought is also visible in the reduced LAI, although on a longer timescale of 1 or 2 years in forests (Kim et al., 2017; Le Dantec et al., 2000). This different response time to water availability for forest LAI and GPP could partly explain the absence of a temporal correlation for some of the sites. The spatial correlation between the LAI and NEE was less strong compared with the GPP, which is in agreement with the results of Chen et al. (2019). The NEE is the sum of carbon uptake by the vegetation (GPP) and carbon loss by ecosystem respiration. Ecosystem respiration varies with climate and soil carbon storage, which are not directly related to the LAI. This could explain the absence of a correlation between the LAI and NEE.

These results partly confirmed our hypothesis. As hypothesized, the correlation between the LAI and surface fluxes was strong in arid regions for water and energy fluxes, and the correlation was absent in humid ENF and DBF. For humid EBF, however, we found a strong correlation between the LAI and water and energy fluxes, and the correlation with the LAI was strong across all aridity gradients for GPP. While carbon uptake is the primary goal of vegetation, independent of the aridity gradient, ecosystem water loss inevitably comes with carbon uptake but also depends on the vapour pressure deficit, available radiation, and soil moisture, which are not directly linked to the LAI.

Our statistical analysis cannot be used to study causality between the LAI and surface fluxes or to study vegetation control on the surface fluxes. The correlation between the LAI and water fluxes is confounded by the effect of soil moisture, especially in arid and semi-arid ecosystems, where both canopy development and LE increase with water availability (Kergoat, 1998; Mallick et al., 2018). Similarly, precipitation is the main controller for spatial variability in both vegetation and GPP (Koster et al., 2014). Furthermore, the LAI is related to vegetation properties, but it is not a direct measure of canopy conductance; despite this, there are similarities, with previous studies showing the stomatal or vegetation control on surface fluxes. A strong vegetation control on water and energy fluxes in arid

and semi-arid regions has been shown on timescales of days or shorter (e.g. Mallick et al., 2016; Mallick et al., 2018); our study also shows that, on large spatio-temporal scale, the correlation between LAI and respective water and energy fluxes is strongest in arid regions. For EBF, however, we found a strong spatial correlation of vegetation versus the respective water and energy fluxes, whereas Padrón et al. (2017) showed that vegetation control in equatorial regions was absent. An interesting follow-up study would be to link stomatal control for different vegetation types (De Kauwe et al., 2017) to the canopy-scale pattern investigated in this study.

Our analyses provide insight into how and when the vegetation LAI is related to surface fluxes. The results show that the LAI is a good predictor of spatial variability in GPP across different vegetation types and aridity gradients. Furthermore, the analysis suggests that the LAI could be used to describe canopy-scale spatio-temporal variability in water and energy fluxes in SAV, GRA, and EBF. However, the LAI is not a good predictor for water and energy fluxes in ENF and DBF nor for NEE. It is important to be aware of these limitations when using the LAI to describe or estimate water, energy, and carbon fluxes in climate models or extrapolation methods. This study provides insight into the link between surface fluxes and the LAI and could be used to improve predictions of the effects of land cover change on surface fluxes.

3.5 Conclusions

The objective of this study was to gain insight into the link between the vegetation LAI and land–atmosphere fluxes for different vegetation types along an aridity gradient. We studied this link at a large spatio-temporal scale using flux tower measurements of water, energy, and carbon, combined with satellite-derived LAI data. The data analysis led to the following conclusions:

The link between the LAI and the respective water and energy fluxes depends on vegetation type and aridity. The correlation of the LAI with water and energy fluxes is strong in SAV, GRA, and EBF. In DBF and ENF, however, no significant correlation was found. Contrary to water and energy fluxes, the spatial correlation between the LAI and GPP was strong and independent of the vegetation type and aridity. This suggests that using the LAI to model or extrapolate surface fluxes of water and energy is very possible in SAV, GRA, and EBF, but it is limited in DBF and ENF.

As hypothesized, the link between the LAI and water and energy fluxes was strong in arid, water-limited conditions and was absent or weak for humid, radiation-limited conditions. EBF, which was found over a high range of aridity conditions, although mostly in humid environments, forms an exception: the spatial correlation between the LAI and the respective water and energy fluxes was strong, despite the overall humid conditions.

This research – facilitated by the recent availability of large global datasets of remotely sensed LAI, flux tower data, and cloud-computing platforms – has added to the understanding of the LAI interaction with surface fluxes and could help to improve modelling or extrapolating surface fluxes.

Chapter 4

Remote sensing of vegetation during the 2018 European drought

Abstract

Forest and grassland have a different drought coping strategy. Trees control their stomata to reduce water loss, while grasslands take the risk to lose their aboveground biomass. Both the increased stomatal control and reduction in green leaf area decrease the evaporation, through a reduction of the surface conductance. Here we study how remote sensing data reflected the reduction in surface conductance in forest and grassland during the 2018 Central European drought. For six study sites, surface conductance was derived from eddy covariance measurements. The surface conductance was combined with MODIS sensor derived optical and thermal infrared based indices: the LST, LST-Ta, TCI, NDMI, NDVI, and VCI. The results show that for grassland, all studied optical and thermal infrared indices were sensitive to the reduction in G_s. For the forest sites, the optical indices were not sensitive to the reduction in G_s, but the thermal infrared indices LST, LST-Ta, and TCI, were sensitive to the reduction in G_s. The results were however not uniform across all forest and grassland sites. The results indicate that a different strategy is required to monitor the effects of drought on the water, energy, and carbon cycle in grassland and forest.

4.1 Introduction

During the summer of 2018, Central and Northern Europe experienced drought and unusually hot weather (Peters et al., 2020). The exceptional sunny conditions in spring 2018 worsened the summer drought through enhanced evaporation of the residual soil moisture (Bastos et al., 2020). The drought led to a large-scale 'browndown' of the landscape due to early leaf senescence in grasslands, cropland, and forests (Brun et al., 2020; Buras et al., 2020; Peters et al., 2020). The drought resulted in large-scale tree mortality (Schuldt et al., 2020; Senf and Seidl, 2021), and multiple year legacy effects such as increased vulnerability of forests to wild fires and beetle outbreakes (Obladen et al., 2021; Schuldt et al., 2020; Senf and Seidl, 2021).

During a precipitation deficit, low soil moisture availability in the root zone in conjunction with a high atmospheric evaporative demand triggers vegetation reactions. The first obvious response to drought is expressed through strong stomatal regulation to reduce the root-zone water loss. Prolonged soil moisture drought can induce changes in the vegetation state, such as the leaf color, the leaf water content, and leaf turgor. When the drought conditions persist even longer, this can result in the defoliation of the vegetation and mortality. While the stomatal regulation is a rapid and reversible response, the effects on the vegetation state can be irreversible. Both the stomatal regulation and decrease in green leaf area decrease the surface conductance G_s (the aggregated stomatal conductances of the entire canopy) (Fig. 4.1). A decrease in G_s reduces evaporation and reduced evaporation reduces the downwind precipitation, increases in air temperature, and decreases the vegetation CO_2 uptake. The exact vegetation response to drought and impacts on the water, energy, and carbon balance, depends on the timing, intensity, and duration of the drought, as well as the species type (Hateren et al., 2021; Obladen et al., 2021).

In temperate climates, grasslands and forests respond differently to droughts because of their different drought coping strategies (Fig. 4.1). Grasslands take the risk to lose their aboveground biomass, while they survive belowground. Trees cannot take this risk and therefore adopt a more conservative behaviour. Trees increase their stomatal regulation and increase their water use efficiency to decrease water loss, while grasslands maintain high evaporation (Wolf et al., 2013). Grasslands however show an early senescence, while forests maintain high leaf area (Zha et al., 2010). Through these different strategies, grasslands and forests have a different impact on evaporation, precipitation, heat waves, and the carbon balance during drought (Graf et al., 2020; Pranindita et al., 2021b; Teuling et al., 2010; Vicca et al., 2016). Different adaptive strategies also exist between tree species, such as a stronger stomatal regulation for leaves versus needles (Wolf et al., 2013), or a higher sensitivity of Norway spruce to drought compared to pine because of their different rooting depths (Schuldt et al., 2020; Treml et al., 2022). Due to the conservative behaviour of trees, drought is not always directly reflected in the forests' appearance (Mallick et al.,

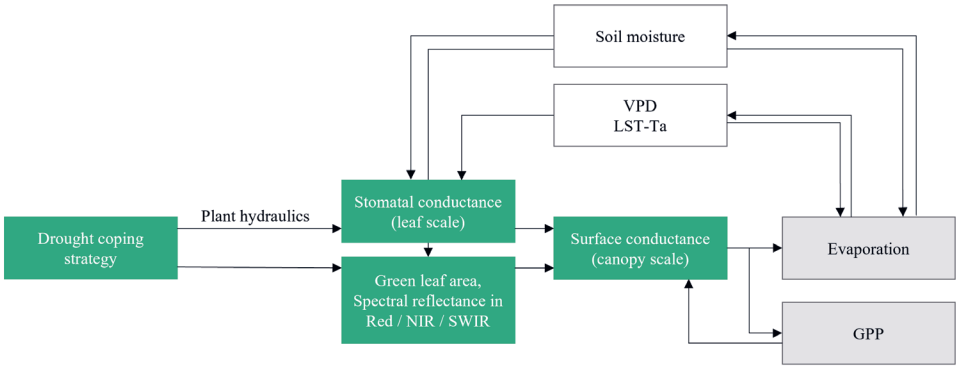

Figure 4.1: Diagram of the vegetation response to drought. Forest and grassland have a different drought coping strategy. Forests reduce their stomatal conductance through strong stomatal regulation, and grasslands decrease their green leaf area. Both decrease the surface conductance and evaporation.

2016), but, the effects are visible in the following years's growth and leaf area (Anderegg et al., 2015; Senf and Seidl, 2021).

Remotely sensing based drought monitoring methods use the optical and thermal infrared part of the electromagnetic spectrum. Optical remote sensing measures the reflection of solar radiation by the soil and the vegetation in the visible, near-infrared, and shortwave infrared wavelengths. The visible wavelengths ($0.4 - 0.7\,\mu m$) can be used to detect, amongst others, changes in leaf chlorophyll content and other leaf pigments, for example during vegetation browning. The near-infrared ($0.7 - 1.4\,\mu m$) can be used to detect changes in vegetation and cell structure, which makes it suitable to detect biophysical changes in the leaf angle and leaf area. Water absorbs radiation in the shortwave infrared wavelengths ($1.3 - 2.5\,\mu m$) and these wavelengths are therefore suitable to detect changes in the canopy and soil water content. Land surface temperature (LST) obtained through thermal infrared remote sensing ($8 - 14\,\mu m$) is extremely sensitive to evaporative cooling and water stress induced variations. Therefore, LST can be used to detect the changes in vegetation functioning and G_s (Mallick et al., 2022; Mallick et al., 2018) when the vegetation state is not (yet) altered (Vicca et al., 2016).

Monitoring the vegetation response to drought is important, to anticipate the effects on vegetation growth and survival, and the water, energy, and carbon fluxes. The different drought coping strategies of forests and grasslands do suggest that monitoring their vegetation response with remotely sensed data requires a different strategy. For forests, the strong stomatal regulation is reflected in LST and other thermal indices, but the absence of a direct biophysical response makes it impossible to detect the reduction in G_s with optical sensors. For grasslands, on the other hand, the early leaf wilting and senescence can

be detected using optical indices. We aim to study how the different vegetation drought responses of forest and grassland are reflected in remote sensing data. We formulated the following hypothesis:

For forest, drought-induced changes in the surface conductance G_s are reflected in thermal infrared based indices, while for grassland, drought-induced changes in the surface conductance G_s are reflected in both thermal infrared and in optical based indices.

To test our hypothesis, we study two deciduous forest sites, two coniferous forest sites, and two grassland sites in Central Europe during the severe 2018 drought. We study changes in G_s on the different sites and link these to commonly used remote sensing drought indices derived from optical and thermal infrared data.

4.2 Methods

We calculated G_s from flux tower measurements, and compared these with MODIS sensor derived vegetation indices. We focused our analyses on the 2018 'drought year' and compare these values to the 2015 - 2017 'reference years'.

4.2.1 Study sites

Six study sites were selected that met two selection criteria: first, they had a good availability of flux tower and satellite data, and second, they experienced meteorological drought during the summer of 2018 (Fig. 4.2, Table 4.1). Furthermore, sites that benefited from the drought (no reduction in G_s and an increase in evaporation) were excluded. The selected sites were situated in Germany (three sites), Sweden, the Netherlands, and Switzerland (one site each). Two sites were vegetated by deciduous forest (both dominated by beech trees), two by coniferous forest (one pine forest and one spruce forest), and two by grass. All sites experienced a high precipitation deficit during the growing season (Fig. 4.2b).

4.2.2 Flux tower data and calculation of stomatal conductance

Half-hourly land-atmosphere fluxes, meteorological data, and soil moisture data were derived from the European Fluxes Database Cluster and the Integrated Carbon Observation System ICOS (Team and Centre, 2020). From the half hourly data, daily mean VPD and soil moisture content were calculated, if less than seven (12 %) half hourly data points were missing. Daily total precipitation was also calculated when more than 12 % data were missing, because knowing that there was any precipitation was more important than knowing the exact quantity of precipitation.

For the calculation of G_s only data during daytime hours were used (8:00 - 16:00) to account for the time that the vegetation is photosynthesizing (De Kauwe et al., 2017).

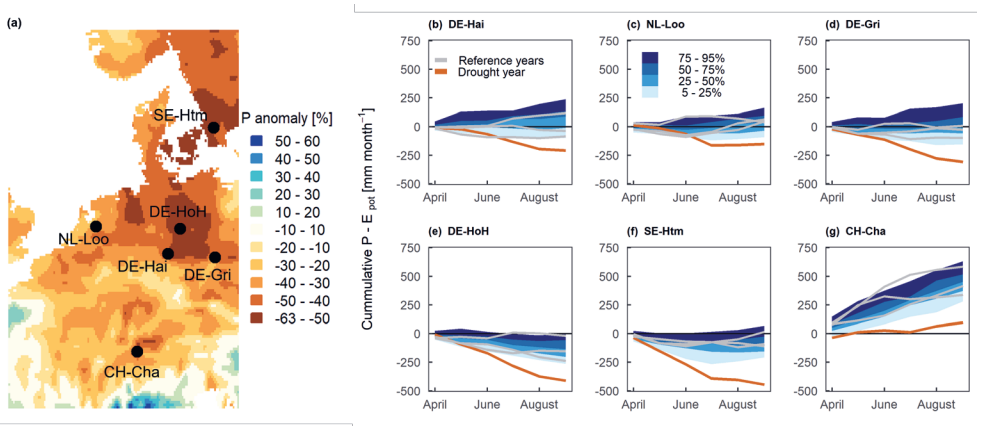

Figure 4.2: The six study sites and their climate. a) The six study sites are located in Central Europe (Table 4.1) and experienced below average precipitation (P) during the 2018 drought. The colours indicate the precipitation anomaly of April - July 2018 compared to the 1981 - 2019 mean. b - g) The percentile distribution of monthly cumulative precipitation deficit (precipitation minus potential evaporation, $P - E_{pot}$) over the growing season (1981 - 2019 mean). The red line represents cumulative precipitation deficit for the 2018 drought year, and the grey lines represent the 2015 - 2017 reference years. The climatological P and E_{pot} were derived from ERA-5 reanalyses data (Hersbach et al., 2018), and MSWEP data (Beck et al., 2019).

The half hourly flux data were discarded in three cases: 1) if the fluxes had a quality label 'poor data' (label 2), 2) if there were atmospherically stable conditions (friction velocity $u^* \leq 0.25$), because flux data is unreliable with insufficient turbulence. For grassland sites, the threshold was set to $u^* \leq 0.05$, to avoid a high data loss, and 3) if there was precipitation at the time of the measurement. The surface conductance G_s was calculated from the inverted Penman-Monteith. This is a commonly used method, however, Wehr and Saleska (2021) recently proposed the flux-gradient equations are more plausible and less prone to biases than the inverted Penman-Monteith equation. G_s was calculated as:

$$G_s = \frac{G_a \gamma LE}{s(R_n - G) - (s + \gamma)LE + G_a M_a c_p D_a} \tag{4.1}$$

where G_a is the aerodynamic conductance [mol m^{-2} s^{-1}], γ is the psychrometric constant [Pa K^{-1}], LE is the latent heat flux [W m^{-2}], s is the slope of the saturation vapour pressure curve at air temperature [Pa K^{-1}], R_n and G are the are the net radiation and soil heat flux [W m^{-2}], M_a is the molar mass of air [kg mol^{-1}], c_p is the heat capacity of air [J kg^{-1} K^{-1}], and the D_a is the vapour pressure deficit [Pa]. The aerodynamic conductance G_a is calculated as:

Table 4.1: The six study sites, their location and their vegetation characteristics.

Site code (Fig. 4.2)	Location	Vegetation type, dominant species	Longitude, Latitude	DOI (/citation)
DE-Hai	Hainich, Germany	Deciduous forest, Beech	10.4522, 51.0792	10.18140/FLX/1440148 Knohl et al. (2020)
DE-HoH	Hohes Holz, Germany	Deciduous forest, Beech	11.2192, 52.0853	10.18160/J1YB-YEHC Rebmann and ICOS ETC (2020)
NL-Loo	Loobos, The, Netherlands	Coniferous forest, Pine	5.7436, 52.1666	10.18140/FLX/1440178 Kruijt and ICOS ETC (2020)
SE-Htm	Hyltemossa, Sweden	Coniferous forest, Spruce	13.4190, 56.0976	Heliasz and ICOS ETC (2020)
DE-Gri	Grillenburg, Germany	Grassland, Grass	13.5126, 50.9500	10.18140/FLX/1440147 Bernhofer and Gruenwald (2021)
CH-Cha	Chamau, Switzerland	Grassland, Grass	8.4104, 47.2102	Buchmann et al. (2021)

$$G_a = \frac{c}{\frac{u}{u^*} + 6.2u^{-\frac{2}{3}}} \tag{4.2}$$

where c is a conversion factor from units of [m s^{-1}] to [mol m^{-2} s^{-1}], (calculated as $c = \frac{P}{R_{gas}T_k}$, where P is the atmospheric pressure [Pa], R_{gas} is the gas constant [J mol^{-1} K^{-1}], and T_k is the air temperature [K]), u is the wind speed [m s^{-1}], and u^* is the friction velocity [m s^{-1}]. Negative values and positive outliers ($G_s > 100$) were deleted. The daily mean G_s was calculated when at least 11 out of 17 data values were available.

4.2.3 Remote sensing data

Remote sensing indices were derived from the MODIS products MOD09GA, MYD09GA, MOD11A1, MYD11A1 (Table 4.2) that were available from the Terra (MOD) and Aqua (MYD) satellites. Both satellites observe the same area twice a day, and the daytime observation was used for the analyses (around 10:30 for Terra and 13:30 for Aqua). For all required data, cloudy (or adjacent clouds) data were discarded based on the quality label.

For the MODIS bands B1, B2, and B7, the mean daily value was calculated from the Terra and Aqua satellite data, and either Terra or Aqua data were used when only one of them was available. For the LST data, the Aqua data were used, because the afternoon overpass time better captures the vegetation stress. However, if the Aqua data were not available, the Terra data were used, that were first adjusted using a linear model between the Aqua and Terra data. Afterwards, six different remote sensing indices were calculated: the NDVI, VCI, NDMI, LST, TCI, and LST-Ta (Table 4.3). The air temperature (Ta)

Table 4.2: The four MODIS vegetation products and their characteristics. The MODIS bands are the bands that were used in the calculation of the vegetation indices.

MODIS product	Satellite	Temporal resolution	Spatial resolution	MODIS bands
MOD09GA	Terra	Daily	500 m	B1 (red), B2 (near-infrared), B7 (shortwave infrared)
MYD09GA	Aqua	Daily	500 m	B1 (red), B2 (near-infrared), B7 (shortwave infrared)
MOD11A1	Terra	Daily	1 km	Daytime LST, calculated from B31 and B32 (thermal infrared)
MYD11A1	Aqua	Daily	1 km	Daytime LST, calculated from B31 and B32 (thermal infrared)

Table 4.3: Vegetation Indices used for drought monitoring. B1, B2, B7, and LST refer to the MODIS bands in table 4.2.

Index	Formula
NDVI Normalized Difference Vegetation Index	$NDVI = \frac{B2-B1}{B2+B1}$
VCI Vegetation Condition Index	$VCI = \frac{NDVI-min(NDVI)}{max(NDVI)-min(NDVI)}$
NDMI Normalized Difference Moisture Index	$NDMI = \frac{B2-B7}{B2+B7}$
LST Land Surface Temperature	
TCI Temperature Condition Index	$TCI = \frac{max(LST)-LST}{max(LST)-min(LST)}$
LST-Ta Land Surface - Air Temperature Difference	$LST - Ta = LST - Ta$

was taken from the flux tower measurements at the moment of satellite overpass (13:30). These six indices are frequently used for vegetation and drought monitoring and are based on a range of different wavelengths: the visible, near-infrared, shortwave infrared, and thermal infrared. The different indices were gap-filled for up to ten days of missing data using a linear model. Afterwards, the Savitzky-Golay filter was used for data smoothing. For LST, TCI, and LST-Ta, no smoothing was applied, because LST is a state variable and shows a high daily variability.

For both the grassland sites, the MODIS pixels of 500 x 500 m and 1 x 1 km reflect a mixed signal of grassland and forest. At the lowest resolution, half of the grassland pixels reflect a forest signal. The forest pixels fully cover a forest land cover.

4.2.4 Analyses

Define unstressed and stressed vegetation
We study the difference between the unstressed and stressed vegetation. 'Unstressed' refers to the time before the drop in G_s, thus before the onset of stomatal regulation and/or changes in leaf color and structure. 'Stressed' refers to the time of low G_s. It is assumed that the drop in G_s indicates the onset of the vegetation drought response. The start of vegetation stress is defined based on the time series of G_s and a comparison between G_s for the drought and reference years. First, we indicated when G_s for 2018 was below 25 % of the reference G_s for multiple days. Afterwards, we indicated the exact shift between the unstressed and stressed vegetation as the moment that the 2018 G_s showed a clear drop.

Compare unstressed and stressed vegetation
G_s and the vegetation indices were compared for the unstressed and drought stressed vegetation. More precisely, the two weeks before the shift in G_s were compared with the four weeks afterwards. Only two weeks were used for the unstressed vegetation, because four weeks includes the green-up phase for some study sites and this would add noise to the data. However, for the site NL-Loo, a three-week period has been used for the calculation of the NDVI, VCI, and NDMI, because no data was available for the two-week period.

4.3 Results

4.3.1 Hydro-meteorology and G_s

A progressive decline in soil moisture was concurrent with an increase in the vapour pressure deficit during the 2018 summer drought (Fig 4.3). The combination of low water availability and high atmospheric demand triggered the vegetation drought response, and G_s declined (Fig. 4.3). This drop in G_s is the result of stomatal regulation and / or a loss in green leaf area, but our data cannot be used to study the importance of these effects for each site. The timing of the drop in G_s and duration differed per study site. The drop in G_s occurred late May, in June, or early July, and low G_s persisted for one to three months. During these months, G_s was around 25 % of the reference G_s. At the end of the growing season, G_s increased to up or above the reference level.

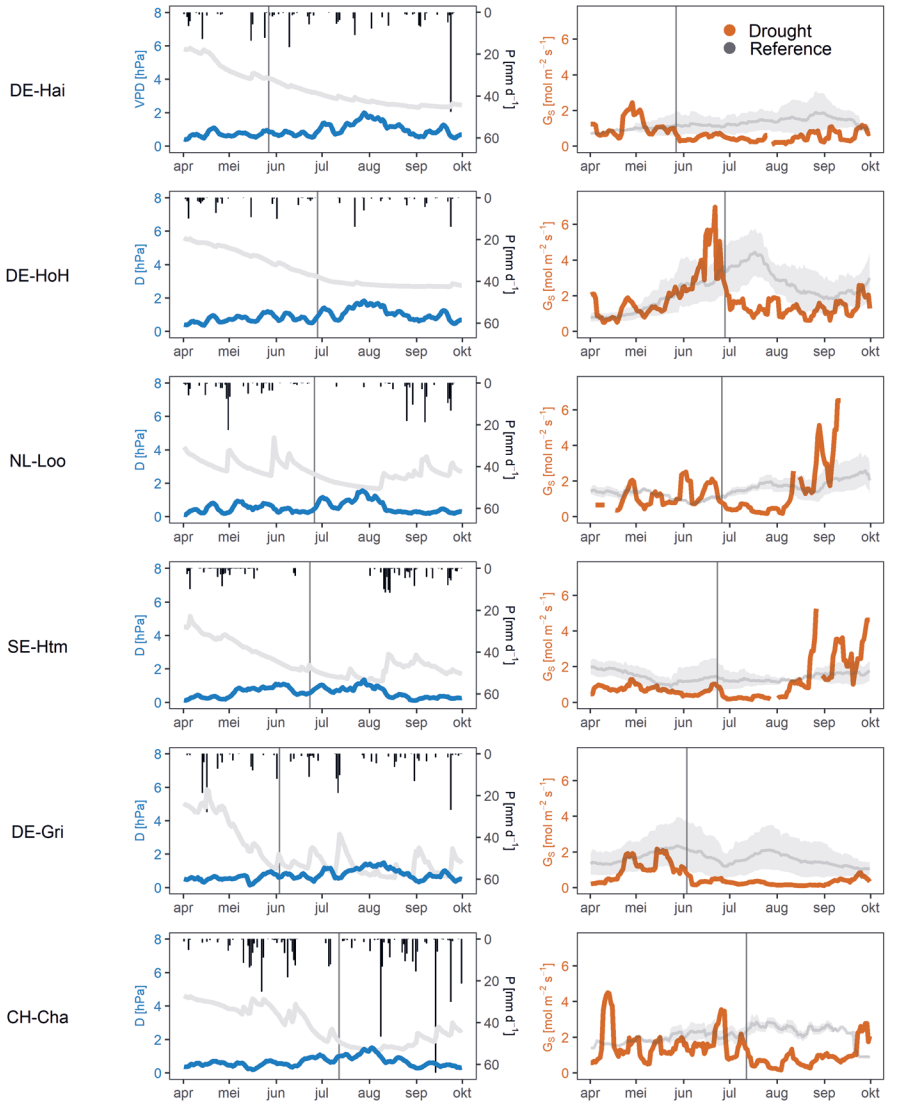

Figure 4.3: Hydro-meteorological measurements during the spring and summer of 2018. The left figures show the vapour pressure deficit (D) in blue, soil moisture in grey (mean value over various depths), and precipitation (P) in black. The soil moisture line presents the trend, but no absolute values. The right figures show the stomatal conductance (G_s) for the drought year 2018 (in red) and the reference years 2015-2017 (in grey). The reference G_s represents the 30-day moving mean conductance for the three years, and the shaded area represents the minimum to maximum value. The drought G_s, soil moisture, and D represent the 7-day moving mean value. The grey vertical lines indicate the transition from unstressed to stressed vegetation.

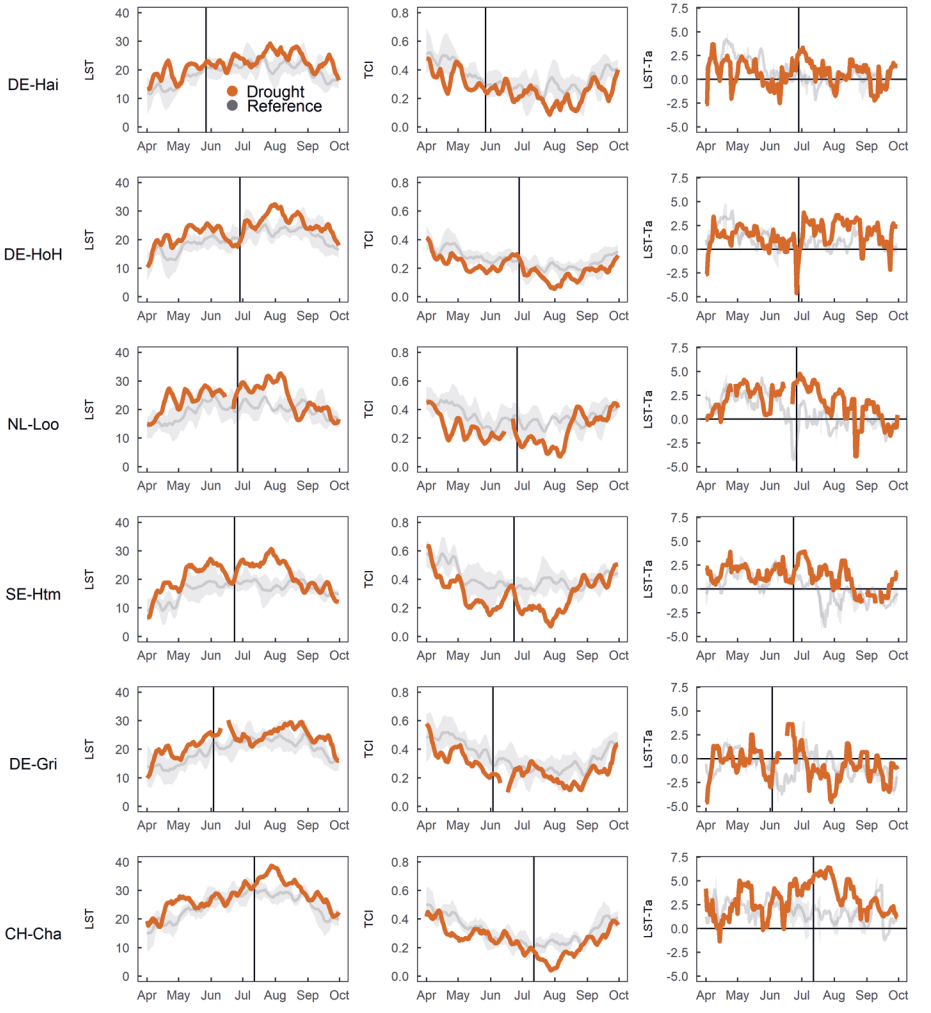

Figure 4.4: Vegetation drought monitoring using thermal indices. The LST, TCI, and LST-Ta drought indices for the 2018 drought year (in red) and 2015 - 2017 reference years (in grey). The drought indices represent the 7-day moving mean value. The grey shaded area represents the minimum to maximum value. The grey vertical lines indicate the transition from unstressed to stressed vegetation, as in figure 4.3.

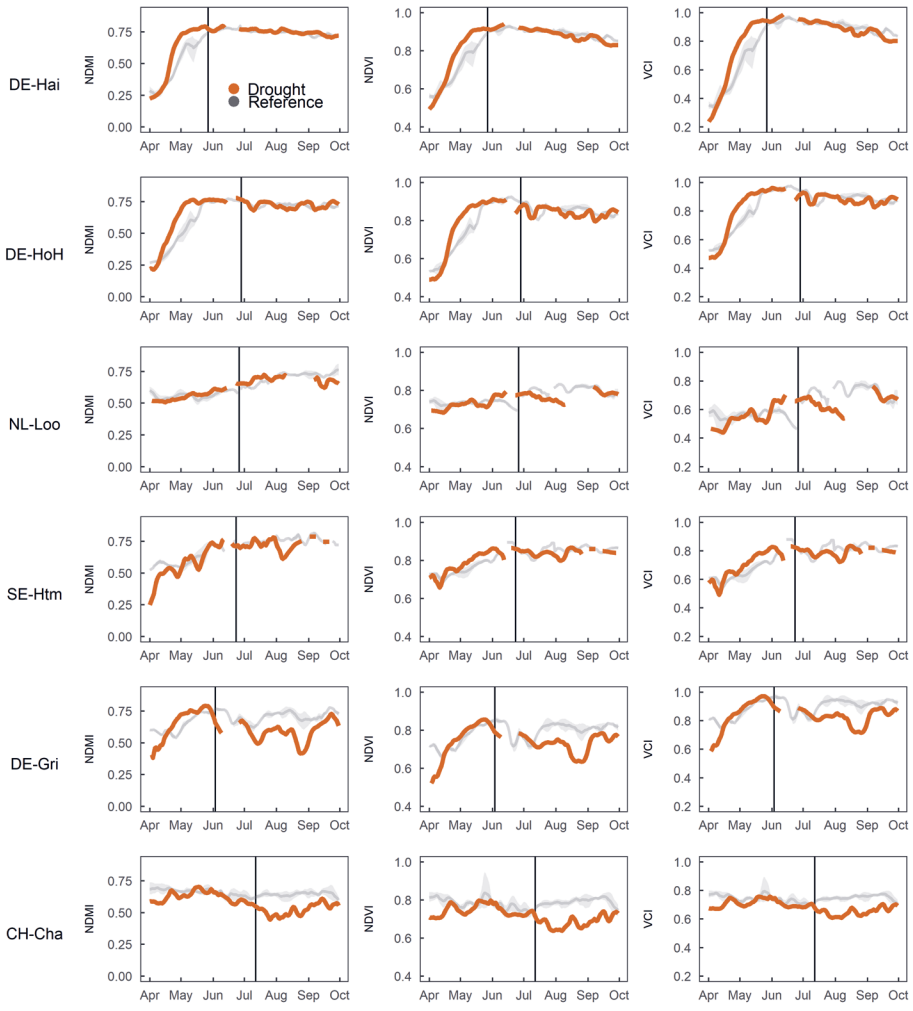

Figure 4.5: Vegetation drought monitoring using optical indices. The NDMI, NDVI, and VCI drought indices for the 2018 drought year (in red) and 2015 - 2017 reference years (in grey). The drought indices represent the 7-day moving mean value. The grey shaded area represents the minimum to maximum value. The grey vertical lines indicate the transition from unstressed to stressed vegetation, as in figure 4.3.

4.3.2 Vegetation indices

The thermal infrared vegetation indices reflected the drought for most of the study sites (Fig 4.4). The deciduous forest site DE-HoH, both coniferous forest sites (NL-Loo and SE-Htm), and the grassland site CH-Cha all showed an increase in LST that coincided with the decrease in surface conductance. In the other sites, LST was also above the reference value during parts of the drought. The TCI (the normalized LST), dropped during (part of) the drought for all of the study sites. The third thermal infrared index, the LST-Ta, showed positive and above average values during the drought for four out of six sites. In spring 2018, the LST showed above average values and the TCI showed below average values for all sites, which reflects the sunny spring conditions. The optical indices showed less temporal variability as compared to the thermal indices (Fig. 4.5). For the two deciduous forest sites, the NDMI, NDVI, and VCI (the normalised NDVI) did reflect the early green-up in spring, but did not reflect the drought. For the pine forest site NL-Loo, the NDMI did not reflect a drought response. The NDVI and VCI dropped in August, a few weeks after the onset of stomatal regulation, but unfortunately no data was available to confirm whether this drop was persistent over a longer time. At the spruce forest site SE-Htm, the different indices did not reflect an anomaly during the drought. At the two grassland sites, the NDMI, NDVI, and VCI were close to the reference values in the month before the drought, but were below average during the drought. At the grasslands, the drop in the optical indices coincided with the drop in G_s.

4.3.3 Comparing unstressed and stressed vegetation

The G_s dropped considerably from the unstressed to the stressed condition for all sites. The drop was smallest for the beech forest site DE-Hai ($-52\,\%$) and largest for the beech forest site DE-HoH, the pine forest site NL-Loo, and the grassland site DE-Gri ($-75\,\%$) (Fig 4.6). The LST increased with up to $7\,^{\circ}\mathrm{C}$ from the unstressed to the stressed condition for all sites, but only a small increase was observed for the beech forest site DE-Hai and the grassland site DE-Gri. The TCI had a comparable result as the LST. The LST-Ta increased for all sites with $1-2\,^{\circ}\mathrm{C}$, except for the beech forest site DE-Hai. Given LST-Ta is directly associated with the sensible heat flux and evaporative fraction, it is considered as a relatively better indicator of drought than the LST. The NDMI showed an irregular response for the forest sites: The NDMI decreased (slightly) for the beech forest sites, increased substantially for the pine forest site, and decreased slightly for the spruce forest site. The NDMI decreased substantially for both grassland sites. The NDVI and VCI showed negligible response in all forest sites, but decreased substantially in both grassland sites from the unstressed to stressed condition. In summary, the thermal indices LST and TCI were sensitive to a change in G_s for four out of six sites, and the LST-Ta was sensitive to the drop in G_s for five out of six sites. The optical indices were not or only slightly sensitive to the drop in G_s in forests, but were sensitive to changes in the grassland G_s.

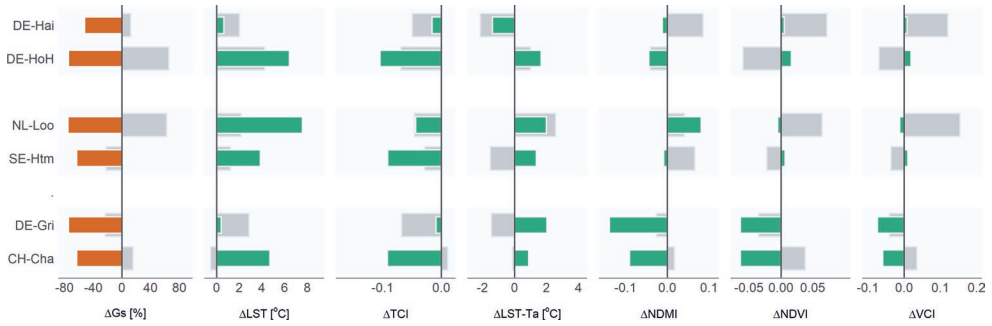

Figure 4.6: Comparing the unstressed and stressed vegetation. The bars reflect the difference in the surface conductance G_s and the vegetation indices between the unstressed to the stressed vegetation. The 'unstressed vegetation' refers to the two weeks before the drop in G_s and the 'stressed vegetation' refers to the four weeks after the drop in G_s. The left three vegetation indices are based on thermal infrared data and the right three indices are based on optical data (visible, near-infrared and shortwave infrared). The red and green bars present the 2018 drought year, while the grey bars present the corresponding weeks for the 2015 - 2017 reference years.

As a comparison to the drought year, we calculated the change in G_s and vegetation indices for the corresponding weeks in the reference years. The differences between these non-drought years and the drought year 2018 can not only be attributed to the change vegetation stress, but also reflect other vegetation changes. In the reference years G_s increased, rather than decreased for four out of six sites. Similarly to the drought year, the LST increased and the TCI decreased for all four forest sites and one grassland site, despite that G_s increased for most sites. This reflects the seasonal course of the LST, rather than a drought responds. LST-Ta decreased for half of the sites. For the reference years, the temporal change in the optical indices the NDMI, NDVI, and VCI had a variable response for each vegetation type. The substantial change in all optical indices for the beech forest site DE-Hai is due to the green-up of the forest in spring, which is reflected in both the NDMI, NDVI, and VCI. For the grassland site DE-Gri, the slight decrease in G_s is accompanied with a decrease in NDMI, NDVI, and VCI, and vice versa for the grassland site CH-Cha.

4.4 Discussion

4.4.1 Limitations of the study

In this chapter we used the terms stressed and unstressed vegetation. We assume that the drop in G_s indicates the onset of the vegetation drought response. We did not study other types of vegetation stress, nor did we study other potential causes of a decreased G_s (such

as mowing). Similarly, we assume that a change in the vegetation indices from unstressed to stressed period visualizes the vegetation response to drought. Unfortunately, it is not certain that the drought caused these changes in the Earth's reflectance and radiation emission, and it is impossible to verify our assumption with complete certainty.

The vegetation indices are calculated from 500×500 m and 1×1 km spatial resolution MODIS data. For both grassland sites, the MODIS pixels also include forest, and the data thus consist of both a grassland and a forest signal. A comparable study with high resolution satellite data is needed to confirm the presented results. Some recently launched satellites with high spatial and high temporal resolution, such as ESA's Sentinel series and NASA's ECOSTRESS thermal infrared satellite would provide a great opportunity for further analyses on future droughts. Unfortunately, these high-resolution data were not yet available over the entire study period.

In this study, the 2018 drought year and the 2015 - 2017 reference years were compared. Ideally reference years would have had an climatically average precipitation and potential evaporation. The three selected reference years unfortunately do not all reflect average conditions. For example for the deciduous forest site DE-HoH, compared to the past 39 years (1981 - 2019), 2016 was the sixth driest and 2017 was the seventh wettest year. Furthermore, the reference years differ from the drought year in the timing of green-up. The drought year experienced an early green-up because of the sunny weather and this impacted the comparison between the drought year and reference years.

4.4.2 The results confirm the hypotheses

We formulated the following hypothesis: 'for forest, drought-induced changes in G_s are reflected in thermal infrared based indices, while for grassland, drought-induced changes in G_s are reflected in both thermal infrared and in optical based indices'.

For three of the four forest sites, the thermal infrared indices were sensitive to changes in G_s. The optical index NDMI, which is calculated from the reflectance in the near-infrared and shortwave infrared data, showed variable drought response, partly due to the seasonal variability of NDMI in the site. The NDVI and VCI were not sensitive to the forest drought response. The results therefore confirm the hypothesis for the forests. The more conservative trees do close their stomata to reduce water loss, which increases the LST and LST-Ta (as reflected in thermal infrared data). However, forests do not initially change their leaf water content, leaf color, or structure, and therefore, there is no change in the optical indices.

For one grassland site, the thermal infrared indices LST and TCI did not reflect the drought. There are a few uncertainties, such as an optional moving event, and the forest signal in the grassland pixel, that could explain this. For the second grassland site, however, the LST and TCI were sensitive to changes in G_s. The LST-Ta, a better indicator for

vegetation drought, was sensitive to changes in G_s for both grassland sites. Furthermore, all optical indices were highly sensitive to the decrease in G_s. The results therefore confirm our hypothesis for grassland. The drop in G_s coincided with a decrease in the optical indices that reflect a reduction in leaf and soil water content, a change in leaf color and / or a change in leaf structure.

The results however also indicate that a reduction in G_s is not always reflected in the thermal infrared indices, and that the grassland and forest sites do not show a similar response.

Previous studies also confirmed that optical vegetation indices did not or only weakly reflect a drought in energy-limited forest (Bachmair et al., 2018; Vicca et al., 2016). Vicca et al. (2016) concluded that the NDVI and NDMI data did not reflect the drought, however the EVI (Enhanced Vegetation Index) and sPRIn (standardi Normalized Photochemical Reflectance Index) did reflect the drought for some of their sites. Both indices did not show a uniform response in preliminary analyses in our study. Buras et al. (2020) found a reduction in the forest NDVI during the 2018 drought, although they also concluded that grassland NDVI was more sensitive. Buras et al. (2020) did not link the reduction in forest NDVI to the timing of the reduction in G_s, and therefore, their results are not necessarily complementary to our results.

The results show that, when one is interested in ecosystem evaporation (and the water, energy, and carbon cycle) during drought, a different monitoring strategy is required for forest and grassland. The results however also show that the vegetation response is not uniform or not uniformly reflected in satellite data over all forest and grassland sites. This is in line with conclusions drawn by for instance Buras et al. (2020) and Vicca et al. (2016). More extensive analyses over different droughts, different study sites, and at higher spatial resolution can provide a better insight in how representative these results are for all forests and grasslands in temperate climate regions.

4.5 Conclusions

Forest and grassland adopt a different drought coping strategy. Forests reduce their stomatal conductance, to reduce water loss. The reduced vegetation-atmosphere exchange of water in grasslands, is largely due to reduction in green leaf area. The aim of this study was to investigate how these different drought coping strategies impact the satellite based drought monitoring. Our results show that:

- During the 2018 drought in Central Europe, the surface conductance G_s reduced with $50-70\,\%$ for all study sites.

- For three of the four forest sites, the reduction in G_s was reflected in thermal infrared indices, but not in any of the optical indices. There was no difference between the deciduous and coniferous forest sites.
- For the grassland sites, the thermal infrared index LST-Ta as well as all optical indices were sensitive to the reduction in G_s.

The results confirm the hypothesis and show that forest and grassland drought monitoring requires a different strategy. To study the effect of drought on the water, energy, and carbon cycle in forests, the focus should be on thermal infrared vegetation indices rather than optical indices. For grasslands however, both the thermal infrared and optical vegetation indices are sensitive to a reduction in G_s. Both the forest and grassland sites do however not show a uniform response, and more research is needed to confirm this conclusion.

Chapter 5

The effect of tree restoration on evaporation and water availability

This chapter is based on:

A. J. Hoek van Dijke, M. Herold, K. Mallick, I. Benedict, M. Machwitz, M. Schlerf, A. Pranindita, J. J. E. Theeuwen, J.-F. Bastin, and A. J. Teuling (2022). "Shifts in regional water availability due to global tree restoration". *Nature Geoscience* 15, 363–368. DOI: https://doi.org/10.1038/s41561-022-00935-0

Abstract

Tree restoration is an effective way to store atmospheric carbon and mitigate climate change. However, large-scale tree cover expansion has long been known to increase evaporation, leading to reduced local water availability and streamflow. More recent studies suggest that increased precipitation, through enhanced atmospheric recycling of evaporated water, can offset this effect. Here we calculate how 900 million hectares of global tree restoration would impact evaporation through an ensemble of data-driven Budyko models, and we calculate the increase in precipitation through the UTrack moisture recycling dataset. We show that the combined effects of directly enhanced evaporation and indirectly enhanced precipitation due to recycling create complex patterns of shifting water resources availability. Large-scale tree cover expansion can increase water availability by up to 6 % in some regions, while decreasing it by up to 38 % in other regions. There is a divergent impact on large river basins: some rivers could lose 6 % of their streamflow due to enhanced evaporation, while for other rivers, the enhanced evaporation is counterbalanced by enhanced recycling. Several so-called 'hot spots for forest restoration' could lose water; including regions that are already facing water scarcity today. Tree restoration significantly shifts terrestrial water fluxes and we emphasize that future tree restoration strategies should consider these hydrological effects.

5.1 Introduction

In June 2021, the United Nations declared the Decade on Ecosystem Restoration to prevent, halt, and reverse the degradation of ecosystems worldwide. Large-scale tree restoration is key in climate change mitigation and for enhancing and protecting biodiversity and ecosystem services (Griscom et al., 2017). Under the current climate conditions, it is estimated that an additional 900 million hectares of tree cover could exist on the Earth's surface (Bastin et al., 2019), without encroaching on agriculture and urban areas (Fig. 5.1). During the past decade, numerous global and regional initiatives were initiated to increase tree cover, and this will play an important role in shaping global land use over the next decades. Despite these ongoing initiatives and the claims that ecosystem restoration is beneficial to all of the Sustainable Development Goals (IRP, 2019), the impact of tree planting on the water cycle and water availability is still poorly understood (Seijger et al., 2021; Wang-Erlandsson et al., 2018). As a result, potential impacts of ecosystem restoration on ensuring water availability both downstream and downwind are often overlooked.

Tree cover expansion impacts water availability locally through its effects on the radiation balance, infiltration and soil water storage, evaporation, streamflow, and precipitation (Ellison, 2018). Traditionally, local impacts of forest cover on streamflow have been investigated mainly using a so-called 'paired catchment approach'. These studies compare two nearby headwater catchments with similar characteristics over a prolonged period, during which one of the catchments underwent land-cover change, while the other did not undergo change. These observational studies have, virtually without exception, concluded that tree planting increases annual evaporation and decreases streamflow (Bosch and Hewlett, 1982; Brown et al., 2005; Farley et al., 2005; Filoso et al., 2017; Jackson et al., 2005; Zhang et al., 2001). This high evaporation is attributed to the deeper roots of trees (facilitating access to water during dry periods), higher leaf area index (increasing the precipitation interception and canopy conductance), lower snow-free albedo (increasing

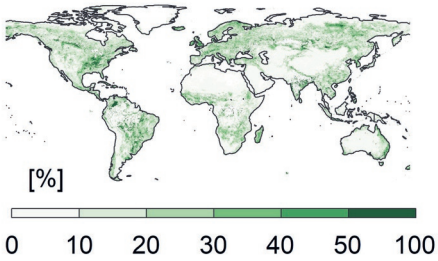

Figure 5.1: Global tree restoration potential. The percentage area of each pixel that is suitable for tree restoration.

the energy available for evaporation), and higher aerodynamic roughness (facilitating turbulent exchange), as compared to the other vegetation types (Farley et al., 2005). Higher evaporation has been reported across different climate zones and tree species, but the magnitude of evaporation differs with climate, tree species, and tree age (Bosch and Hewlett, 1982; Brown et al., 2005). From these studies, it was predicted that large-scale tree restoration will decrease annual mean water availability and streamflow locally (Farley et al., 2005; Huxman et al., 2005; Ning et al., 2020; Sun et al., 2006).

In contrast to these small-scale river basin studies, more recent, large-scale research suggests that the impacts of tree restoration on streamflow are more complex (Ellison, 2018; Ellison et al., 2012; Keys et al., 2016; Meier et al., 2021; Spracklen et al., 2018; Wang-Erlandsson et al., 2018). Through atmospheric feedbacks and transport, the increased evaporation from restored trees will partly recycle back to the terrestrial surface (via so-called evaporation or moisture recycling) and thereby potentially increase downwind rainfall and water availability. Such effects of tree cover change can reach far beyond the river basin- or even continental level: tree-cover change in the Amazon forest could impact precipitation in Canada, northern Europe, and all the way into eastern Asia (Lawrence and Vandecar, 2015). A host of regional and global-scale research has integrated the effects of evaporation recycling in land-cover change studies (Keys et al., 2016; Li et al., 2018; Wang-Erlandsson et al., 2018; Wierik et al., 2021). These studies have shown that evaporation recycling has a major influence on the water availability and that evaporation recycling should be considered in future land-cover change studies.

No study has quantified the effects of large-scale global tree restoration on water availability, by accounting for both the local, direct effect of increased evaporation and the large-scale, indirect effect of evaporation recycling. The recently published datasets of the 'global tree restoration potential'(Bastin et al., 2019) and evaporation recycling (Tuinenburg et al., 2020b) opens up an emerging opportunity for such analyses. In our idealized study, we calculate how large-scale tree restoration (defined as: increasing tree cover in any region, independent of the land-use history) influences water availability (defined as: precipitation water that is not lost through evaporation, the total water available for consumption, on a yearly basis) and streamflow (defined as: the amount of water flowing in a stream, in this study the accumulation of the above defined water availability on the river-basin scale). More precisely, we calculate how a recent estimate of the 'global tree restoration potential' (Bastin et al., 2019, Fig. 5.1) would impact the fluxes of evaporation, precipitation and streamflow. The 'global tree restoration potential' dataset highlights where more trees could naturally grow, without encroaching on agricultural and urban land. To determine how tree restoration impacts the long-term partitioning of precipitation between evaporation and streamflow, we use an ensemble of six data-driven Budyko-models available in the literature that include a calibrated vegetation parameter for forest and non-forest conditions at a 1 km spatial resolution (Oudin et al., 2008; Teuling et al., 2019; Zhang et al., 2001; Zhang et al., 2004; Zhou et al., 2015) (Fig. 5.2).

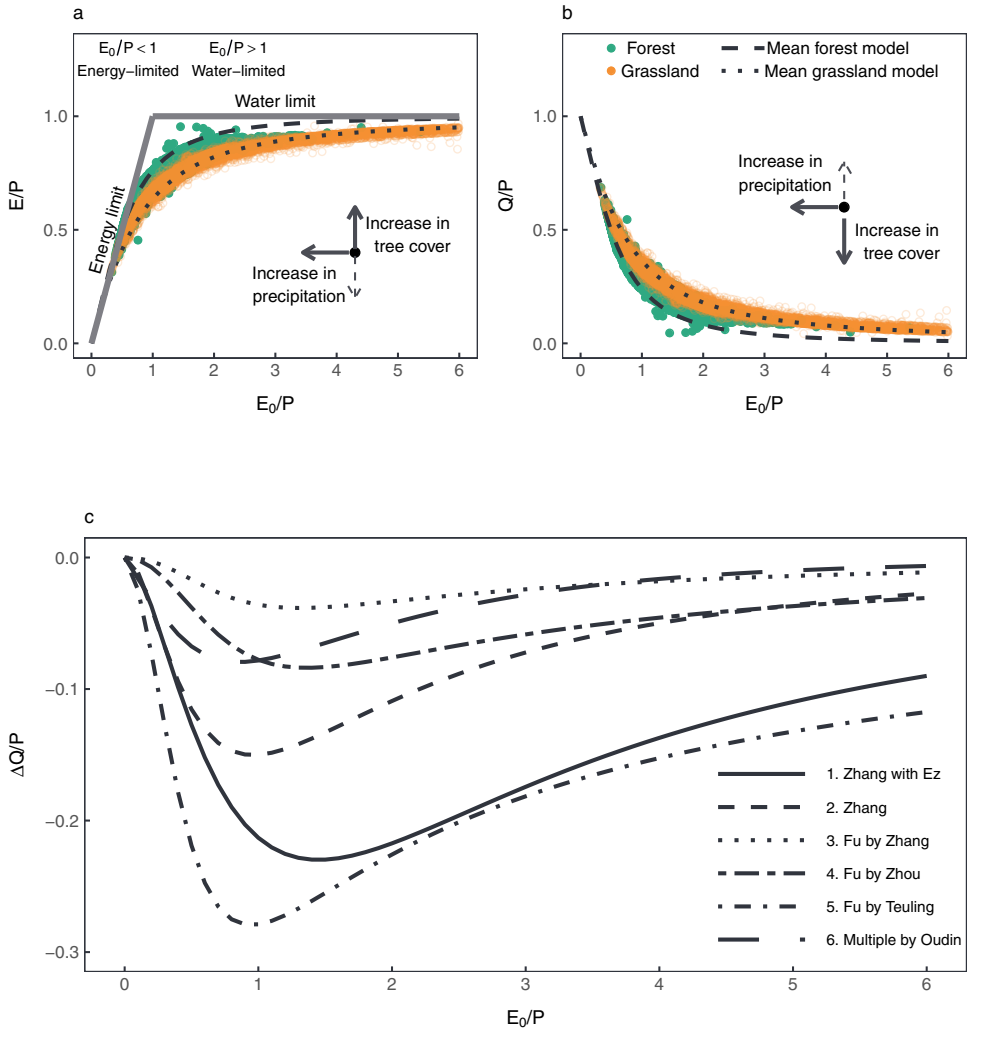

Figure 5.2: The Budyko framework The Budyko framework (Budyko, 1974) parameterizes how the long-term aridity $\frac{E_0}{P}$ (potential evaporation over precipitation ratio) determines the partitioning of precipitation into evaporation and streamflow. (a) displayed the evaporation over precipitation ratio $\frac{E}{P}$, while (b) displays the streamflow over precipitation ratio $\frac{Q}{P}$. The dots display the range of values found in our study for grassland and forest (land-cover based on the IGBP dataset (Loveland et al., 2000)). The lines represent the mean grassland and forest $\frac{E}{P}$ and $\frac{Q}{P}$. The arrows show the direction of movement in the Budyko space for an increase in tree cover (which results in a higher $\frac{E}{P}$ and lower $\frac{Q}{P}$) and an increase in precipitation as a consequence of evaporation recycling (which results in a lower $\frac{E_0}{P}$ and possibly a lower $\frac{E}{P}$ and higher $\frac{Q}{P}$). (c) displays the difference in $\frac{Q}{P}$ between forest and grassland for the six different Budyko used models. The numbers refer to the models in table 5.2.

In addition to the Budyko models, we use the recent UTrack dataset of global evaporation recycling (Tuinenburg et al., 2020a; Tuinenburg et al., 2020b), to calculate where, and to what extent, the increased evaporation could increase (downwind) precipitation. This dataset is created using a state-of-the-art Lagrangian moisture tracking model (Tuinenburg and Staal, 2020) and presents the monthly climatological mean evaporation recycling. We assume that tree restoration would intensify the current evaporation recycling patterns as presented in the UTrack dataset. This approach focusses on the regional distribution of evaporated water but does not take into account the effect that land-cover change has on local precipitation or atmospheric circulation and recycling patterns. These assumptions are further addressed in the discussion.

5.2 Methods

5.2.1 Overview

We calculate how a realistic scenario of large-scale tree restoration (restoring 900 million hectares of tree cover (Bastin et al., 2019)) would impact the fluxes of evaporation (E), precipitation (P) and streamflow (Q). The methodology includes four steps (Table 5.1). (1) We use Budyko-models to calculate E and Q before restoration. (2) We use Budyko-models to calculate E and Q after restoration without evaporation recycling. (3) We use the UTrack dataset to calculate P after restoration based on increase in E calculated from step 1 and 2. (4) We use Budyko-models to calculate E and Q after restoration with evaporation recycling. The calculation of E and Q without evaporation recycling (step 2) is a local approach, that assumes that evaporation increases with tree restoration, but does not consider the effects of evaporation recycling. The calculation of E and Q with evaporation recycling (step 4) takes into account that the evaporated water partly recycles back to the Earth's land surface and increases P.

5.2.2 Input data to calculate E and Q

E and Q before tree restoration (step 1) are calculated using climatological P (MSWEP V2.8, Beck et al. (2019)), climatological potential evaporation (WorldClim V2, Trabucco and Zomer (2018)), and current tree cover (Hansen tree cover V1.7, Hansen et al. (2013)). For E and Q after restoration (step 2 and 4) we use tree cover after restoration (Hansen tree cover + Tree Restoration Potential, where we set the maximum tree cover after restoration to 1). E and Q with evaporation recycling (step 4) are calculated using P after restoration (MSWEP P + P from evaporation recycling calculated in step 3). We assume that tree restoration does not affect potential evaporation. All input data were resampled to 0.008 33 ° spatial resolution (1 km at the equator).

Table 5.1: The four steps applied to calculate the change in evaporation (E), precipitation (P) and streamflow (Q) without and with evaporation recycling. The E_0 is the potential evaporation and TC is the tree cover.

Step	Model / Dataset	Input E	Input E_0	Input P	Input TC	Output
1	6 Budyko models		E_0 before restoration	P before restoration	TC before restoration	E and Q before restoration
2	6 Budyko models		E_0 before restoration	P before restoration	TC after restoration*	E and Q after restoration without recycling
3	Utrack dataset	ΔE without recycling (step 1 + 2)				Increase in P
4	6 Budyko models		E_0 before restoration	P after restoration** (step 3)	TC after restoration*	E and Q after restoration with recycling

* TC after restoration is calculated from TC before restoration + the tree restoration potential
** P after restoration is calculated from P before restoration + increase in P (step 3)

5.2.3 Budyko-models to calculate E and Q

E and Q before and after restoration are calculated using six different Budyko-type models (Oudin et al., 2008; Teuling et al., 2019; Zhang et al., 2001; Zhang et al., 2004; Zhou et al., 2015) (Fig. 5.2c, Table 5.2). These models reflect global annual patterns in P partitioning between E and Q. The general form of the equations is:

$$\frac{E}{P} = f(\frac{E_o}{P}, \omega) \tag{5.1}$$

where $\frac{E}{P}$ is the fraction of precipitation partitioned into evaporation, $\frac{E_o}{P}$ is the aridity index and ω is a model parameter. Previous studies have suggested that the parameter ω is closely related to vegetation type or vegetation coverage (Zhang et al., 2001). Six models were available in the literature that have a calibrated ω parameter for forest and grassland cover. These models were calibrated using river basin or lysimeter data from different climate zones. The parameter ω_{trees} was calibrated with data from both natural forests (the major part of the data) and plantations. ω_{grass}, the vegetation parameter for grassland was calibrated using grassland data only, or both grassland and cropland data (Table 5.2). The semi-empirical Budyko models reflect the yearly, catchment integrated, effect of differences in interception, the plant available water, evaporation, the soil water storage capacity, and the energy balance between grassland and forest. For each of the six Budyko models, E and Q before and after restoration (without and with evaporation recycling) are calculated as:

$$E = E_{\text{trees}} * TC + E_{\text{grass}} * NTC \tag{5.2}$$

$$Q = Q_{\text{trees}} * TC + Q_{\text{grass}} * NTC \tag{5.3}$$

where E_{trees} and Q_{trees} [mm yr^{-1}] are E and Q calculated for trees, TC is the tree cover, E_{grass} and Q_{grass} are E and Q calculated for grassland, and NTC is the no-tree cover, where:

$$NTC = 1 - TC \tag{5.4}$$

NTC thus, includes among others bare land, shrub land, and built-up area. Evaporation from these land-cover types is different from evaporation from grassland and cropland. We expect that these differences are negligible because bare land is generally very arid, where E is close to zero (both the Budyko E and true E), and build-up area has a limited extent. The Budyko vegetation parameters for shrubland (when calculated) closely resemble the parameters for grassland and cropland (Oudin et al., 2008; Zhou et al., 2015).

Mean yearly Q before restoration was validated against streamflow data for 19 river basins (Fig. 5.3). The validation shows a good agreement over orders of magnitude, except for the Murray-Darling and Colorado basins, where water extraction likely causes the models to overestimate observed runoff.

The changes in E and Q were calculated from the difference between E and Q before and after restoration. The results were resampled to 0.5 ° spatial resolution for the calculation of evaporation recycling.

5.2.4 Evaporation recycling – calculation of precipitation

We used the UTtrack dataset (Tuinenburg et al., 2020a; Tuinenburg et al., 2020b) of global atmospheric moisture recycling (at 0.5 ° spatial resolution) to calculate where the additional evaporated water from restored trees would rain out (P after restoration in step 3). The UTrack dataset was created using the state-of-the-art Lagrangian moisture tracking model UTrack (Tuinenburg and Staal, 2020). The dataset presents the monthly climatological mean evaporation recycling for each pixel. We aggregated the dataset's monthly mean evaporation recycling to yearly mean evaporation recycling to be able to combine it with the yearly Budyko-models. This yearly aggregation of the UTrack dataset ignores the seasonality in direction and magnitude of atmospheric moisture transport that exists in some regions (Meier et al., 2021; Tuinenburg et al., 2020b). This aggregation was preferred above a disaggregation of the Budyko results, because the Budyko model assumes zero change in water storage and can therefore only be applied on a multi-year mean timescale. Restoring tree cover could increase soil storage capacity and increase dry season water availability (Ellison et al., 2017). Thus the Budyko models cannot be used to calculate evaporation at a monthly timescale. As a comparison, evaporation recycling was

Table 5.2: The four steps of the methodology. These steps are applied to calculate the change in evaporation (E), precipitation (P) and streamflow (Q) without and with evaporation recycling. The E_0 is the potential evaporation and TC is the tree cover. ω_g and ω_f are the calibrated vegetation parameters for grassland and forest.

Model	Functional form*	Calibrated ω	Details
1	$\frac{E}{P} = \frac{1+\omega\frac{E_0}{P}}{1+\omega\frac{E_0}{P}+\frac{P}{E_0}}$	$\omega_g = 0.5$ $\omega_f = 2.0$	Model developed and calibrated by Zhang et al. (2001). Calibrated using 240 global river basins. ω_f is calculated using natural and plantations data, and ω_g is calibrated using grassland and cropland data.
2	$\frac{E}{P} = \frac{1+\omega\frac{E_z}{P}}{1+\omega\frac{E_z}{P}+\frac{P}{E_z}}$	$\omega_g = 0.5$ $\omega_f = 2.0$	As Model 1. E_0 is also calibrated (E_z). $E_{z,grass} = 1100$, $E_{z,trees} = 1410$
3	$\frac{E}{P} = 1 + \frac{E_0}{P} - (1 + (\frac{E_0}{P})^{\omega})^{\frac{1}{\omega}}$	$\omega_g = 2.55$ $\omega_f = 2.84$	Model developed by Fu in 1981, calibrated by Zhang et al. (2004). Calibrated based on 200 Australian and 270 worldwide river basins. ω_f and ω_g are calibrated using river basins ≤ 75 % forest and grassland cover.
4	$\frac{E}{P} = 1 + \frac{E_0}{P} - (1 + (\frac{E_0}{P})^{\omega})^{\frac{1}{\omega}}$	$\omega_g = 2.28$ $\omega_f = 2.83$	Model developed by Fu in 1981, calibrated by Zhang et al. (2004). Calibrated with 1420 river basins with forest (ω_f, and grassland and cropland (ω_g) cover.
5	$\frac{E}{P} = 1 + \frac{aE_0}{P} - (1 + (\frac{aE_0}{P})^{\omega})^{\frac{1}{\omega}}$	$\omega_g = 1.7$ $\omega_f = 3.1$	Model developed by Fu in 1981, calibrated by Teuling et al. (2019). Calibrated based on European Lysimeter data. Teuling et al. (2019) introduced the adjusted potential evaporation ($aE_0 = 1.6E_0$) to account for lysimeter observations above the energy line.
6	a) $\frac{E}{P} = 1 - exp(-\frac{\omega E_0}{P})$	$\omega_g = 0.977$ $\omega_f = 1.248$	Mean E calculated from five Budyko equations of: a) Schreiber, b) Ol'DeKop, c) Turc, d) Budyko, and e) Zhang. Oudin et al. (2008) introduced ω in these equations to capture the vegetation effects. The formulas are calibrated using data from 1508 river basins in United States, United Kingdom, Sweden and France.
	b) $\frac{E}{P} = \omega\frac{E_0}{P}tanh((\omega\frac{E_0}{P})^{-1})$	$\omega_g = 0.767$ $\omega_f = 0.910$	
	c) $\frac{E}{P} = \frac{1}{(1+(\omega\frac{E_0}{P})^{-2})^{0.5}}$	$\omega_g = 0.831$ $\omega_f = 1.025$	
	d) $\frac{E}{P} = (\frac{E_0}{P}(1 - exp(-\omega\frac{E_0}{P}))tanh(\frac{P}{E_0}))^{0.5}$	$\omega_g = 0.762$ $\omega_f = 1.125$	
	e) $\frac{E}{P} = \frac{1+\omega\frac{E_0}{P}}{1+\omega\frac{E_0}{P}+\omega+\frac{P}{E_0}}$	$\omega_g = 0.682$ $\omega_f = 1.404$	

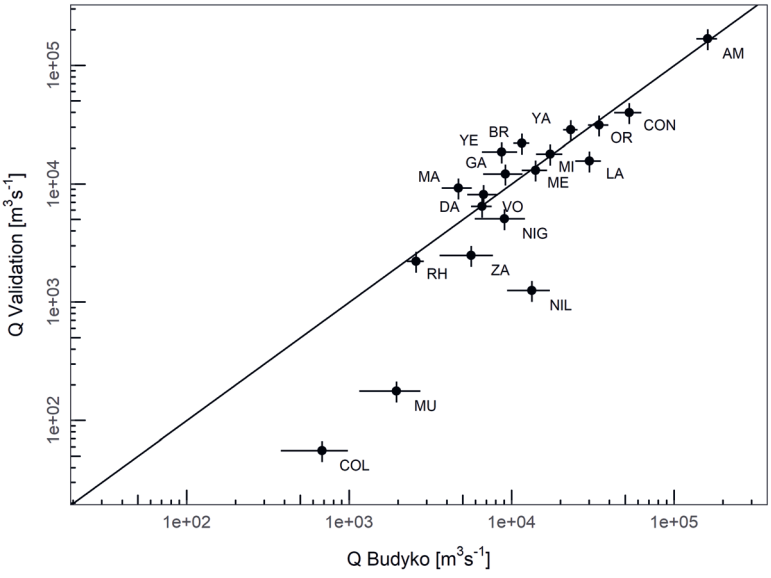

Figure 5.3: Validation of the streamflow calculation. Model ensemble mean versus observed streamflow (Q) measurements (GRDC, n.d.) for 19 validated river basins. The error bars for Q Budyko indicate the standard deviation over the six Budyko models. The error bars for Q validation indicate a 20 % error. The river basins are: Amazon (AM), Brahmaputra (BR), Colorado (COL), Congo (CON), Danube (DA), Ganges (GA), La Plata (LA), Mackenzie 18 (MA), Mekong (ME), Mississippi (MI), Murray-Darling (MU), Niger (NIG), Nile (NIL), Orinoco (OR), Rhine (RH), Volga (VO), Yangtze (YA), Yenisei (YE), and Zambezi (ZA).

also calculated using a monthly timestep for the river basins of the Mississippi, Orange, and Ganges-Brahmaputra (Fig. 5.4). When using a monthly time step, the total yearly evaporation is disaggregated over twelve months, relative to the magnitude of evaporation for each month in the ERA5-reanalysis data (Muñoz Sabater, 2019, accessed January 2020). The monthly and yearly calculations have similar patterns and values, but there are differences of up to $1\,\mathrm{mm\,yr^{-1}}$.

In our approach we assume that increased evaporation will amplify the current evaporation recycling patterns. It is commonly assumed that land-cover change impacts evaporation recycling (patterns), but the effects of land-cover change on evaporation recycling processes are poorly understood and difficult to determine (Spracklen et al., 2018). There is currently no possibility to include these processes at high resolution at global scale, and therefore we use the UTrack dataset as the best available option.

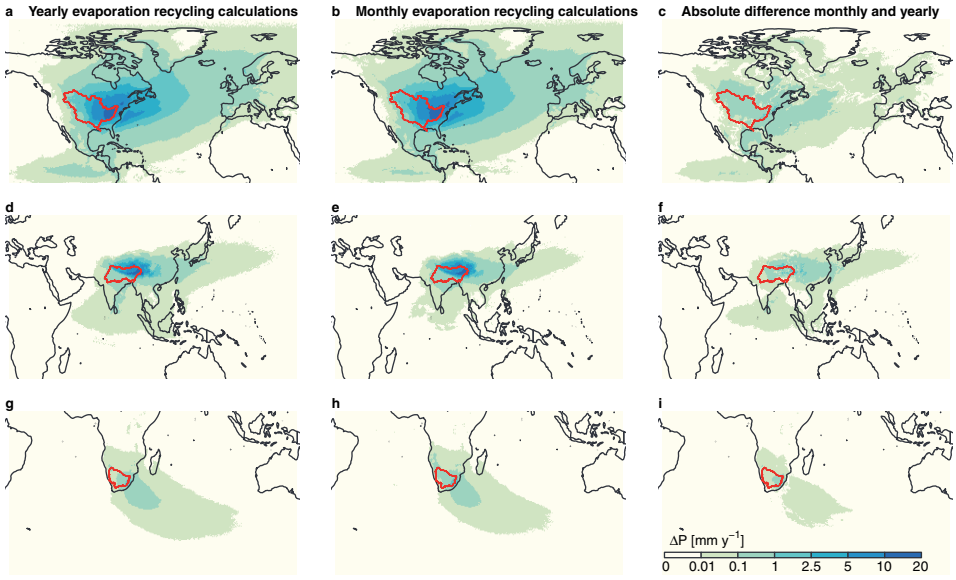

Figure 5.4: Difference between yearly and monthly calculation of evaporation recycling from three river basins. In our study, we present the results based on a yearly evaporation recycling calculation. This figure displays the difference between the applied yearly calculation and a monthly calculation of evaporation recycling. For the yearly calculation, the monthly evaporation recycling from the UTrack dataset is aggregated to yearly evaporation recycling. For the monthly calculation, the increase in evaporation (from Budyko) is disaggregated over twelve months, relative to the local monthly evaporation from the ERA5-reanalysis product (Muñoz Sabater, 2019, accessed January 2020). Both the yearly and the monthly calculation in this figure display the yearly aggregated evaporation recycling. The figures display the increase in precipitation following an tree-restoration induced increase in evaporation from three different river basins: (a-c) Mississippi basin, (d-f) Ganges-Brahmaputra basin, and (g-i) Orange basin. (a, d, and g) display the yearly calculation, (b, e, and h) display the monthly calculation, and (c, f, and i) display the absolute difference between the monthly and yearly calculation.

5.3 Results

5.3.1 Impact on water fluxes with and without evaporation recycling

Under the current precipitation and potential evaporation, large-scale tree restoration would lead to a direct local increase in terrestrial evaporation of on average $8.2 \pm 5.5\,\mathrm{mm\,yr^{-1}}$, which is an increase of 1.2 % (Fig. 5.5a). The standard deviation characterizes the variation over the six Budyko models. The sign of the average evaporation effect is clear, but the underlying distribution is heavily skewed, and the direct increase in evaporation can exceed

$250\,\mathrm{mm\,yr^{-1}}$ in the South American tropical forest. When we include the indirect effects of increased evaporation on the atmospheric moisture content and precipitation, we find that 68 % of this extra evaporated water would rain out over land (Fig. 5.5b). Following tree restoration, terrestrial precipitation would increase with $4.8 \pm 3.1\,\mathrm{mm\,yr^{-1}}$ on average due to recycling of increased evaporation (an average increase of 0.7 %). While the patterns in the direct evaporation effect are determined by the patterns in tree restoration and local climate, the indirect evaporation-recycling effect of tree restoration on precipitation happens at the continental scale and is determined by atmospheric circulation.

Without the effect of evaporation recycling, global mean water availability would decrease by $8.2 \pm 5.3\,\mathrm{mm\,yr^{-1}}$ (Fig. 5.5c). When we include the process of evaporation recycling on the water budget calculations (thus taking into account that the evaporated water will partly rain out over land), water availability would decrease by $5.3 \pm 5.6\,\mathrm{mm\,yr^{-1}}$ (Fig. 5.5d). There is however a large spatial variability with regions showing a decreasing (up to 38 %) or increasing (up to 6 %) water availability. The United Kingdom for example has a high tree restoration potential and therefore a high increase in evaporation. There is however low evaporation recycling due to the dominant westerly moisture transport from the country towards Eurasia and due to a low tree restoration potential upwind in the Atlantic Ocean. Therefore, streamflow in the United Kingdom will decrease more substantially as compared to the other regions. The low latitudes and the Tibetan Plateau, however, show an increase in water availability. In these regions, local evaporation recycling is high, for example due to strong convection above the tropical forest, or strong orographic lift in the mountainous regions, and travel distances of the atmospheric moisture are relatively short (Tuinenburg et al., 2020b; Van Der Ent and Savenije, 2011). The results suggest that for half of the Earth's surface (47 %), the indirect water cycle effects of large-scale tree restoration could offset the direct evaporation effects, thus resulting in slight increases in water availability rather than decreases (Fig. 5.6).

5.3.2 Global tree restoration has varying effects on streamflow

To evaluate the impacts of tree restoration at the river-basin scale, we aggregate the direct effects (via increased evaporation) and indirect effects (through increased precipitation) for 21 large river basins. For all the river basins, enhanced evaporation reduces streamflow (up to 9 %), but streamflow reduction can be close to zero, when increasing precipitation outweighs the increasing evaporation (Fig. 5.7).

The increased precipitation is a combination of local recycling (when evaporated water rains out within the same river basin) and recycling of water from other, further upwind, regions. For several tropical basins with a high local evaporation recycling, the high recycling nearly completely compensates for the loss of water through evaporation. Most river basins with a low wetness index (water-limited basins) have a low tree restoration potential simply because arid regions can only support tree growth if there is significant

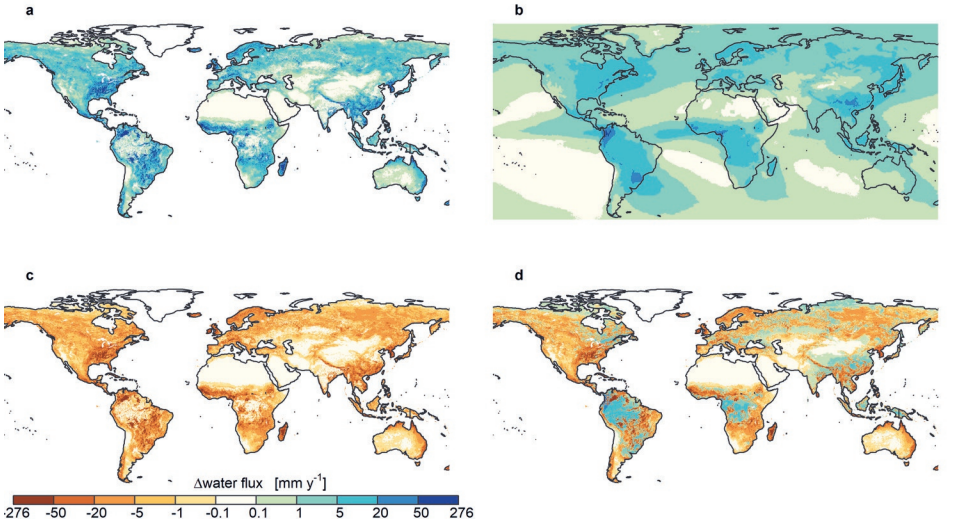

Figure 5.5: Impacts of forest restoration on water fluxes and water availability. (c-f) show the absolute annual change in water fluxes after tree restoration. Change in: (c) evaporation, (d) precipitation, (e) water availability without evaporation recycling, and (f) water availability with evaporation recycling. Note that (e) is the inverse of (c): without the feedback of evaporation recycling, the local increase in evaporation equals the local decrease in water availability. All maps display the 0.1 ° mean values, except for (b) which displays the 0.5 ° mean value.

groundwater convergence (Roebroek et al., 2020). These arid river basins have a small absolute change in evaporation and precipitation. Overall, following tree restoration, streamflow will decrease for most of the world's important river basins, despite the indirect effect of evaporation recycling.

5.3.3 Implications for water availability

Our study shows that large-scale tree restoration will shift water availability regionally. The hot spots for forest restoration could face a strong reduction in the water availability (Fig. 5.8a) because water supply by evaporation recycling is not enough to compensate for water loss through evaporation. On the other hand, regions with no or limited tree restoration potential could see an increase in water availability due to the lateral transport of evaporated water into the region. This shows the importance of a proper strategical planning of forest restoration projects (Ellison et al., 2019). Forest restoration could locally enhance precipitation through land-atmosphere interactions (Meier et al., 2021), but these effects are complex and not included in our calculations. This enhanced precipitation could partly offset the high water loss in regions with high tree restoration.

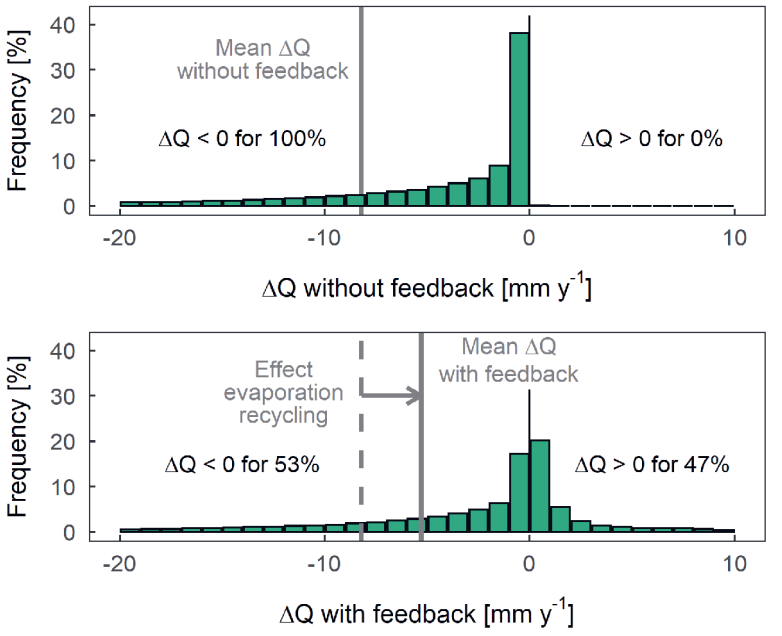

Figure 5.6: Water availability with and without streamflow A histogram of the distribution of the global changes in water availability without and with evaporation recycling. 89 % (without recycling) and 91 % (with recycling) of the data fall within the displayed range of $-20\,\mathrm{mm\,yr^{-1}}$ to $10\,\mathrm{mm\,yr^{-1}}$.

Another important finding is that this tree restoration scenario could further decrease annual water availability in several regions that are already facing water scarcity (Fig. 5.8b). Rainfall supply for some of these regions is largely of oceanic origin (Tuinenburg et al., 2020b; Van Der Ent and Savenije, 2011) and these regions therefore, do not, or only to a small extent, see an increase in precipitation after restoration. On the other hand, this tree restoration scenario has the potential to increase water availability in currently water scarce regions. Despite that several regions could see a decrease in annually aggregated water availability, local water availability in the dry season could actually increase. Trees are known to increase soil porosity and soil organic carbon (Lal, 1996). Therefore, tree restoration, especially in treeless regions, promotes the infiltration capacity and the soil water storage capacity, and reduces the overland flow (Bargués Tobella et al., 2014; Ellison, 2018; Ellison et al., 2017; Ilstedt et al., 2016). After tree restoration, the soils could thus potentially store more water, that would slowly be released during the dry season (Ellison et al., 2019). The true impact of tree restoration on water availability in the water scarce regions may thus not be necessarily negative, and the impact depends on combination of various aspects with high seasonal variability.

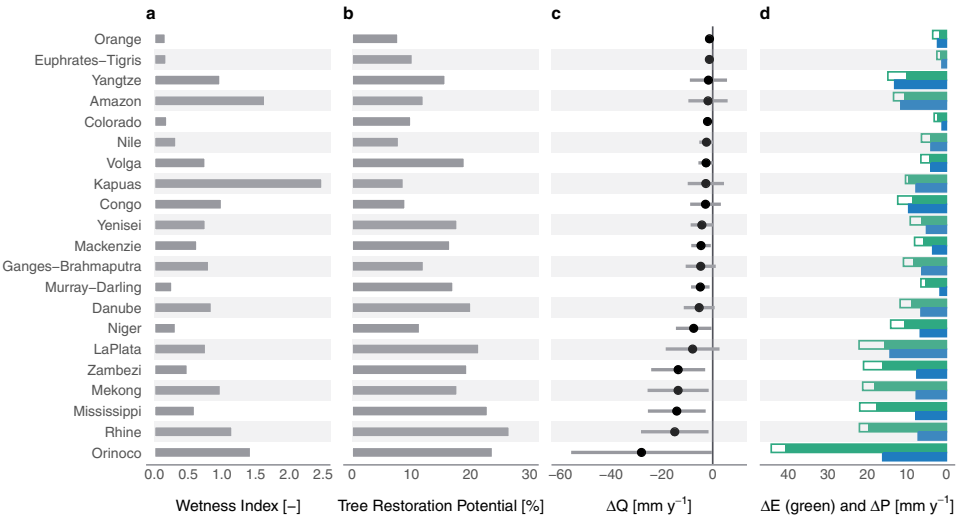

Figure 5.7: Impacts of global tree restoration on hydrological fluxes in selected river basins. (a) mean wetness index (potential evaporation over precipitation ratio) and (b) tree restoration potential for each river basin. (c) The change in streamflow (ΔQ) with evaporation recycling. The dots indicate the mean river basin change in streamflow, and the bars indicate one standard deviation (the variation over the six Budyko models). (d) The change in evaporation (ΔE in green) and precipitation (ΔP in blue). The green bar indicates the increase in evaporation without evaporation recycling, and the green line indicates the increase in evaporation with evaporation recycling (the increase in evaporation when taking into account the increased precipitation). The river basins are sorted from the lowest to the highest decrease in streamflow. The river basin boundaries are taken from Lehner et al. (2008)

5.4 Discussion

The presented results are calculated using state-of-the-art data and methods, but several feedbacks and processes are not included in the analyses. Our approach does not account for the potential impacts of increased tree cover on atmospheric circulation and land-atmosphere interactions. Tree restoration could locally enhance convergence, cloud cover and precipitation and change the travelling direction and distance of atmospheric moisture (Ellison and Ellis, 2020; Meier et al., 2021; Spracklen et al., 2018; Xu et al., 2021). Research suggests that forests could even impact large-scale wind patterns and draw atmospheric moisture from the oceans to the continents (Makarieva and Gorshkov, 2007; Sheil and Murdiyarso, 2009), although the importance of this effect is still debated. These different feedbacks are poorly understood and difficult to incorporate in the present study, because most evaporation recycling models rely on meteorological reanalysis data, which are only valid under current land-cover conditions. The land-atmosphere interactions and potential

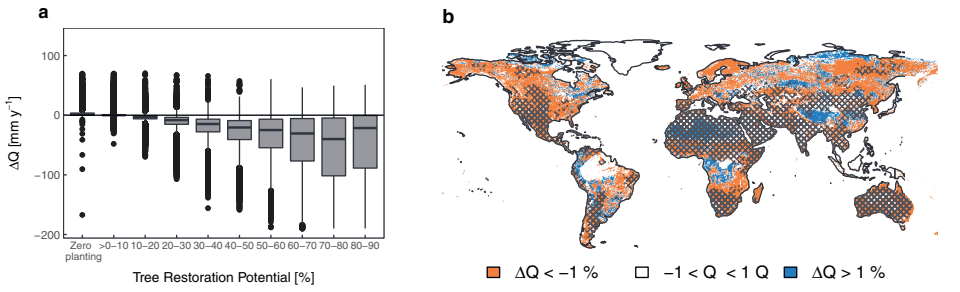

Figure 5.8: Implications of the percentage restored area and the implications for water scarcity. (a) Water availability could decrease in 'hot spots for tree restoration'. (b) Water availability will decrease in several regions that currently face water scarcity: the colour indicates whether local water availability will decrease (red) or increase (blue) following the studied tree restoration scenario. The cross-hatched regions currently face freshwater scarcity for at least three months per year, and the bold hatched regions face freshwater scarcity for at least nine months per year (Mekonnen and Hoekstra, 2016). Note that we quantified the change in water availability on an annual timescale. The sign of change could vary seasonally, and water availability could, for example, decrease on a yearly basis, but remain equal, or even increase in the dry season.

changes in atmospheric circulation could impact the exact location and magnitude of increased precipitation. These processes could partly, but not fully, compensate for the enhanced evaporation, and this will unlikely affect the main results of this study, as presented below. In addition to data-driven studies, coupled land surface models have been used to reconstruct the effects of land-cover change on water availability (Swann et al., 2018; Yosef et al., 2018). Because of the large number of model parameters and feedbacks, their estimates of local impacts are less constrained by observations, and as a result more uncertain.

Furthermore, this study presents the impact of tree restoration under current climate conditions. However, global warming, and the tree restoration itself, will shift temperature and precipitation patterns (Bonan, 2008; Perugini et al., 2017), and these are not considered in our analyses. Higher temperatures could reduce the global tree restoration potential with 25 % towards 2050. Furthermore, higher temperatures will increase the potential evaporation and annual precipitation (Konapala et al., 2020), which causes a vertical shift in the Budyko framework (Fig. 5.2c). Climate warming will impact the atmosphere's dynamics which possibly results in a poleward shift of the Hadley cells and storm tracks, and a shift in magnitude of the jet streams (Coumou et al., 2018; Jennifer and Natasa, 2015; Shaw, 2019; Vecchi et al., 2006). The shifting global circulation will impact the patterns and magnitude of evaporation recycling.

5.5 Conclusions

This is the first study that estimated the effects of global large-scale tree restoration on water fluxes, including evaporation recycling. The results show that tree restoration shifts water availability and streamflow both at local and continental scales, and that the patterns of increasing and decreasing water availability are complex throughout the globe. Following tree restoration, the increased precipitation could increase water availability locally, however, we find a global net loss of water availability over the continents. These conclusions are consistent with other data-driven or model-based studies to the effects of land-cover change on water fluxes (Meier et al., 2021; Swann et al., 2018). We stress that future tree restoration strategies should consider the hydrological effects. Applying smart tree restoration strategies are necessary to secure the water supply locally and remotely or enhance the water supply in water-scarce regions.

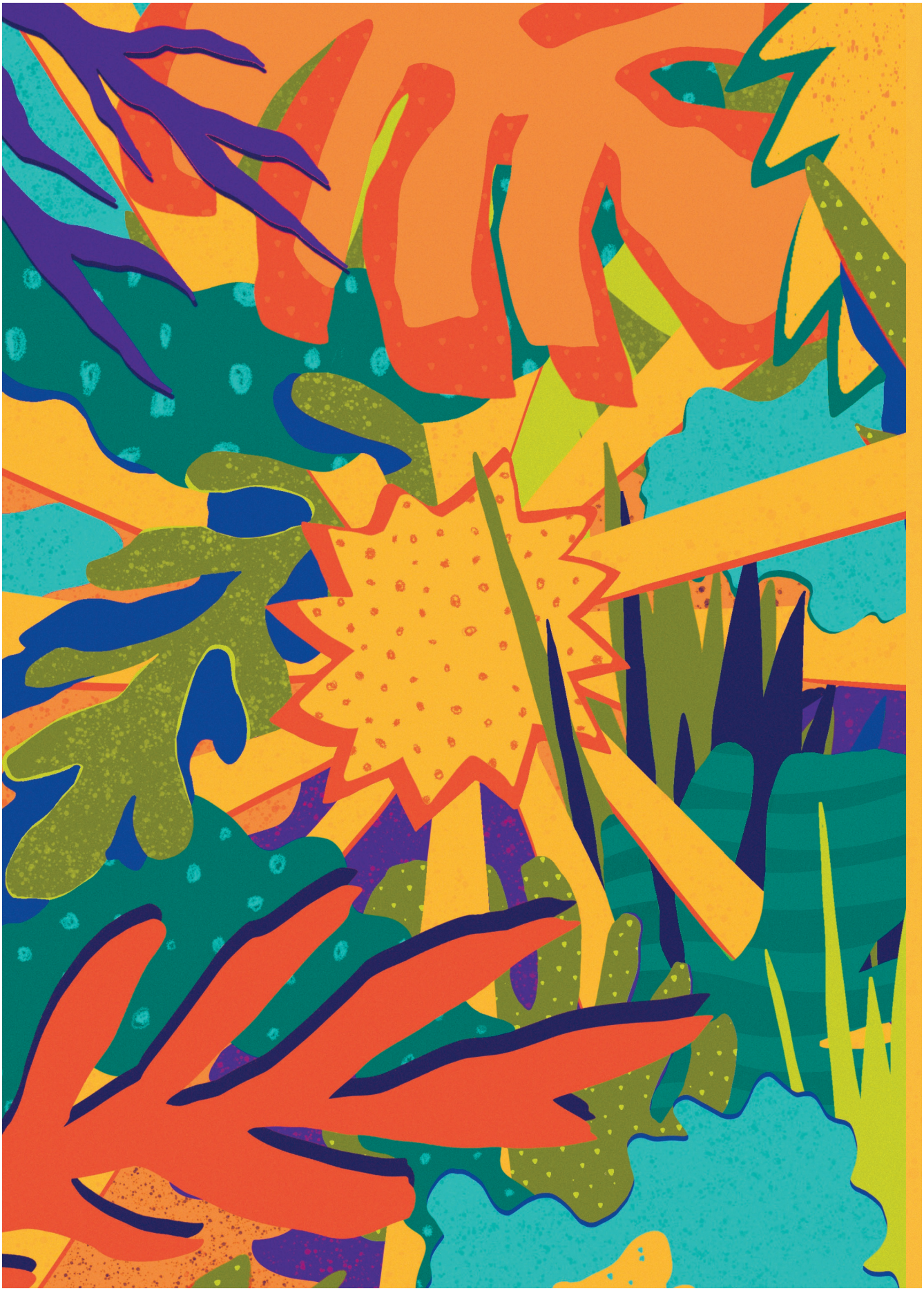

Chapter 6

Synthesis

6.1 Linking evaporation and vegetation characteristics

This thesis studied the **link** between evaporation and vegetation characteristics. The link means that there is a relation between those two, but it does not specify whether we can speak of causality or correlation. Correlation and causation are related, but correlation does not imply causation. In the first part of this thesis, we studied the correlation between evaporation or transpiration and vegetation. We hypothesised to find a positive correlation between the NDVI or LAI and evaporation, because the interception evaporation, the surface conductance, and the aerodynamic roughness increase with leaf area, and these factors generally increase evaporation (Farley et al., 2005). However, water availability could be a confounding factor, because both evaporation and LAI increase with water availability (Iio et al., 2014; Roebroek et al., 2020). In the second part of this thesis, we assume that changes in the vegetation characteristics cause a change in the evaporation.

In this thesis, we use **evaporation** data acquired using different measurement techniques. Every research question requires data at a specific spatial and temporal scale, for a specific vegetation type and climate. The different measurements discussed in this thesis all have distinct characteristics, strengths and weaknesses which makes them useful to answer specific research questions. In chapter 2, measurements of the sap velocity (the velocity of the sap stream in the tree trunk) were used. The total volume of the sap stream equals the total transpiration of a tree. The sap velocity measurements were performed continuously on a single tree, and they are the best option to study tree- differences in transpiration. In chapter 3 ecosystem evaporation measurements from eddy covariance flux towers were used. These flux tower measurements encompass a spatial scale of $100-1000$ m in two directions (Kim et al., 2006) and we scaled the measurements to yearly total evaporation. These yearly mean data reflect the year-to-year availability of energy and water for (ideally) one vegetation and soil type, but do not include any information on temporal or seasonal variability. In chapter 4 similar flux tower measurements of evaporation were used, but on a daily timescale. These measurements thus reflect the day-to-day variability in radiation, water availability, and stomatal control, as well as the seasonal variability related to temperature and vegetation characteristics. In chapter 5, catchment-scale measurements of evaporation were used, derived from the difference between the precipitation and the streamflow. These measurements reflect the long-term catchment evaporation and climate characteristics for a certain landscape and vegetation cover.

We studied several **vegetation characteristics** and vegetation types. Our main focus is on the NDVI and the LAI that reflect the leaf chlorophyll content and leaf and vegetation structure (referred to as the 'vegetation green biomass'). The LAI is derived from a radiative transfer model or empirical relation with NDVI (when the radiative transfer

model fails). Other applied remote sensing indicators reflect the vegetation green biomass (the VCI), moisture content (the NDMI), or surface temperature or vegetation stress (the LST, TCI, and LST-Ta). Furthermore, we studied various vegetation types that all differ in rooting characteristics, leaf characteristics (e.g. evergreen versus deciduous species), and drought coping strategies.

6.2 Main findings

In chapter 1.5, we defined two main research objectives and in this chapter, we discuss the main findings for both objectives.

Research Objective 1: Study the link between ground-based observations of evaporation and satellite remote sensing observations of vegetation

In chapter 2 and chapter 3 we investigate the correlation between satellite remote sensing observations of vegetation green biomass and ground-based measurements of evaporation. Several earlier studies found a (strong) positive correlation between the NDVI or LAI and evaporation or transpiration (Nagler et al., 2005; Szilagyi, 2000). Based on these studies and the effect of LAI on evaporation (through the albedo, interception and the conductance), we hypothesised to find a positive correlation between vegetation green biomass and evaporation. The chapters 2 and 3 used different measurements of vegetation and evaporation, and they differed in their study area and vegetation type, and spatial and temporal resolution of the data. Chapter 2 showed that the correlation between sap velocity and NDVI is time-variable and inconsistent. At the start of the growing season there is a positive correlation, which changes into a negative correlation during the rest of the growing season. And during the drought in 2015, there was no correlation. Chapter 3 showed that there was a positive correlation between evaporation and LAI for grassland, savanna and evergreen broadleaf forest, while there was no correlation between evaporation and LAI for deciduous broadleaf forest and evergreen needleleaf forest.

Chapter 4 investigated how a drought-induced reduction in surface conductance was reflected in the thermal infrared and optical satellite indices. For the grassland sites, the reduction in surface conductance was reflected in both thermal infrared and optical remote sensing data. For the forest sites, on the other hand, the thermal infrared did reflect the drought response while the optical indices did not reflect the drought response.

These three chapters thus conclude that, under several conditions, the spatial or temporal variability in vegetation green biomass links with the spatial or temporal variability in evaporation or transpiration, but under other circumstances, there is no spatial or temporal link between vegetation green biomass and evaporation or transpiration. Below, a few of these circumstances are discussed.

- Temporal variability In chapter 2, for a deciduous broadleaf forest, we found a positive correlation between the NDVI and sap velocity over time: the vegetation green-up coincided with the increase in evaporation. In chapter 3, we found a positive correlation between intra-anual variability in LAI and evaporation for savanna, and part of the grassland, forest sites. Thus in several cases, the intra- and inter-annual changes in evaporation were reflected in the vegetation green biomass.

- Spatial resolution of the remote sensing data In chapter 2 we explained the time-variant and inconsistent correlation as the result of the high spatial correlation of the data. However, in chapter 3, with a similar vegetation type, but a coarse resolution spatial, and yearly mean, data, also no correlation between LAI and evaporation was found. This suggests that the high-spatial resolution (alone) did not explain the absence of a consistent, positive correlation.

- Vegetation type In both chapters 2 and 3, the link between vegetation green biomass and sap velocity or evaporation were negative or insignificant in temperate forest, and in chapter 3, the link between LAI and evaporation was insignificant in the boreal forest, but significant in the tropical forest, savanna and grassland. The effect of LAI on evaporation is two fold, the soil evaporation decreases with increasing LAI, while the interception evaporation and the transpiration increase with increasing LAI. Therefore, the LAI has a different impact on the total evaporation in ecosystems with a high and low LAI. Furthermore, the vegetation types are found in different climates.

- Water availability Chapters 2, 3, and 4 indicate that both climatically water availability (aridity) and droughts play an important role in the occurrence, strength, and slope of the correlation between vegetation green biomass and evaporation or transpiration. In chapter 3 a significant positive correlation between evaporation and LAI was found for the water-limited savanna and grassland, and no significant correlation was found for the energy-limited temperate and boreal forest. Furthermore, for arid regions, the correlation had a steeper slope compared to the humid regions. In chapter 2, the correlation between NDVI and sap velocity changed during the drought. Early in the drought, stomata closed to prevent further water loss, which decreased evaporation. The vegetation's greenness, biomass, or leaf area was however was not affected by the drought. Therefore, the negative correlation before the drought, changed into 'no correlation' during the drought. Chapter 4 showed that the effect of drought on evaporation and NDVI was different for forest and grassland. The grassland and forest experienced a similar reduction in stomatal conductance. While the grassland NDVI did reflect this change in vegetation's functioning, the forest NDVI did not reflect this.

- Soil characteristics In chapter 2 sap velocity decreased during the summer drought in 2015, and the rate of change depended on the geology. Trees on the sandstone

maintained high sap velocity, while sap velocity was reduced for trees on the marl and schist. This was explained by the higher water storage capacity of the sandstone region. Geology did not however impact changes in the NDVI. This shows that the different geologies changed the slope of the correlation between the NDVI and evaporation.

- Seasonality in chapter 3, the spatial correlation between NDVI and evaporation changed from the spring to the summer season. While the correlation was positive in spring, the correlation was negative or absent in summer, independent of the water-limitation conditions.

In summary, there are many different aspects that impact the correlation between vegetation green biomass and evaporation or transpiration, and most of these aspects can be linked to the availability of water. The results suggest that both the aridity and short-term changes in water availability (droughts) play an important role in the occurrence, strength, and slope of the correlation between evaporation and the vegetation green biomass. Under water-limited conditions, both the vegetation green biomass and the evaporation are strongly controlled by water availability (commonly measured as the root zone soil moisture or precipitation) (Iio et al., 2014; Roebroek et al., 2020). Therefore, with a slight increase in precipitation, both the LAI and evaporation increase. This con-founding effect of water availability likely explains (part of) the correlation between evaporation and vegetation green biomass in water-limited regions. Furthermore, in water-limited environments, there is a stronger biological control of evaporation, through stomatal regulation. In contrary, in the energy-limited environments, leaf area and evaporation are less strongly controlled by water availability, and also the biological control is less prominent. The importance of water availability does however not fully explain why we did find a positive correlation for the tropical forest. Other explanations such as the albedo or the saturation of the remote sensing signal in forest may play an additional role but also these factors do not explain why there is a strong positive correlation in the tropical forest.

From the results of this thesis, a positive correlation between evaporation and the vegetation green biomass seems to be an exception rather than the rule. A more extensive analyses at different spatial and temporal scales and in different vegetation types, should provide a better insight in when satellite measurements of the vegetation can be used to monitor evaporation. An interesting follow-up hypothesis would be 'The vegetation green biomass reflects variability in evaporation only when and where both their spatial and temporal variability are driven by water availability'.

Research Objective 2: Study the effect of drought and land-cover change on evaporation

Europe and other parts of the terrestrial surface will face an increase in the duration, intensity and occurrence of droughts in a warmer future (Böhnisch et al., 2021; Dai, 2013).

In 2003, 2010, and 2018, Central Europe experienced three major summer droughts and these impacted the carbon sink function of forests, heat waves, river runoff, crop yield, and forest mortality, as well as the economy and human health (Beillouin et al., 2020; Naumann et al., 2021; Orth and Destouni, 2018; Senf et al., 2020; Stanke et al., 2013; Vicca et al., 2016). Chapter 4 showed how evaporation and the surface conductance changed during the Central European drought of 2018. Our six study sites experienced a $50-70\,\%$ reduction in surface conductance and a reduction in evaporation of up to $47\,\%$ (and a negligible reduction in evaporation for two sites). The drought had a different impact on temperate forests and grasslands, which was in line with the hypothesis. While forests generally adopt a more conservative behaviour, and close their stomata to prevent depletion of the soil water, grasslands keep evaporating water at high rate, which results in a high above-ground biomass loss when the soil moisture content drops considerably (Graf et al., 2020; Teuling et al., 2010; Wolf et al., 2013). The focus of chapter 4 is Europe's temperate climate zone, where vegetation growth and evaporation are usually energy-limited rather than water-limited. The response described here is likely different in other climate zones, for example where the vegetation is more adapted to water limitation, and where severe multi-year droughts occurred, such as the Australian Millennium drought and the 2011 – 2017 California drought.

Tree restoration is a hot topic in climate change mitigation studies, as an option to reduce the atmospheric CO_2 content (Bastin et al., 2019). In chapter 5, the effect of large-scale tree restoration on evaporation was studied. The chapter showed that tree restoration could locally increase evaporation with up to $250\,\mathrm{mm\,yr^{-1}}$, ($41\,\%$). On average, terrestrial evaporation could increase with $8.2\,\mathrm{mm\,yr^{-1}}$, ($1.2\,\%$). The increase in evaporation increases with the percentage surface area reforested (Brown et al., 2005) and is highest in humid regions.

Also increased atmospheric CO_2 concentrations and global warming will have a significant impact on future evaporation. The increased atmospheric CO_2 concentration could increase the stomatal resistance to evaporation, while at the same time increasing the leaf area index (Piao et al., 2007), and the increased temperature will increase the potential evaporation (Milly and Dunne, 2016). So far, it remains unclear whether the sum of these processes will increase or decrease future water fluxes and water availability (Milly and Dunne, 2016; Roderick et al., 2015). The combined impact of climate change and land-cover change on evaporation will differ per region and will differ over time (Bao et al., 2019; Guo et al., 2014; Heo et al., 2015; Li et al., 2017; Teuling et al., 2019; Yan et al., 2016). Yan et al. (2016) for example showed that for a catchment in northern China, future land-cover change could enhance the effects of climate change in half of the year, and reduce it in the other half of the year. This makes it important to assess the effects of land-cover change and climate change combined, in order to anticipate the future changes in evaporation, as well as how these changes propagate further into the water, energy, and carbon cycle.

6.3 The LAI and land-atmosphere fluxes

The LAI is a key variable in land-atmosphere fluxes because of it's effect on photosynthesis, evaporation, and transpiration. Therefore, the LAI and NDVI are frequently used to estimate evaporation or to study the vegetation control on evaporation (Crowhurst et al., 2021; Padrón et al., 2017; Wang et al., 2014).

This thesis suggests that, in energy-limited forests, evaporation does not increase with LAI. However, paired catchment studies and lysiemeter data suggest that forests (with a high LAI) generally have a higher evaporation than grasslands, also in energy-limited forests. Thus, at certain spatial-temporal scales, the LAI (alone) cannot be used to explain the difference between forest and grassland evaporation. The LAI is intuitive and freely available through for example the MODIS dataset, which makes it an attractive data source. It is however important to remain critical towards what the LAI does and does not controls or reflects.

6.4 Satellite-based evaporation estimations

Satellite remote sensing data provides a great opportunity to estimate evaporation over larger areas, at high and low resolution, including inaccessible regions, and with minimal costs. This makes the satellite data a popular data source for evaporation monitoring. Several satellite-based and hybrid methods exist to estimate or scale evaporation, and most of them make use of the NDVI or LAI. This thesis concludes that a statistical correlation between evaporation and satellite measurements of NDVI and LAI is the exception rather than the rule and in the current paragraph we explore how this conclusion impacts evaporation monitoring from space. Commonly used methods for estimating or scaling evaporation include:

1. The NDVI and LAI are used to calculate the fractional vegetation cover to separate between evaporating surfaces (the soil and the vegetation) and transpiring surfaces. A model based on potential evaporation, a crop factor, and a water stress factor are used to calculate the soil evaporation and transpiration separately to estimate the total evaporation (e.g. Chiesi et al., 2013; Maselli et al., 2014).
2. The NDVI is used to derive a spatio-temporal crop coefficient, optionally with a water-stress term for arid or water-stressed conditions (e.g. Hunink et al., 2017; Kamble et al., 2013; Mutiibwa and Irmak, 2013; Park et al., 2017).
3. Surface energy balance models use the NDVI to parameterize the aerodynamic roughness length and displacement height, which are needed to calculate the sensible heat flux (Bastiaanssen et al., 1998; Su, 2002). Penman-Monteith based models use the NDVI to parameterize the surface conductance (Zhang et al., 2009).

4. The surface temperature - NDVI triangle is used to derive a soil moisture stress scalar to constrain the evaporation. If pixels from different surface conditions are plotted in an LST-NDVI scatterplot, they form a triangle pattern. The evaporative fraction and the Priestley–Taylor coefficient – the ratio potential evaporation over equilibrium evaporation – can be parameterized from that triangle. The evaporation fraction and Priestley-Taylor coefficient are used to calculate the evaporation (e.g. Jiang and Islam, 2001; Mallick et al., 2009; Zhu et al., 2017).

5. NDVI or LAI are used as a proxy for stomatal conductance or absorbed photosynthetically active radiation, to scale in situ measured evaporation over larger regions (e.g. Kim et al., 2006; Rahman et al., 2001).

A few of these methods are purely empirical and rely on a positive correlation between NDVI or LAI and evaporation. However, such correlations are co-incidental and they are unable to explain the ecophysiology of evaporation. Inherent to empirical models, these models require a location and time specific parameter. In this thesis, several aspects have been discussed that impact these parameters. First, we show that these models unlikely work for large spatio-temporal scale monitoring of evaporation in energy-limited forests. Second, evaporation differs between vegetation types, despite that they have a similar LAI or NDVI. Third, for a seemingly similar vegetation cover and climate, the hidden geological factors or seasonality could impact the correlation between vegetation and evaporation.

The physically based models do not explicitly rely on a positive correlation between the evaporation and vegetation green biomass, but they do for example use vegetation indices to parameterise the surface and aerodynamic conductance. This is an oversimplification of different internal processes and this needs to be done carefully. Liu et al. (2007) for example showed that these parameterisation can create large errors in the estimated evaporation. The STIC model (Surface Temperature Initiated Closure model) (Mallick et al., 2014; Mallick et al., 2018) is an interesting alternative to these models. The model integrates the land surface temperature into the Penman-Monteith model and does not require any parameterisation of the aerodynamic and surface conductance when calculating the evaporation. In summary, satellite-based estimations or scaling of evaporation are not trivial and it is important to remain critical to when and where these models can or should not be used.

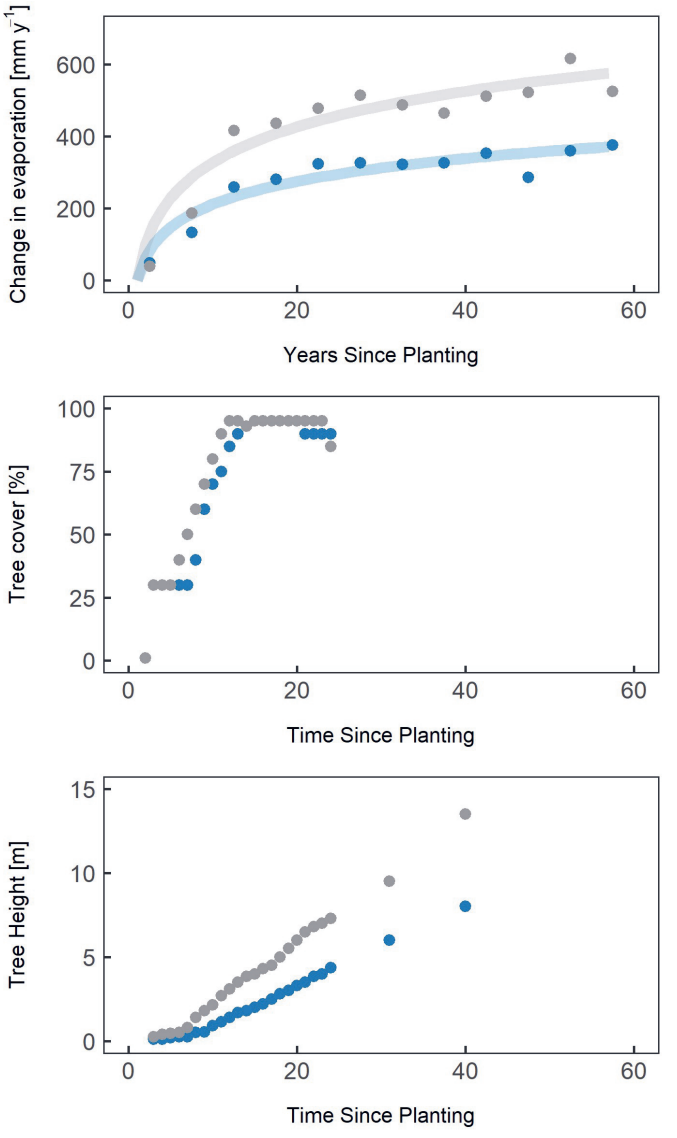

Figure 6.1: Evaporation and vegetation development after forest restoration takes several decades. The increase in evaporation with forest development in a lysiemeter continues for many decades (the dots represent the five year mean value). The forest reached a maximum tree cover of 95% after 14 years, and the tree height increased during the first 40 years, and for the further years, no data was available. The deciduous forest (mainly oak) is depicted in blue, and the pine forest is depicted in grey. Data from the Castricum Lysiemeters (Stuyfzand, 1984; Van der Hoeven, 2011).

Complexity of satellite-based evaporation monitoring under global change

Chapter 2 and 4 of this thesis showed that a statistical correlation between evaporation and vegetation green biomass changed during a drought: while the forest evaporation decreased, the forest's looks, such as the leaf colour, the structure, or the leaf angle, remained unchanged. The vegetation's optical indices did therefore not reflect the change in evaporation. Similarly during a land-cover change or after a forest disturbance, the vegetation's looks do not reflect the evaporation and transpiration. The response time of evaporation to a land-cover change is several decades (Teuling and Hoek van Dijke, 2020), and this long time results from several below-ground and above-ground vegetation characteristics that develop over different time scales (Fig. 6.1). For example, the recovery time of LAI after disturbance is around 42 years, while the response time of below-ground biomass is around 96 years (Fu et al., 2017). Furthermore, satellite-based vegetation characteristics such as the NDVI and LAI reflect various above-ground aspects, that do not all impact the evaporation. Buma (2012) for example showed that after a forest fire, the NDVI signal was dominated by low vegetation rather than the forest, and while the NDVI had recovered within a few years, the forest itself took much longer to recover.

The NDVI and LAI do not reflect relevant vegetation characteristics such as the stomatal control and root development. Therefore, global change adds another layer of complexity to using remote sensing data of vegetation for evaporation monitoring.

6.5 Ecosystem restoration: balancing the water costs of carbon sequestration

In June 2021, the United Nations launched the Decade on Ecosystem Restoration to prevent, halt, and reverse the degradation of ecosystems worldwide. Large-scale tree restoration has major benefits for carbon sequestration and climate change mitigation, but also for protecting the biodiversity and ecosystem services. The United Nations claim that ecosystem restoration is beneficial to all of the Sustainable Development Goals (IRP, 2019). This thesis however showed that large-scale tree restoration can shift global water availability, including reducing water availability in water scarce regions. We showed that large-scale tree restoration impacts local and downstream water availability through enhanced evaporation, while it also impacts regional, downwind, water availability through enhanced precipitation. Strategic tree restoration policies are required to reduce the local 'downsides' of tree restoration and increase the regional 'benefits' of tree restoration on water availability.

To limit local unwanted reductions in water availability, strategic restoration should focus on locations that do not face water limitation today, and limit tree restoration in regions that do face water limitation today, or will likely face strong reductions in water availability under the future climate. Also, restoration in regions that provide water to rivers should

be considered carefully. Another aspect is the species type: natural tree species are more efficient in using the available water resources without depleting them than (monoculture) plantations, and natural species have a more positive impact on other ecosystem services (Bosch and Hewlett, 1982; Calder and Aylward, 2006; Liu et al., 2018). Tree restoration could be beneficial to water availability, because it could improve the soil infiltration capacity and soil water holding capacity, and therefore even increase water availability during the dry season (Bruijnzeel, 2004; Lal, 1996; Zimmermann and Elsenbeer, 2008). A better understanding of the these positive impacts of tree restoration on water availability and a translation into guidelines would provide the opportunity to include these geological aspects in forestation projects. Another important and often overlooked aspect of strategic tree restoration lies in securing water availability for downwind regions. Forests for example have an important function in securing water availability for downwind agricultural regions (Keys et al., 2019; O'Connor et al., 2021; Pranindita et al., 2021a). To balance the water costs of carbon sequestration, we need a broad recognition of all of these hydrological impacts.

Successful tree restoration requires large international collaborations, rather than the local water and forest authorities or national governments that are in charge of executing the tree restoration projects. Furthermore, a better understanding of the hydrological effects, and a translation of the research results into restoration guidelines, would facilitate future land conversion projects. Strategic restoration involves more than the spatial planning and planting, but also prolonged monitoring of the vegetation to reduce the number of reforestation failures. Castro et al. (2021) introduced the term 'precision forest restoration' to emphasises that more efforts are needed to ensure that restoration projects will grow into self-regulated forests.

Large-scale tree restoration projects (whether 'strategic' or not) are an ideal opportunity to study a few of the important scientific questions. For example, under what circumstances can the enhanced soil infiltration and soil water holding capacity feed back into enhanced water availability during the dry season? Or how does tree restoration impact local precipitation, a question that is so far mostly addressed using spatial comparisons, rather than temporal (e.g. Meier et al., 2021). Another topic of interest is how tree restoration impacts the supply of moisture to downwind regions during a drought (Pranindita et al., 2021b). Involving researchers in large-scale tree restoration projects allows for addressing these questions. It will however remain difficult to isolate the effects of land-cover change from climate change and natural variability.

6.6 Beyond evaporation: the water, energy and carbon cycle

Droughts, climate change, and land-cover change have and will have a significant impact on local evaporation, and changes in evaporation propagate further into the water, energy, and carbon cycle. Therefore, global change can impact the meteorology and climate, the occurrence of heatwaves, the atmospheric carbon balance, and the growth and survival of the vegetation. Below we discuss how droughts and land-cover change impact the water, energy, and carbon cycle and vegetation.

To assess the effects of a drought on water, energy, and carbon, its timing is important. A warm or dry anomaly in spring can increase evaporation as well as vegetation growth and carbon uptake when water is not a limiting factor to photosynthesis. This effect was for example observed during spring 2003 and spring 2018 (Bastos et al., 2020; Ramonet et al., 2020). The enhanced evaporation during these spring droughts increased the severity of the summer droughts a few months later (Bastos et al., 2020; Seneviratne et al., 2012). A summer drought generally has an opposite effect on water, energy, and carbon. A reduced water availability during summer can accelerate the evaporation at first, through the high evaporative demand, but will eventually reduce evaporation through stomatal control or a change in the green leaf area. The reduced evaporation can propagate into a downwind drought, through reduced evaporation recycling (González-Hidalgo et al., 2018; Herrera-Estrada et al., 2019), while forests can also help to maintain some level of precipitation in downwind regions (Pranindita et al., 2021a). The effects on the temperature are also non-universal across species. Whilst tress adopt a conservative behaviour and reduce evaporation rates through stomatal control, the sensible heat flux and air temperatures increases. Grasslands however first maintain high evaporation rate and therefore reduce the sensible heat flux compared to forests (Teuling et al., 2010). During the summer drought of 2018, prolonged stomatal regulation reduced the carbon uptake and increased the atmospheric CO_2 content (Smith et al., 2020). The reduced photosynthesis resulted in one of the highest agricultural yield losses in the recent decades (Beillouin et al., 2020). The 2018 drought and other recent droughts also had a major impact on forest growth and survival. For forests, the effects on vegetation growth cannot always be detected in the drought year itself, but the legacy effects in reduced tree ring growth and reduced leaf area are visible over the next few years (Kannenberg et al., 2019; Schuldt et al., 2020; Yu and Liu, 2019). The growth reduction weakens forests and makes them more vulnerable to insect outbreaks and fires (Allen et al., 2010; Obladen et al., 2021). In Sweden, for example, the beetle-induced mortality for spruce increased from 0.15 million m^3 in 1990-2010 to 7 million m^3 in 2019 and 2020, as a consequence of the drought in 2018 (Öhrn et al., 2021). Prolonged droughts and repeated drought events have also led to widespread tree mortality (Brun et al., 2020; Schuldt et al., 2020; Senf et al., 2020) through a failure of the

tree hydraulic system, often in combination with carbon starvation (Adams et al., 2017; Choat et al., 2018; Kono et al., 2019).

In chapter 5 we calculated the hydrological effects of 900 million hectares of tree restoration. This large-scale tree restoration scenario would increase the forest carbon stock with 133.2 to 276.2 GtC (Bastin et al., 2019). We calculated that the accompanied change in evaporation could increase precipitation with 4.8 ± 3.1 mm y^{-1} (a few percent) through evaporation recycling and decrease streamflow with up to 47 % or increase it with up to 24 %. Wang-Erlandsson et al. (2018) showed that the effect of regional land cover change on local precipitation can be as high as the effects of local land-cover change, through the effect of evaporation recycling. While the effect of land-cover change on evaporation and precipitation is generally considered to be more or less homogeneous over the earth's surface, the effect on the air temperature is different for the tropical and boreal regions. In tropical regions, forest planting decreases the temperature, because the increase in evaporation outweighs the effect of increasing albedo. In boreal climate zones, forest planting increases the temperature, because the albedo effect (snow-covered short vegetation versus forest) outweighs the increased evaporation effect (Perugini et al., 2017). This local increase or decrease in air temperature can be up to 2 °C, and local forest cover change could increase or decrease global air temperature by op to 1 °C (Perugini et al., 2017).

6.7 More opportunities for measuring evaporation from space

During the past decades, we have seen a strong increase in the spatial and temporal resolution of remote sensing data. However the limited satellite revisit time and spatial resolution did still limit the analyses in this thesis. For example during the dry summer months of 2015 (chapter 2) it was cloudy on all Landsat pictures (once every 14 days) and the MODIS grassland pixels (chapter 4) represented not only grassland, but also forest or agricultural land. A few recently launched missions would allow for these studies at higher spatial or temporal resolution. These missions include the ESA Sentinel series ($10 - 1000$ m spatial resolution and a (bi-)weekly revisit time), and NASA's ECOSTRESS thermal satellite (69 38 m spatial resolution, $4 - 5$ day revisit time). Upcomming missions will further improve the monitoring of evaporation through high spatio-temporal measurements. These include the French-Indian LST mission Trishna (57 m resolution and 3 day revisit time), ESA's Copernicus thermal mission LSTM (50 m spatial resolution, $1 - 3$ day revisit time) and hyperspectral mission CHIME ($20 - 30$ m spatial resolution, $10 - 12.5$ day revisit time), and NASA's thermal infrared mission SBG (60 m spatial resolution, sub-monthly revisit time). These future missions will play an important role in the future monitoring of evaporation and vegetation stress. Using these new, freely available, satellite data,

one can study small-scale variability in ecosystem evaporation, related to for example the soil type or species, or study changes during a drought. Geostationary satellite data cover large spatial areas at kilometer-scale spatial resolution, but very high, sub-hourly, temporal resolution. Their data is not commonly used in evaporation monitoring, but their high temporal resolution would allow for near-real time evaporation monitoring. Furthermore, geostationary satellites are very suitable for continental-scale monitoring of evaporation.

Future improvements in remote sensing of evaporation lie among others in the improvement of modelling approaches and the synergistic use of multiple satellite sensors. The LST is a key component of most satellite evaporation monitoring methods, because it reflects the surface energy balance and short-term vegetation water stress. LST retrieval can be improved through a synergistic use of thermal infrared, shortwave infrared, and microwave radiation. Currently, the LST is most frequently retrieved from thermal infrared data, but LST could also be retrieved from microwave radiation which has the benefit that it can see through the clouds. Microwave based LST has a higher uncertainty but could strongly increase the opportunities for evaporation monitoring for all-weather conditions (Damm et al., 2018; Jimenez et al., 2018). Also sensitive shortwave infrared bands could be used to map water use and water stress when LST is not available (Mallick et al., 2019). Furthermore, other stress indicators could complement the LST, to improve the monitoring of (water) stressed ecosystems. Potential interesting stress indicators are Solar-Induced Fluorescence (SIF, Frankenberg et al., 2011), or specific narrow waveband spectral measurements that reflect the xanthophyll pigments (PRI indices, Gamon et al., 1992) or the abundance of chlorophyll (CARI indices, Kim, 1994). Both SIF, PRI, and CARI reflect drought stress, although the sensitivity depends on the vegetation type and aridity (Ballester et al., 2018; Jiao et al., 2019; Liu et al., 2021; Vicca et al., 2016).

The word 'latent' from latent heat finds its origin in the Latin word 'latere' which means 'lie hidden' or 'concealed'. And indeed, the latent heat flux or evaporation are invisible and difficult to measure. Several ground-based evaporation measurement methods exist to make the invisible evaporation visible and one characteristic is that these generally have a small spatial extent ánd a high temporal resolution (such as micro-meteorological methods, lysiemeters, or eddy covariance methods) or a large spatial extent ánd a low temporal resolution (catchment scale water budget techniques). Remote sensing however allows for studying evaporation over a large range of spatial and temporal scales (from 10 m to the global scale, from sub-daily to multiyear temporal scale) and for example allows for studying catchment evaporation at high daily basis. Remote sensing evaporation models also have the great potential to monitor evaporation in remote areas such as the arid or tropical regions where research is still strongly measurement-limited. To use satellite remote sensing evaporation in answering future research questions, it is however essential to discuss the validity of current satellite-based evaporation monitoring methods under global change.

References

Adams, H. D., M. J. B. Zeppel, W. R. L. Anderegg, H. Hartmann, S. M. Landhäusser, D. T. Tissue, T. E. Huxman, P. J. Hudson, T. E. Franz, C. D. Allen, L. D. L. Anderegg, G. A. Barron-Gafford, D. J. Beerling, D. D. Breshears, T. J. Brodribb, H. Bugmann, R. C. Cobb, A. D. Collins, L. T. Dickman, H. Duan, B. E. Ewers, L. Galiano, D. A. Galvez, N. Garcia-Forner, M. L. Gaylord, M. J. Germino, A. Gessler, U. G. Hacke, R. Hakamada, A. Hector, M. W. Jenkins, J. M. Kane, T. E. Kolb, D. J. Law, J. D. Lewis, J.-M. Limousin, D. M. Love, A. K. Macalady, J. Martínez-Vilalta, M. Mencuccini, P. J. Mitchell, J. D. Muss, M. J. O'Brien, A. P. O'Grady, R. E. Pangle, E. A. Pinkard, F. I. Piper, J. A. Plaut, W. T. Pockman, J. Quirk, K. Reinhardt, F. Ripullone, M. G. Ryan, A. Sala, S. Sevanto, J. S. Sperry, R. Vargas, M. Vennetier, D. A. Way, C. Xu, E. A. Yepez, and N. G. McDowell (2017). "A multi-species synthesis of physiological mechanisms in drought-induced tree mortality". *Nature Ecology & Evolution* 1.9, 1285–1291. DOI: https://doi.org/10.1038/s41559-017-0248-x.

Allen, C. D., A. K. Macalady, H. Chenchouni, D. Bachelet, N. McDowell, M. Vennetier, T. Kitzberger, A. Rigling, D. D. Breshears, E. H. Hogg, P. Gonzalez, R. Fensham, Z. Zhang, J. Castro, N. Demidova, J. H. Lim, G. Allard, S. W. Running, A. Semerci, and N. Cobb (2010). "A global overview of drought and heat-induced tree mortality reveals emerging climate change risks for forests". *Forest Ecology and Management* 259.4, 660–684. DOI: https://doi.org/10.1016/j.foreco.2009.09.001.

Allen, R. G., L. S. Pereira, D. Raes, and M. Smith (1998). *Crop evapotranspiration : guidelines for computing crop water requirements*. FAO irrigation and drainage paper, 0254-5284 ; 56. Rome: Food and Agriculture Organization of the United Nations.

Anderegg, W. R. L., C. Schwalm, F. Biondi, J. J. Camarero, G. Koch, M. Litvak, K. Ogle, J. D. Shaw, E. Shevliakova, A. P. Williams, A. Wolf, E. Ziaco, and S. Pacala (2015). "Pervasive drought legacies in forest ecosystems and their implications for carbon cycle models". *Science* 349.6247, 528–532. DOI: https://doi.org/10.1126/science.aab1833.

Asbjornsen, H., G. R. Goldsmith, M. S. Alvarado-Barrientos, K. Rebel, F. P. Van Osch, M. Rietkerk, J. Chen, S. Gotsch, C. Tobon, D. R. Geissert, A. Gomez-Tagle, K. Vache, and T. E. Dawson (2011). "Ecohydrological advances and applications in plant-water

relations research: a review". *Journal of Plant Ecology* 4.1-2, 3–22. DOI: https://doi.org/10.1093/jpe/rtr005.

Asner, G. P., J. M. O. Scurlock, and J. A. Hicke (2003). "Global synthesis of leaf area index observations: implications for ecological and remote sensing studies". *Global Ecology and Biogeography* 12.3, 191–205. DOI: https://doi.org/10.1046/j.1466-822X.2003.00026.x.

Awada, T., R. El-Hage, M. Geha, D. A. Wedin, J. A. Huddle, X. Zhou, J. Msanne, R. A. Sudmeyer, D. L. Martin, and J. R. Brandle (2013). "Intra-annual variability and environmental controls over transpiration in a 58-year-old even-aged stand of invasive woody Juniperus virginiana L. in the Nebraska Sandhills, USA". *Ecohydrology* 6.5, 731–740. DOI: https://doi.org/10.1002/eco.1294.

Bachmair, S., M. Tanguy, J. Hannaford, and K. Stahl (2018). "How well do meteorological indicators represent agricultural and forest drought across Europe?" *Environmental Research Letters* 13.3, 034042. DOI: https://doi.org/10.1088/1748-9326/aaafda.

Bagley, J. E., A. R. Desai, K. J. Harding, P. K. Snyder, and J. A. Foley (2014). "Drought and deforestation: Has land cover change influenced recent precipitation extremes in the Amazon?" *Journal of Climate* 27.1, 345–361. DOI: https://doi.org/10.1175/JCLI-D-12-00369.1.

Baldocchi, D., E. Falge, L. Gu, R. Olson, D. Hollinger, S. Running, P. Anthoni, C. Bernhofer, K. Davis, R. Evans, J. Fuentes, A. Goldstein, G. Katul, B. Law, X. Lee, Y. Malhi, T. Meyers, W. Munger, W. Oechel, U. K. T. Paw, K. Pilegaard, H. P. Schmid, R. Valentini, S. Verma, T. Vesala, K. Wilson, and S. Wofsy (2001). "FLUXNET: A New Tool to Study the Temporal and Spatial Variability of Ecosystem-Scale Carbon Dioxide, Water Vapor, and Energy Flux Densities". *Bulletin of the American Meteorological Society* 82.11, 2415–2434. DOI: https://doi.org/10.1175/1520-0477(2001)082<2415:FANTTS>2.3.CO;2.

Baldocchi, D. D., R. J. Luxmoore, and J. L. Hatfield (1991). "Discerning the forest from the trees: an essay on scaling canopy stomatal conductance". *Agricultural and Forest Meteorology* 54.2, 197–226. DOI: https://doi.org/10.1016/0168-1923(91)90006-C.

Ballester, C., P. Zarco-Tejada, E. Nicolás, J. Alarcón, E. Fereres, D. Intrigliolo, and V. Gonzalez-Dugo (2018). "Evaluating the performance of xanthophyll, chlorophyll and structure-sensitive spectral indices to detect water stress in five fruit tree species". *Precision Agriculture* 19.1, 178–193. DOI: https://doi.org/10.1007/s11119-017-9512-y.

Bao, Z., J. Zhang, G. Wang, Q. Chen, T. Guan, X. Yan, C. Liu, J. Liu, and J. Wang (2019). "The impact of climate variability and land use/cover change on the water balance in the Middle Yellow River Basin, China". *Journal of Hydrology* 577. DOI: https://doi.org/10.1016/j.jhydrol.2019.123942.

Barcza, Z., A. Kern, L. Haszpra, and N. Kljun (2009). "Spatial representativeness of tall tower eddy covariance measurements using remote sensing and footprint analysis". *Agricultural and Forest Meteorology* 149.5, 795–807. DOI: https://doi.org/10.1016/j.agrformet.2008.10.021.

Baret, M., S. Pepin, and D. Pothier (2018). "Hydraulic limitations in dominant trees as a contributing mechanism to the age-related growth decline of boreal forest stands". *Forest Ecology and Management* 427, 135–142. DOI: https://doi.org/10.1016/j.foreco.2018.05.043.

Bargués Tobella, A., H. Reese, A. Almaw, J. Bayala, A. Malmer, H. Laudon, and U. Ilstedt (2014). "The effect of trees on preferential flow and soil infiltrability in an agroforestry parkland in semiarid Burkina Faso". *Water Resources Research* 50.4, 3342–3354. DOI: https://doi.org/10.1002/2013WR015197.

Bastiaanssen, W. G. M., M. Menenti, R. A. Feddes, and A. A. M. Holtslag (1998). "A remote sensing surface energy balance algorithm for land (SEBAL). 1. Formulation". *Journal of Hydrology* 212-213, 198–212. DOI: https://doi.org/10.1016/S0022-1694(98)00253-4.

Bastin, J.-F., Y. Finegold, C. Garcia, D. Mollicone, M. Rezende, D. Routh, C. M. Zohner, and T. W. Crowther (2019). "The global tree restoration potential". *Science* 365.6448, 76–79. DOI: https://doi.org/10.1126/science.aax0848.

Bastos, A., Z. Fu, P. Ciais, P. Friedlingstein, S. Sitch, J. Pongratz, U. Weber, M. Reichstein, P. Anthoni, A. Arneth, V. Haverd, A. Jain, E. Joetzjer, J. Knauer, S. Lienert, T. Loughran, P. C. McGuire, W. Obermeier, R. S. Padrón, H. Shi, H. Tian, N. Viovy, and S. Zaehle (2020). "Impacts of extreme summers on European ecosystems: a comparative analysis of 2003, 2010 and 2018". *Philosophical Transactions of the Royal Society B: Biological Sciences* 375.1810, 20190507. DOI: https://doi.org/10.1098/rstb.2019.0507.

Bates, C. G. and A. J. Henry (1928). "Second phase of streamflow experiment at Wagon Wheel Gap, Colo". *Monthly Weather Review* 56.3, 79–80. DOI: https://doi.org/10.1175/1520-0493(1928)56<79:sposea>2.0.co;2.

Beck, H. E., E. F. Wood, M. Pan, C. K. Fisher, D. G. Miralles, A. I. J. M. v. Dijk, T. R. McVicar, and R. F. Adler (2019). "MSWEP V2 Global 3-Hourly 0.1° Precipitation: Methodology and Quantitative Assessment". *Bulletin of the American Meteorological Society* 100.3, 473–500. DOI: https://doi.org/10.1175/bams-d-17-0138.1.

Beer, C., M. Reichstein, P. Ciais, G. D. Farquhar, and D. Papale (2007). "Mean annual GPP of Europe derived from its water balance". *Geophysical Research Letters* 34.5. DOI: https://doi.org/10.1029/2006gl029006.

Beillouin, D., B. Schauberger, A. Bastos, P. Ciais, and D. Makowski (2020). "Impact of extreme weather conditions on European crop production in 2018". *Philosophical*

Transactions of the Royal Society B: Biological Sciences 375.1810, 20190510. DOI: https://doi.org/10.1098/rstb.2019.0510.

Bernhofer, C. and J. Gruenwald (2021). *Fluxnet Product, Grillenburg, 2003-12-31–2020-12-31*.

Bierkens, M. F. P., V. A. Bell, P. Burek, N. Chaney, L. E. Condon, C. H. David, A. Roo, P. Döll, N. Drost, J. S. Famiglietti, M. Flörke, D. J. Gochis, P. Houser, R. Hut, J. Keune, S. Kollet, R. M. Maxwell, J. T. Reager, L. Samaniego, E. Sudicky, E. H. Sutanudjaja, N. Giesen, H. Winsemius, and E. F. Wood (2015). "Hyper-resolution global hydrological modelling: what is next?" *Hydrological Processes* 29.2, 310–320. DOI: https://doi.org/10.1002/hyp.10391.

Blackman, C. J., D. Creek, C. Maier, M. J. Aspinwall, J. E. Drake, S. Pfautsch, A. O'Grady, S. Delzon, B. E. Medlyn, D. T. Tissue, and B. Choat (2019). "Drought response strategies and hydraulic traits contribute to mechanistic understanding of plant dry-down to hydraulic failure". *Tree Physiology* 39.6, 910–924. DOI: https://doi.org/10.1093/treephys/tpz016.

Boegh, E., R. N. Poulsen, M. Butts, P. Abrahamsen, E. Dellwik, S. Hansen, C. B. Hasager, A. Ibrom, J. K. Loerup, K. Pilegaard, and H. Soegaard (2009). "Remote sensing based evapotranspiration and runoff modeling of agricultural, forest and urban flux sites in Denmark: From field to macro-scale". *Journal of Hydrology* 377.3-4, 300–316. DOI: https://doi.org/10.1016/j.jhydrol.2009.08.029.

Böhnisch, A., M. Mittermeier, M. Leduc, and R. Ludwig (2021). "Hot Spots and Climate Trends of Meteorological Droughts in Europe–Assessing the Percent of Normal Index in a Single-Model Initial-Condition Large Ensemble". *Frontiers in Water* 3. DOI: https://doi.org/10.3389/frwa.2021.716621.

Bonan, G. B. (2008). "Forests and climate change: forcings, feedbacks, and the climate benefits of forests". *Science* 320.5882, 1444–9. DOI: https://doi.org/10.1126/science.1155121.

Bosch, J. M. and J. D. Hewlett (1982). "A review of catchment experiments to determine the effect of vegetation changes on water yield and evapotranspiration". *Journal of Hydrology* 55.1, 3–23. DOI: https://doi.org/10.1016/0022-1694(82)90117-2.

Brown, A. E., L. Zhang, T. A. McMahon, A. W. Western, and R. A. Vertessy (2005). "A review of paired catchment studies for determining changes in water yield resulting from alterations in vegetation". *Journal of Hydrology* 310.1, 28–61. DOI: https://doi.org/10.1016/j.jhydrol.2004.12.010.

Bruijnzeel, L. A. (2004). "Hydrological functions of tropical forests: not seeing the soil for the trees?" *Agriculture, Ecosystems & Environment* 104.1, 185–228. DOI: https://doi.org/10.1016/j.agee.2004.01.015.

Brun, P., A. Psomas, C. Ginzler, W. Thuiller, M. Zappa, and N. E. Zimmermann (2020). "Large-scale early-wilting response of Central European forests to the 2018 extreme

drought". *Global Change Biology* 26.12, 7021–7035. DOI: https://doi.org/10.1111/gcb.15360.

Buchmann, N., I. Feigenwinter, K. Fuchs, and L. Merbold (2021). *Fluxnet Product, Chamau grassland, 2004-12-31–2020-12-31*.

Budyko, M. (1974). *Climate and Life*. Academic Press, New York, NY, USA.

Buma, B. (2012). "Evaluating the utility and seasonality of NDVI values for assessing post-disturbance recovery in a subalpine forest". *Environmental Monitoring and Assessment* 184.6, 3849–3860. DOI: https://doi.org/10.1007/s10661-011-2228-y.

Buras, A., A. Rammig, and C. S. Zang (2020). "Quantifying impacts of the 2018 drought on European ecosystems in comparison to 2003". *Biogeosciences* 17.6, 1655–1672. DOI: https://doi.org/10.5194/bg-17-1655-2020.

Burgess, S. S. O., M. Adams, N. Turner, C. Beverly, C. Ong, A. Khan, and T. Bleby (2001). "An improved heat pulse method to measure low and reverse rates of sap flow in woody plants". *Tree Physiology* 21, 589–598. DOI: https://doi.org/0.1093/treephys/21.9.589.

Calder, I. R. and B. Aylward (2006). "Forest and Floods". *Water International* 31.1, 87–99. DOI: https://doi.org/10.1080/02508060608691918.

Campbell, G. S., C. Calissendorff, and J. H. Williams (1991). "Probe for Measuring Soil Specific Heat Using A Heat-Pulse Method". *Soil Science Society of America Journal* 55.1, 291–293. DOI: https://doi.org/10.2136/sssaj1991.03615995005500010052x.

Canadell, J., R. Jackson, J. Ehleringer, H. Mooney, O. Sala, and S. E.-D. (1996). "Maximum rooting depth of vegetation types at the global scale". *Maximum rooting depth of vegetation types at the global scale. Oecologia* 108, 583–595. DOI: https://doi.org/10.1007/BF00329030.

Carter, C. and S. Liang (2018). "Comprehensive evaluation of empirical algorithms for estimating land surface evapotranspiration". *Agricultural and Forest Meteorology* 256-257, 334–345. DOI: https://doi.org/10.1016/j.agrformet.2018.03.027.

Castro, J., F. Morales-Rueda, F. B. Navarro, M. Löf, G. Vacchiano, and D. Alcaraz-Segura (2021). "Precision restoration: a necessary approach to foster forest recovery in the 21st century". *Restoration Ecology* 29.7, e13421. DOI: https://doi.org/10.1111/rec.13421.

Čermák, J., J. Kučera, and N. Nadezhdina (2004). "Sap flow measurements with some thermodynamic methods, flow integration within trees and scaling up from sample trees to entire forest stands". *Trees* 18.5, 529–546. DOI: https://doi.org/10.1007/s00468-004-0339-6.

Chaney, N. W., P. Metcalfe, and E. F. Wood (2016). "HydroBlocks: a field-scale resolving land surface model for application over continental extents". *Hydrological Processes* 30.20, 3543–3559. DOI: https://doi.org/10.1002/hyp.10891.

Chen, S., J. Zou, Z. Hu, and Y. Lu (2019). "Climate and Vegetation Drivers of Terrestrial Carbon Fluxes: A Global Data Synthesis". *Advances in Atmospheric Sciences* 36.7, 679–696. DOI: https://doi.org/10.1007/s00376-019-8194-y.

Chiesi, M., B. Rapi, P. Battista, L. Fibbi, B. Gozzini, R. Magno, A. Raschi, and F. Maselli (2013). "Combination of ground and satellite data for the operational estimation of daily evapotranspiration". *European Journal of Remote Sensing* 46.1, 675–688. DOI: https://doi.org/10.5721/EuJRS20134639.

Chiu, C.-W., H. Komatsu, A. Katayama, and K. Otsuki (2016). "Scaling-up from tree to stand transpiration for a warm-temperate multi-specific broadleaved forest with a wide variation in stem diameter". *Journal of Forest Research* 21.4, 161–169. DOI: https://doi.org/10.1007/s10310-016-0532-7.

Choat, B., T. J. Brodribb, C. R. Brodersen, R. A. Duursma, R. López, and B. E. Medlyn (2018). "Triggers of tree mortality under drought". *Nature* 558.7711, 531–539. DOI: https://doi.org/10.1038/s41586-018-0240-x.

Cleugh, H., R. Leuninga, Q. Mu, and R. S.W. (2007). "Regional evaporation estimates from flux tower and MODIS satellite data". *Remote Sensing of Environment* 106.3, 285–304. DOI: https://doi.org/10.1016/j.rse.2006.07.007.

Cleverly, J., D. Eamus, N. Restrepo Coupe, C. Chen, W. Maes, L. Li, R. Faux, N. S. Santini, R. Rumman, Q. Yu, and A. Huete (2016). "Soil moisture controls on phenology and productivity in a semi-arid critical zone". *Sci Total Environ* 568, 1227–37. DOI: https://doi.org/10.1016/j.scitotenv.2016.05.142.

Costa, M. H., M. C. Biajoli, L. Sanches, A. C. M. Malhado, L. R. Hutyra, H. R. da Rocha, R. G. Aguiar, and A. C. de Araújo (2010). "Atmospheric versus vegetation controls of Amazonian tropical rain forest evapotranspiration: Are the wet and seasonally dry rain forests any different?" *Journal of Geophysical Research: Biogeosciences* 115.G4. DOI: https://doi.org/10.1029/2009jg001179.

Coumou, D., G. Di Capua, S. Vavrus, L. Wang, and S. Wang (2018). "The influence of Arctic amplification on mid-latitude summer circulation". *Nature Communications* 9.1, 2959. DOI: https://doi.org/10.1038/s41467-018-05256-8.

Cramer, W., A. Bondeau, F. I. Woodward, I. C. Prentice, R. A. Betts, V. Brovkin, P. M. Cox, V. Fisher, J. A. Foley, A. D. Friend, C. Kucharik, M. R. Lomas, N. Ramankutty, S. Sitch, B. Smith, A. White, and C. Young-Molling (2001). "Global response of terrestrial ecosystem structure and function to CO2 and climate change: Results from six dynamic global vegetation models". *Global Change Biology* 7.4, 357–373. DOI: https://doi.org/10.1046/j.1365-2486.2001.00383.x.

Crowhurst, D., S. Dadson, J. Peng, and R. Washington (2021). "Contrasting controls on Congo Basin evaporation at the two rainfall peaks". *Climate Dynamics* 56.5-6, 1609–1624. DOI: https://doi.org/10.1007/s00382-020-05547-1.

Dai, A. (2011). "Drought under global warming: A review". *Wiley Interdisciplinary Reviews: Climate Change* 2.1, 45–65. DOI: https://doi.org/10.1002/wcc.81.

– (2013). "Increasing drought under global warming in observations and models". *Nature Climate Change* 3.1, 52–58. DOI: https://doi.org/10.1038/nclimate1633.

Damm, A., E. Paul-Limoges, E. Haghighi, C. Simmer, F. Morsdorf, F. Schneider, C. van der Tol, M. Migliavacca, and U. Rascher (2018). "Remote sensing of plant-water relations: An overview and future perspectives". *Journal of Plant Physiology* 227, 3–19. DOI: https://doi.org/10.1016/j.jplph.2018.04.012.

Davi, H., K. Soudani, T. Deckx, E. Dufrene, V. Le Dantec, and C. FranÇois (2006). "Estimation of forest leaf area index from SPOT imagery using NDVI distribution over forest stands". *International Journal of Remote Sensing* 27.5, 885–902. DOI: https://doi.org/10.1080/01431160500227896.

De Jong, S. and V. Jetten (2007). "Estimating spatial patterns of rainfall interception from remotely sensed vegetation indices and spectral mixture analysis". *International Journal of Geographical Information Science* 21.5, 529–545. DOI: https://doi.org/10.1080/13658810601064884.

De Kauwe, M. G., B. E. Medlyn, J. Knauer, and C. A. Williams (2017). "Ideas and perspectives: how coupled is the vegetation to the boundary layer?" *Biogeosciences* 14.19, 4435–4453. DOI: https://doi.org/10.5194/bg-14-4435-2017.

Dos Santos, V., F. Laurent, C. Abe, and F. Messner (2018). "Hydrologic Response to Land Use Change in a Large Basin in Eastern Amazon". *Water* 10.4, 429. DOI: https://doi.org/10.3390/w10040429.

Duursma, R. A., P. Kolari, M. Perämmäki, M. Pulkkinen, A. Mäkelä, E. Nikinmaa, P. Hari, M. Aurela, P. Berbigier, C. Bernhofer, T. Grünwald, D. Loustau, M. Mölder, H. Verbeeck, and T. Vesala (2009). "Contributions of climate, leaf area index and leaf physiology to variation in gross primary production of six coniferous forests across Europe: A model-based analysis". *Tree Physiology* 29.5, 621–639. DOI: https://doi.org/10.1093/treephys/tpp010.

Eklundh, L. (1998). "Estimating relations between AVHRR NDVI and rainfall in East Africa at 10-day and monthly time scales". *International Journal of Remote Sensing* 19.3, 563–568. DOI: https://doi.org/10.1080/014311698216198.

Ellison, D. (2018). "Forests and Water. UNFF13 Background Analytical Study 2 on Forests and Water". *Report commissioned for the thirteenth session of the United Nations Forum on Forests*.

Ellison, D. and E. Ellis (2020). "Forest cover, windspeed, and precipitation: A south American case study of the impact of forest ecosystems on wind and rainfall patterns". In: *EGU General Assembly 2020*, EGU2020–22235. DOI: https://doi.org/10.5194/egusphere-egu2020-22235.

Ellison, D., M. N. Futter, and K. Bishop (2012). "On the forest cover-water yield debate: From demand- to supply-side thinking". *Global Change Biology* 18.3, 806–820. DOI: https://doi.org/10.1111/j.1365-2486.2011.02589.x.

Ellison, D., L. Wang-Erlandsson, R. J. Van Der Ent, and M. v. noordwijk (2019). "Upwind forests: managing moisture recycling for nature-based resilience". *Unasylva* 70. DOI: https://doi.org/10.4060/CA6842EN.

Ellison, D., C. E. Morris, B. Locatelli, D. Sheil, J. Cohen, D. Murdiyarso, V. Gutierrez, M. v. Noordwijk, I. F. Creed, J. Pokorny, D. Gaveau, D. V. Spracklen, A. B. Tobella, U. Ilstedt, A. J. Teuling, S. G. Gebrehiwot, D. C. Sands, B. Muys, B. Verbist, E. Springgay, Y. Sugandi, and C. A. Sullivan (2017). "Trees, forests and water: Cool insights for a hot world". *Global Environmental Change* 43, 51–61. DOI: https://doi.org/10.1016/j.gloenvcha.2017.01.002.

Elmore, A. J., S. M. Guinn, B. J. Minsley, and A. D. Richardson (2012). "Landscape controls on the timing of spring, autumn, and growing season length in mid-Atlantic forests". *Global Change Biology* 18.2, 656–674. DOI: https://doi.org/10.1111/j.1365-2486.2011.02521.x.

Esau, I. N. and T. J. Lyons (2002). "Effect of sharp vegetation boundary on the convective atmospheric boundary layer". *Agricultural and Forest Meteorology* 114.1-2, 3–13. DOI: https://doi.org/10.1016/S0168-1923(02)00154-5.

Evaristo, J. and J. J. McDonnell (2019). "Global analysis of streamflow response to forest management". *Nature*. DOI: https://doi.org/10.1038/s41586-019-1306-0.

Fang, H., F. Baret, S. Plummer, and G. Schaepman-Strub (2019). "An Overview of Global Leaf Area Index (LAI): Methods, Products, Validation, and Applications". *Reviews of Geophysics* 57.3, 739–799. DOI: https://doi.org/10.1029/2018rg000608.

Farley, K. A., E. G. Jobbágy, and R. B. Jackson (2005). "Effects of afforestation on water yield: a global synthesis with implications for policy". *Global Change Biology* 11.10, 1565–1576. DOI: https://doi.org/10.1111/j.1365-2486.2005.01011.x.

Fei, S., J. M. Desprez, K. M. Potter, I. Jo, J. A. Knott, and C. M. Oswalt (2017). "Divergence of species responses to climate change". *Science Advances* 3.5, e1603055. DOI: https://doi.org/10.1126/sciadv.1603055.

Ferguson, C. R., E. F. Wood, and R. K. Vinukollu (2012). "A Global Intercomparison of Modeled and Observed Land–Atmosphere Coupling". *Journal of Hydrometeorology* 13.3, 749–784. DOI: https://doi.org/10.1175/jhm-d-11-0119.1.

Filoso, S., M. Bezerra, K. Weiss, and M. Palmer (2017). "Impacts of forest restoration on water yield: a systematic review". *PLoS ONE* 12.8, e0183210. DOI: https://doi.org/10.1371/journal.pone.0183210.

Ford, C. R., R. M. Hubbard, and J. M. Vose (2011). "Quantifying structural and physiological controls on variation in canopy transpiration among planted pine and hard-

wood species in the southern Appalachians". *Ecohydrology* 4.2, 183–195. DOI: https://doi.org/10.1002/eco.136.

Ford, C. R., M. McGuire, R. Mitchell, and R. Teskey (2004). "Assessing variation in the radial profile of sap flux density in pinus species and its effect on daily water use". *Tree Physiology* 24, 241–249. DOI: https://doi.org/10.1093/treephys/24.3.241.

Forkel, M., M. Drüke, M. Thurner, W. Dorigo, S. Schaphoff, K. Thonicke, W. Von Bloh, and N. Carvalhais (2019). "Constraining modelled global vegetation dynamics and carbon turnover using multiple satellite observations". *Scientific Reports* 9.1, 18757. DOI: https://doi.org/10.1038/s41598-019-55187-7.

Frankenberg, C., J. B. Fisher, J. Worden, G. Badgley, S. S. Saatchi, J.-E. Lee, G. C. Toon, A. Butz, M. Jung, A. Kuze, and T. Yokota (2011). "New global observations of the terrestrial carbon cycle from GOSAT: Patterns of plant fluorescence with gross primary productivity". *Geophysical Research Letters* 38.17. DOI: https://doi.org/10.1029/2011GL048738.

Fu, Z., D. Li, O. Hararuk, C. Schwalm, Y. Luo, L. Yan, and S. Niu (2017). "Recovery time and state change of terrestrial carbon cycle after disturbance". *Environmental Research Letters* 12.10, 104004. DOI: https://doi.org/10.1088/1748-9326/aa8a5c.

Gamon, J., J. Peñuelas, and C. Field (1992). "A narrow-waveband spectral index that tracks diurnal changes in photosynthetic efficiency". *Remote Sensing of Environment* 41.1, 35–44. DOI: https://doi.org/10.1016/0034-4257(92)90059-S.

Gamon, J. A., C. B. Field, M. L. Goulden, K. L. Griffin, A. E. Hartley, G. Joel, Pe, xf, J. uelas, and R. Valentini (1995). "Relationships between NDVI, canopy structure, and photosynthesis in three Californian vegetation types". *Ecological Applications* 5.1, 28–41. DOI: https://doi.org/10.2307/1942049.

Gebauer, T., V. Horna, and C. Leuschner (2012). "Canopy transpiration of pure and mixed forest stands with variable abundance of European beech". *Journal of Hydrology* 442-443, 2–14. DOI: https://doi.org/10.1016/j.jhydrol.2012.03.009.

Glenn, E. P., P. L. Nagler, and A. R. Huete (2010). "Vegetation Index Methods for Estimating Evapotranspiration by Remote Sensing". *Surveys in Geophysics* 31.6, 531–555. DOI: https://doi.org/10.1007/s10712-010-9102-2.

Gómez, J. A., J. V. Giráldez, and E. Fereres (2001). "Rainfall interception by olive trees in relation to leaf area". *Agricultural Water Management* 49.1, 65–76. DOI: https://doi.org/10.1016/S0378-3774(00)00116-5.

González-Hidalgo, J. C., S. M. Vicente-Serrano, D. Peña-Angulo, C. Salinas, M. Tomas-Burguera, and S. Beguería (2018). "High-resolution spatio-temporal analyses of drought episodes in the western Mediterranean basin (Spanish mainland, Iberian Peninsula)". *Acta Geophysica* 66.3, 381–392. DOI: https://doi.org/10.1007/s11600-018-0138-x.

Graf, A., A. Klosterhalfen, N. Arriga, C. Bernhofer, H. Bogena, F. Bornet, N. Brüggemann, C. Brümmer, N. Buchmann, J. Chi, C. Chipeaux, E. Cremonese, M. Cuntz, J. Dušek, T. S. El-Madany, S. Fares, M. Fischer, L. Foltýnová, M. Gharun, S. Ghiasi, B. Gielen, P. Gottschalk, T. Grünwald, G. Heinemann, B. Heinesch, M. Heliasz, J. Holst, L. Hörtnagl, A. Ibrom, J. Ingwersen, G. Jurasinski, J. Klatt, A. Knohl, F. Koebsch, J. Konopka, M. Korkiakoski, N. Kowalska, P. Kremer, B. Kruijt, S. Lafont, J. Léonard, A. De Ligne, B. Longdoz, D. Loustau, V. Magliulo, I. Mammarella, G. Manca, M. Mauder, M. Migliavacca, M. Mölder, J. Neirynck, P. Ney, M. Nilsson, E. Paul-Limoges, M. Peichl, A. Pitacco, A. Poyda, C. Rebmann, M. Roland, T. Sachs, M. Schmidt, F. Schrader, L. Siebicke, L. Šigut, E.-S. Tuittila, A. Varlagin, N. Vendrame, C. Vincke, I. Völksch, S. Weber, C. Wille, H.-D. Wizemann, M. Zeeman, and H. Vereecken (2020). "Altered energy partitioning across terrestrial ecosystems in the European drought year 2018". *Philosophical Transactions of the Royal Society B: Biological Sciences* 375.1810, 20190524. DOI: https://doi.org/10.1098/rstb.2019.0524.

Granier, A., D. Loustau, and N. Bréda (2000). "A generic model of forest canopy conductance dependent on climate, soil water availability and leaf area index". *Annals of Forest Science* 57.8, 755–765. DOI: https://doi.org/10.1051/forest:2000158.

GRDC (n.d.). *In-situ river discharge data*. Global Runoff Data Centre, GRDC. World Meteorological Organization. Accessed 19 April 2021.

Griscom, B. W., J. Adams, P. W. Ellis, R. A. Houghton, G. Lomax, D. A. Miteva, W. H. Schlesinger, D. Shoch, J. V. Siikamäki, P. Smith, P. Woodbury, C. Zganjar, A. Blackman, J. Campari, R. T. Conant, C. Delgado, P. Elias, T. Gopalakrishna, M. R. Hamsik, M. Herrero, J. Kiesecker, E. Landis, L. Laestadius, S. M. Leavitt, S. Minnemeyer, S. Polasky, P. Potapov, F. E. Putz, J. Sanderman, M. Silvius, E. Wollenberg, and J. Fargione (2017). "Natural climate solutions". *Proceedings of the National Academy of Sciences of the United States of America* 114.44, 11645–11650. DOI: https://doi.org/10.1073/pnas.1710465114.

Gu, C., J. Ma, G. Zhu, H. Yang, K. Zhang, Y. Wang, and C. Gu (2018). "Partitioning evapotranspiration using an optimized satellite-based ET model across biomes". *Agricultural and Forest Meteorology* 259, 355–363. DOI: https://doi.org/10.1016/j.agrformet.2018.05.023.

Guo, J., Z. Zhang, J. Zhou, S. Wang, and P. Strauss (2014). "Decoupling Streamflow Responses to Climate Variability and Land Use/Cover Changes in a Watershed in Northern China". *Journal of the American Water Resources Association* 50.6, 1425–1438. DOI: https://doi.org/10.1111/jawr.12197.

Hansen, M. C., P. V. Potapov, R. Moore, M. Hancher, S. A. Turubanova, A. Tyukavina, D. Thau, S. V. Stehman, S. J. Goetz, T. R. Loveland, A. Kommareddy, A. Egorov, L. Chini, C. O. Justice, and J. R. G. Townshend (2013). "High-resolution global

maps of 21st-century forest cover change". *Science* 342.6160, 850–853. DOI: https://doi.org/10.1126/science.1244693.

Hashimoto, H., W. Wang, C. Milesi, M. White, S. Ganguly, M. Gamo, R. Hirata, R. Myneni, and R. Nemani (2012). "Exploring Simple Algorithms for Estimating Gross Primary Production in Forested Areas from Satellite Data". *Remote sensing* 4.1, 303–326. DOI: https://doi.org/10.3390/rs4010303.

Hasler, N. and R. Avissar (2007). "What controls evapotranspiration in the Amazon Basin?" *Journal of Hydrometeorology* 8, 380–395. DOI: https://doi.org/10.1175/JHM587.1.

Hassler, S. K., M. Weiler, and T. Blume (2018). "Tree-, stand- and site-specific controls on landscape-scale patterns of transpiration". *Hydrology and Earth System Sciences* 22.1, 13–30. DOI: https://doi.org/10.5194/hess-22-13-2018.

Hateren, T. C. van, M. Chini, P. Matgen, and A. J. Teuling (2021). "Ambiguous Agricultural Drought: Characterising Soil Moisture and Vegetation Droughts in Europe from Earth Observation". *Remote Sensing* 13.10. DOI: https://doi.org/10.3390/rs13101990.

Hatton, T. J. and H. .-I. Wu (1995). "Scaling theory to extrapolate individual tree water use to stand water use". *Hydrological Processes* 9.5-6, 527–540. DOI: https://doi.org/10.1002/hyp.3360090505.

Heinsch, F. A., M. Zhao, S. W. Running, J. S. Kimball, R. R. Nemani, K. J. Davis, P. V. Bolstad, B. D. Cook, A. R. Desai, D. M. Ricciuto, B. E. Law, W. C. Oechel, H. Kwon, H. Luo, S. C. Wofsy, A. L. Dunn, J. W. Munger, D. D. Baldocchi, L. Xu, D. Y. Hollinger, A. D. Richardson, P. C. Stoy, M. B. S. Siqueira, R. K. Monson, S. P. Burns, and L. B. Flanagan (2006). "Evaluation of remote sensing based terrestrial productivity from MODIS using regional tower eddy flux network observations". *IEEE Transactions on Geoscience and Remote Sensing* 44.7, 1908–1923. DOI: https://doi.org/10.1109/TGRS.2005.853936.

Heliasz, M. and ICOS ETC (2020). *Drought-2018 ecosystem eddy covariance flux product from Hyltemossa*. DOI: https://doi.org/10.18160/17FF-96RT.

Heo, J., J. Yu, J. R. Giardino, and H. Cho (2015). "Impacts of climate and land-cover changes on water resources in a humid subtropical watershed: A case study from East Texas, USA". *Water and Environment Journal* 29.1, 51–60. DOI: https://doi.org/10.1111/wej.12096.

Hernandez-Santana, V., A. Hernandez-Hernandez, M. A. Vadeboncoeur, and H. Asbjornsen (2015). "Scaling from single-point sap velocity measurements to stand transpiration in a multispecies deciduous forest: uncertainty sources, stand structure effect, and future scenarios". *Canadian Journal of Forest Research* 45.11, 1489–1497. DOI: https://doi.org/10.1139/cjfr-2015-0009.

Herrera-Estrada, J. E., J. A. Martinez, F. Dominguez, K. L. Findell, E. F. Wood, and J. Sheffield (2019). "Reduced Moisture Transport Linked to Drought Propagation

Across North America". *Geophysical Research Letters* 46.10, 5243–5253. DOI: https://doi.org/10.1029/2019GL082475.

Hersbach, H., B. Bell, P. Berrisford, G. Biavati, A. Horányi, J. Muñoz Sabater, J. Nicolas, C. Peubey, R. Radu, I. Rozum, D. Schepers, A. Simmons, C. Soci, D. Dee, and J.-N. Thépaut (2018). *ERA5-Land monthly averaged data from 1950 to present*. DOI: https://doi.org/10.24381/cds.68d2bb30.

Hoek van Dijke, A. J., M. Herold, K. Mallick, I. Benedict, M. Machwitz, M. Schlerf, A. Pranindita, J. J. E. Theeuwen, J.-F. Bastin, and A. J. Teuling (2022). "Shifts in regional water availability due to global tree restoration". *Nature Geoscience* 15, 363–368. DOI: https://doi.org/10.1038/s41561-022-00935-0.

Hoek van Dijke, A. J., K. Mallick, M. Schlerf, M. Machwitz, M. Herold, and A. J. Teuling (2020). "Examining the link between vegetation leaf area and land–atmosphere exchange of water, energy, and carbon fluxes using FLUXNET data". *Biogeosciences* 17.17, 4443–4457. DOI: https://doi.org/10.5194/bg-17-4443-2020.

Hoek van Dijke, A. J., K. Mallick, A. J. Teuling, M. Schlerf, M. Machwitz, S. K. Hassler, T. Blume, and M. Herold (2019). "Does the Normalized Difference Vegetation Index explain spatial and temporal variability in sap velocity in temperate forest ecosystems?" *Hydrol. Earth Syst. Sci.* 23.4, 2077–2091. DOI: https://doi.org/10.5194/hess-23-2077-2019.

Huete, A. R. (1988). "A soil-adjusted vegetation index (SAVI)". *Remote Sensing of Environment* 25.3, 295–309. DOI: https://doi.org/10.1016/0034-4257(88)90106-X.

Hunink, J., J. Eekhout, J. de Vente, S. Contreras, P. Droogers, and A. Baille (2017). "Hydrological modelling using satellite-based crop coefficients: a comparison of methods at the basin scale". *Remote Sensing* 9.2, 174–189. DOI: https://doi.org/10.3390/rs9020174.

Huxman, T. E., B. P. Wilcox, D. D. Breshears, R. L. Scott, K. A. Snyder, E. E. Small, K. Hultine, W. T. Pockman, and R. B. Jackson (2005). "Ecohydrological Implications of Woody Plant Encroachment". *Ecology* 86.2, 308–319.

Iio, A., K. Hikosaka, N. P. R. Anten, Y. Nakagawa, and A. Ito (2014). "Global dependence of field-observed leaf area index in woody species on climate: a systematic review". *Global Ecology and Biogeography* 23.3, 274–285. DOI: https://doi.org/10.1111/geb.12133.

Ilstedt, U., A. Bargués Tobella, H. R. Bazié, J. Bayala, E. Verbeeten, G. Nyberg, J. Sanou, L. Benegas, D. Murdiyarso, H. Laudon, D. Sheil, and A. Malmer (2016). "Intermediate tree cover can maximize groundwater recharge in the seasonally dry tropics". *Scientific Reports* 6.1, 21930. DOI: https://doi.org/10.1038/srep21930.

IPCC (2012). *Summary for Policymakers. In: Managing the Risks of Extreme Events and Disasters to Advance Climate Change Adaptation*. A Special Report of Working Groups I, II of the Intergovernmental Panel on Climate Change. Cambridge University

Press, Cambridge, UK, and New York, NY, USA. DOI: https://doi.org/10.1017/CBO9781139177245.002.

IRP (2019). *Land Restoration for Achieving the Sustainable Development Goals: An International Resource Panel Think Piece*. Report.

Jackson, R. B., E. G. Jobbáagy, R. Avissar, S. B. Roy, D. J. Barrett, C. W. Cook, K. A. Farley, D. C. le Maitre, B. A. McCarl, and B. C. Murray (2005). "Trading Water for Carbon with Biological Carbon Sequestration". *Science* 310.5756, 1944–1947.

Jarvis, P. G. (1976). "The Interpretation of the Variations in Leaf Water Potential and Stomatal Conductance Found in Canopies in the Field". *Philosophical Transactions of the Royal Society of London. Series B, Biological Sciences* 273.927, 593–610.

Jarvis, P. and K. McNaughton (1986). "Stomatal Control of Transpiration: Scaling Up from Leaf to Region". In: ed. by A. MacFadyen and E. Ford. Vol. 15. Advances in Ecological Research. Academic Press, 1–49. DOI: https://doi.org/10.1016/S0065-2504(08)60119-1.

Jennifer, F. and S. Natasa (2015). "Evidence linking rapid Arctic warming to mid-latitude weather patterns". *Philosophical Transactions of the Royal Society A.* 373, 20140170. DOI: https://doi.org/10.1098/rsta.2014.0170.

Jeong, S. J., C. H. Ho, H. J. Gim, and M. E. Brown (2011). "Phenology shifts at start vs. end of growing season in temperate vegetation over the Northern Hemisphere for the period 1982-2008". *Global Change Biology* 17.7, 2385–2399. DOI: https://doi.org/10.1111/j.1365-2486.2011.02397.x.

Jia, X., T. S. Zha, B. Wu, Y. Q. Zhang, J. N. Gong, S. G. Qin, G. P. Chen, D. Qian, S. Kellomäki, and H. Peltola (2014). "Biophysical controls on net ecosystem CO2 exchange over a semiarid shrubland in northwest China". *Biogeosciences* 11.17, 4679–4693. DOI: https://doi.org/10.5194/bg-11-4679-2014.

Jiang, L. and S. Islam (2001). "Estimation of surface evaporation map over Southern Great Plains using remote sensing data". *Water Resources Research* 37.2, 329–340. DOI: https://doi.org/doi:10.1029/2000WR900255.

Jiao, W., Q. Chang, and L. Wang (2019). "The Sensitivity of Satellite Solar-Induced Chlorophyll Fluorescence to Meteorological Drought". *Earth's Future* 7.5, 558–573. DOI: https://doi.org/10.1029/2018EF001087.

Jimenez, C., C. Prigent, F. Aires, and S. Ermida (2018). "All-weather land surface temperature estimates from microwave satellite observations, over several decades and real time: methodology and comparison with infrared estimates". In: *EGU General Assembly 2018*, 16003.

Jung, E. Y., D. Otieno, B. Lee, J. H. Lim, S. K. Kang, M. W. T. Schmidt, and J. Tenhunen (2011a). "Up-scaling to stand transpiration of an Asian temperate mixed-deciduous

forest from single tree sapflow measurements". *Plant Ecology* 212.3, 383–395. DOI: https://doi.org/10.1007/s11258-010-9829-3.

Jung, M., M. Reichstein, H. A. Margolis, A. Cescatti, A. D. Richardson, M. A. Arain, A. Arneth, C. Bernhofer, D. Bonal, J. Chen, D. Gianelle, N. Gobron, G. Kiely, W. Kutsch, G. Lasslop, B. E. Law, A. Lindroth, L. Merbold, L. Montagnani, E. J. Moors, D. Papale, M. Sottocornola, F. Vaccari, and C. Williams (2011b). "Global patterns of land-atmosphere fluxes of carbon dioxide, latent heat, and sensible heat derived from eddy covariance, satellite, and meteorological observations". *Journal of Geophysical Research: Biogeosciences* 116.3. DOI: https://doi.org/10.1029/2010JG001566.

Kamble, B., A. Kilic, and K. Hubbard (2013). "Estimating crop coefficients using remote sensing-based vegetation index". *Remote Sensing* 5.4, 1588–1602. DOI: https://doi.org/10.3390/rs5041588.

Kang, S., S. W. Running, J.-H. Lim, M. Zhao, C.-R. Park, and R. Loehman (2003). "A regional phenology model for detecting onset of greenness in temperate mixed forests, Korea: an application of MODIS leaf area index". *Remote Sensing of Environment* 86.2, 232–242. DOI: https://doi.org/10.1016/S0034-4257(03)00103-2.

Kannenberg, S. A., K. A. Novick, M. R. Alexander, J. T. Maxwell, D. J. P. Moore, R. P. Phillips, and W. R. L. Anderegg (2019). "Linking drought legacy effects across scales: From leaves to tree rings to ecosystems". *Global Change Biology* 25.9, 2978–2992. DOI: https://doi.org/10.1111/gcb.14710.

Kergoat, L. (1998). "A model for hydrological equilibrium of leaf area index on a global scale". *Journal of Hydrology* 212-213, 268–286. DOI: https://doi.org/10.1016/S0022-1694(98)00211-X.

Keys, P. W., M. Porkka, L. Wang-Erlandsson, I. Fetzer, T. Gleeson, and L. J. Gordon (2019). "Invisible water security: Moisture recycling and water resilience". *Water Security* 8, 100046. DOI: https://doi.org/10.1016/j.wasec.2019.100046.

Keys, P. W., L. Wang-Erlandsson, and L. J. Gordon (2016). "Revealing Invisible Water: Moisture Recycling as an Ecosystem Service". *PLOS ONE* 11.3, e0151993. DOI: https://doi.org/10.1371/journal.pone.0151993.

Kim, J., Q. Guo, D. Baldocchi, M. Leclerc, L. Xu, and H. Schmid (2006). "Upscaling fluxes from tower to landscape: Overlaying flux footprints on high-resolution (IKONOS) images of vegetation cover". *Agricultural and Forest Meteorology* 136, 132–146. DOI: https://doi.org/10.1016/j.agrformet.2004.11.015.

Kim, K., M.-c. Wang, S. Ranjitkar, S.-h. Liu, J.-c. Xu, and R. J. Zomer (2017). "Using leaf area index (LAI) to assess vegetation response to drought in Yunnan province of China". *Journal of Mountain Science* 14.9, 1863–1872. DOI: https://doi.org/10.1007/s11629-016-3971-x.

Kim, M. (1994). "The Use of Narrow Spectral Bands for Improving Remote Sensing Estimations of Fractionally Absorbed Photosynthetically Active Radiation". *Doctoral dissertation, University of Maryland at College Park*.

Kirchner, J. W., W. R. Berghuijs, S. T. Allen, M. Hrachowitz, R. Hut, and D. M. Rizzo (2020). "Streamflow response to forest management". *Nature* 578.7794, E12–E15. DOI: https://doi.org/10.1038/s41586-020-1940-6.

Knohl, A., L. Siebicke, F. Tiedemann, O. Kolle, and ICOS ETC (2020). *Drought-2018 ecosystem eddy covariance flux product from Hainich*. DOI: https://doi.org/10.18160/D4ET-BFPS.

Konapala, G., A. K. Mishra, Y. Wada, and M. E. Mann (2020). "Climate change will affect global water availability through compounding changes in seasonal precipitation and evaporation". *Nature Communications* 11.1, 3044. DOI: https://doi.org/10.1038/s41467-020-16757-w.

Kono, Y., A. Ishida, S.-T. Saiki, K. Yoshimura, M. Dannoura, K. Yazaki, F. Kimura, J. Yoshimura, and S.-i. Aikawa (2019). "Initial hydraulic failure followed by late-stage carbon starvation leads to drought-induced death in the tree Trema orientalis". *Communications Biology* 2.1, 8. DOI: https://doi.org/10.1038/s42003-018-0256-7.

Köppen, W. (1936). "Das geographische System der Klimate". In: *Handbuch der Klimatologie*. Ed. by W. Köppen and G. Geiger. Berlin: Gebrüder Borntraeger.

Koster, R. D., G. K. Walker, G. J. Collatz, and P. E. Thornton (2014). "Hydroclimatic Controls on the Means and Variability of Vegetation Phenology and Carbon Uptake". *Journal of Climate* 27.14, 5632–5652. DOI: https://doi.org/10.1175/jcli-d-13-00477.1.

Kruijt, B. and ICOS ETC (2020). *Drought-2018 ecosystem eddy covariance flux product from Loobos*. DOI: https://doi.org/10.18160/MV3K-WM09.

Kutsch, W. L., N. Hanan, B. Scholes, I. McHugh, W. Kubheka, H. Eckhardt, and C. Williams (2008). "Response of carbon fluxes to water relations in a savanna ecosystem in South Africa". *Biogeosciences* 5.6, 1797–1808. DOI: https://doi.org/10.5194/bg-5-1797-2008.

Lal, R. (1996). "Deforestation and land-use effects on soil degradation and rehabilitation in western Nigeria. I. Soil physical and hydrological properties". *Land Degradation & Development* 7.1, 19–45. DOI: https://doi.org/10.1002/(SICI)1099-145X(199603)7:1<19::AID-LDR212>3.0.CO;2-M.

Law, B. E., E. Falge, L. Gu, D. D. Baldocchi, P. Bakwin, P. Berbigier, K. Davis, A. J. Dolman, M. Falk, J. D. Fuentes, A. Goldstein, A. Granier, A. Grelle, D. Hollinger, I. A. Janssens, P. Jarvis, N. O. Jensen, G. Katul, Y. Mahli, G. Matteucci, T. Meyers, R. Monson, W. Munger, W. Oechel, R. Olson, K. Pilegaard, K. T. Paw U, H. Thorgeirsson, R. Valentini, S. Verma, T. Vesala, K. Wilson, and S. Wofsy (2002). "Environmental controls over carbon dioxide and water vapor exchange of terrestrial vegetation". *Agricultural*

and Forest Meteorology 113.1, 97–120. DOI: https://doi.org/10.1016/S0168-1923(02)00104-1.

Lawrence, D. and K. Vandecar (2015). "Effects of tropical deforestation on climate and agriculture". *Nature Climate Change* 5.1, 27–36. DOI: https://doi.org/10.1038/nclimate2430.

Lawrence, P. J. and T. N. Chase (2010). "Investigating the climate impacts of global land cover change in the community climate system model". *International Journal of Climatology* 30.13, 2066–2087. DOI: https://doi.org/10.1002/joc.2061.

Le Dantec, V., E. Dufrêne, and B. Saugier (2000). "Interannual and spatial variation in maximum leaf area index of temperate deciduous stands". *Forest Ecology and Management* 134.1, 71–81. DOI: https://doi.org/10.1016/S0378-1127(99)00246-7.

Lehner, B., K. Verdin, and A. Jarvis (2008). "New global hydrography derived from spaceborne elevation data". *Eos, Transactions, AGU* 89.10, 93–94.

Li, G., F. Zhang, Y. Jing, Y. Liu, and G. Sun (2017). "Response of evapotranspiration to changes in land use and land cover and climate in China during 2001–2013". *Science of The Total Environment* 596-597, 256–265. DOI: https://doi.org/10.1016/j.scitotenv.2017.04.080.

Li, Y., S. Piao, L. Z. X. Li, A. Chen, X. Wang, P. Ciais, L. Huang, X. Lian, S. Peng, Z. Zeng, K. Wang, and L. Zhou (2018). "Divergent hydrological response to large-scale afforestation and vegetation greening in China". *Science Advances* 4.5, eaar4182. DOI: https://doi.org/10.1126/sciadv.aar4182.

Liddell, M. (2013a). *Cape Tribulation Ozflux tower site*. Dataset. DOI: https://doi.org/102.100.100/14242.

– (2013b). *Cow Bay OzFlux tower site*. Dataset. DOI: https://doi.org/102.100.100/14244.

Lindroth, A., F. Lagergren, M. Aurela, B. Bjarnadottir, T. Christensen, E. Dellwik, A. Grelle, A. Ibrom, T. Johansson, H. Lankreijer, S. Launiainen, T. Laurila, M. Mölder, E. Nikinmaa, K. Pilegaard, B. D. Sigurdsson, and T. Vesala (2008). "Leaf area index is the principal scaling parameter for both gross photosynthesis and ecosystem respiration of Northern deciduous and coniferous forests". *Tellus, Series B: Chemical and Physical Meteorology* 60 B.2, 129–142. DOI: https://doi.org/10.1111/j.1600-0889.2006.00330.x.

Liu, C. L. C., O. Kuchma, and K. V. Krutovsky (2018). "Mixed-species versus monocultures in plantation forestry: Development, benefits, ecosystem services and perspectives for the future". *Global Ecology and Conservation* 15, e00419. DOI: https://doi.org/10.1016/j.gecco.2018.e00419.

Liu, S., L. Lu, D. Mao, and L. Jia (2007). "Evaluating parameterizations of aerodynamic resistance to heat transfer using field measurements". *Hydrology and Earth System Sciences* 11.2, 769–783. DOI: https://doi.org/10.5194/hess-11-769-2007.

Liu, Y., C. Dang, H. Yue, C. Lyu, and X. Dang (2021). "Enhanced drought detection and monitoring using sun-induced chlorophyll fluorescence over Hulun Buir Grassland, China". *Science of The Total Environment* 770, 145271. DOI: https://doi.org/10.1016/j.scitotenv.2021.145271.

Loveland, T. R., B. C. Reed, J. F. Brown, D. O. Ohlen, Z. Zhu, L. Yang, and J. W. Merchant (2000). "Development of a global land cover characteristics database and IGBP DISCover from 1 km AVHRR data". *International Journal of Remote Sensing* 21.6-7, 1303–1330. DOI: https://doi.org/10.1080/014311600210191.

Lu, Z., P. A. Miller, Q. Zhang, D. Wårlind, L. Nieradzik, J. Sjolte, Q. Li, and B. Smith (2019). "Vegetation Pattern and Terrestrial Carbon Variation in Past Warm and Cold Climates". *Geophysical Research Letters* 46.14, 8133–8143. DOI: https://doi.org/10.1029/2019gl083729.

Makarieva, A. M. and V. G. Gorshkov (2007). "Biotic pump of atmospheric moisture as driver of the hydrological cycle on land". *Hydrol. Earth Syst. Sci.* 11.2, 1013–1033. DOI: https://doi.org/10.5194/hess-11-1013-2007.

Mallick, K., D. Baldocchi, and co-authors (2022). "Water Stress Explains the Aerodynamic versus Radiometric Surface Temperature Paradox in Thermal-based Evaporation Modeling". *Geophysical Research Letters, (in revision).*

Mallick, K., A. J. Jarvis, E. Boegh, J. B. Fisher, D. T. Drewry, K. P. Tu, S. J. Hook, G. Hulley, J. Ardö, J. Beringer, A. Arain, and D. Niyogi (2014). "A Surface Temperature Initiated Closure (STIC) for surface energy balance fluxes". *Remote Sensing of Environment* 141, 243–261. DOI: https://doi.org/10.1016/j.rse.2013.10.022.

Mallick, K., M. Schlerf, G. Boulet, T. Udelhoven, J. Beringer, J. Cleverly, and A. Jarvis (2019). "A Novel Approach for Simultaneous Estimation of High Spatial Resolution LST, Evapotranspiration and Water Stress by Integrating SWIR Information into Surface Energy Balance Model". In: *Living Planet Symposium 2019.*

Mallick, K., I. Trebs, E. Boegh, L. Giustarini, M. Schlerf, D. T. Drewry, L. Hoffmann, C. Von Randow, B. Kruijt, A. Araùjo, S. Saleska, J. R. Ehleringer, T. F. Domingues, J. P. H. B. Ometto, A. D. Nobre, O. Luiz Leal De Moraes, M. Hayek, J. William Munger, and S. C. Wofsy (2016). "Canopy-scale biophysical controls of transpiration and evaporation in the Amazon Basin". *Hydrology and Earth System Sciences* 20.10, 4237–4264. DOI: https://doi.org/10.5194/hess-20-4237-2016.

Mallick, K., B. K. Bhattacharya, V. U. M. Rao, D. R. Reddy, S. Banerjee, H. Venkatesh, V. Pandey, G. Kar, J. Mukherjee, S. P. Vyas, A. S. Gadgil, and N. K. Patel (2009). "Latent heat flux estimation in clear sky days over Indian agroecosystems using noontime

satellite remote sensing data". *Agricultural and Forest Meteorology* 149.10, 1646–1665. DOI: https://doi.org/10.1016/j.agrformet.2009.05.006.

Mallick, K., E. Toivonen, I. Trebs, E. Boegh, J. Cleverly, D. Eamus, H. Koivusalo, D. Drewry, S. K. Arndt, A. Griebel, J. Beringer, and M. Garcia (2018). "Bridging Thermal Infrared Sensing and Physically-Based Evapotranspiration Modeling: From Theoretical Implementation to Validation Across an Aridity Gradient in Australian Ecosystems". *Water Resources Research* 54.5, 3409–3435. DOI: https://doi.org/10.1029/2017wr021357.

Maselli, F., D. Papale, M. Chiesi, G. Matteucci, L. Angeli, A. Raschi, and G. Seufert (2014). "Operational monitoring of daily evapotranspiration by the combination of MODIS NDVI and ground meteorological data: Application and evaluation in Central Italy". *Remote Sensing of Environment* 152, 279–290. DOI: https://doi.org/10.1016/j.rse.2014.06.021.

Meier, R., J. Schwaab, S. I. Seneviratne, M. Sprenger, E. Lewis, and E. L. Davin (2021). "Empirical estimate of forestation-induced precipitation changes in Europe". *Nature Geoscience* 14.7, 473–478. DOI: https://doi.org/10.1038/s41561-021-00773-6.

Meinzer, F. C., G. Goldstein, N. M. Holbrook, P. Jackson, and C. J. (1993). "Stomatal and environmental control of transpiration in a lowland tropical forest tree". *Plant, Cell & Environment* 16.4, 429–436. DOI: https://doi.org/10.1111/j.1365-3040.1993.tb00889.x.

Mekonnen, M. and A. Hoekstra (2016). "Four billion people facing severe water scarcity". *Science Advances* 2.2, e1500323. DOI: https://doi.org/10.1126/sciadv.1500323.

Milly, P. and K. Dunne (2016). "Potential evapotranspiration and continental drying". *Nature Climate Change* 6, 946–949. DOI: https://doi.org/10.1038/nclimate3046.

Miralles, D. G., W. Brutsaert, A. J. Dolman, and J. H. Gash (2020). "On the Use of the Term "Evapotranspiration"". *Water Resources Research* 56.11, e2020WR028055. DOI: https://doi.org/10.1029/2020WR028055.

Miralles, D. G., R. A. M. De Jeu, J. H. Gash, T. R. H. Holmes, and A. J. Dolman (2011). "Magnitude and variability of land evaporation and its components at the global scale". *Hydrology and Earth System Sciences* 15.3, 967–981. DOI: https://doi.org/10.5194/hess-15-967-2011.

Mitchell, P. J., R. G. Benyon, and P. N. J. Lane (2012). "Responses of evapotranspiration at different topographic positions and catchment water balance following a pronounced drought in a mixed species eucalypt forest, Australia". *Journal of Hydrology* 440-441, 62–74. DOI: https://doi.org/10.1016/j.jhydrol.2012.03.026.

Monteith, J. (1965). "Evaporation and Environment". *The state and movement of water in living organism. 19th Symp. Soc. Exptl. Biol.*, 205–234.

Müller, B., M. Bernhardt, and K. Schulz (2014). "Identification of catchment functional units by time series of thermal remote sensing images". *Hydrology and Earth System Sciences* 18, 5345–5329. DOI: https://doi.org/10.5194/hess-18-5345-2014.

Muñoz Sabater, J. (2019, accessed January 2020). *ERA5-Land monthly averaged data from 1981 to present*. Dataset. DOI: https://doi.org/10.24381/cds.68d2bb3.

Mutanga, O. and L. Kumar (2019). "Google earth engine applications". *Remote Sensing* 11.5. DOI: https://doi.org/10.3390/rs11050591.

Mutiibwa, D. and S. Irmak (2013). "AVHRR-NDVI-based crop coefficients for analyzing long-term trends in evapotranspiration in relation to changing climate in the U.S. High Plains". *Water Resources Research* 49.1, 231–244. DOI: https://doi.org/10.1029/2012wr012591.

Myneni, R., Y. Knyazikhin, and T. Park (2015). "MCD15A2H MODIS/Terra+Aqua Leaf Area Index/FPAR 8-day L4 Global 500m SIN Grid V006 [data set]". *NASA EOSDIS Land Processes DAAC*. DOI: https://doi.org/10.5067/MODIS/MCD15A2H.006.

Nagler, P., J. Cleverly, E. Glenn, D. Lampkin, A. Huete, and Z. Wan (2005). "Predicting riparian evapotranspiration from MODIS vegetation indices and meteorological data". *Remote Sensing of Environment* 94.1, 17–30. DOI: https://doi.org/10.1016/j.rse.2004.08.009.

Naumann, G., C. Cammalleri, L. Mentaschi, and L. Feyen (2021). "Increased economic drought impacts in Europe with anthropogenic warming". *Nature Climate Change* 11, 485–491. DOI: https://doi.org/10.1038/s41558-021-01044-3.

Ning, T., Z. Li, Q. Feng, W. Chen, and Z. Li (2020). "Effects of forest cover change on catchment evapotranspiration variation in China". *Hydrological Processes* 34.10, 2219–2228. DOI: https://doi.org/10.1002/hyp.13719.

O'Toole, J. C. and R. T. Cruz (1980). "Response of Leaf Water Potential, Stomatal Resistance, and Leaf Rolling to Water Stress". *Plant Physiology* 65.3, 428–432. DOI: https://doi.org/10.1104/pp.65.3.428.

O'Connor, J. C., M. J. Santos, S. C. Dekker, K. T. Rebel, and O. A. Tuinenburg (2021). "Atmospheric moisture contribution to the growing season in the Amazon arc of deforestation". *Environmental Research Letters* 16.8, 084026. DOI: https://doi.org/10.1088/1748-9326/ac12f0.

Obladen, N., P. Dechering, G. Skiadaresis, W. Tegel, J. Keßler, S. Höllerl, S. Kaps, M. Hertel, C. Dulamsuren, T. Seifert, M. Hirsch, and A. Seim (2021). "Tree mortality of European beech and Norway spruce induced by 2018-2019 hot droughts in central Germany". *Agricultural and Forest Meteorology* 307, 108482. DOI: https://doi.org/10.1016/j.agrformet.2021.108482.

Obrist, D., P. S. J. Verburg, M. H. Young, J. S. Coleman, D. E. Schorran, and J. Arnone (2003). "Quantifying the effects of phenology on ecosystem evapotranspiration in planted

grassland mesocosms using EcoCELL technology". *Agricultural and Forest Meteorology* 118.3-4, 173–183. DOI: https://doi.org/10.1016/S0168-1923(03)00111-4.

Öhrn, P., M. Berlin, M. Elfstrand, P. Krokene, and A. M. Jönsson (2021). "Seasonal variation in Norway spruce response to inoculation with bark beetle-associated bluestain fungi one year after a severe drought". *Forest Ecology and Management* 496, 119443. DOI: https://doi.org/10.1016/j.foreco.2021.119443.

Oki, T. and S. Kanae (2006). "Global hydrological cycles and world water resources". *Science* 313.5790, 1068–1072. DOI: https://doi.org/10.1126/science.1128845.

Oliveira, J. V. de, D. B. d. S. Ferreira, P. K. Sahoo, G. R. C. Sodré, E. B. de Souza, and J. C. B. Queiroz (2018). "Differences in precipitation and evapotranspiration between forested and deforested areas in the Amazon rainforest using remote sensing data". *Environmental Earth Sciences* 77.239. DOI: https://doi.org/10.1007/s12665-018-7411-9.

Orth, R. and G. Destouni (2018). "Drought reduces blue-water fluxes more strongly than green-water fluxes in Europe". *Nature Communications* 9.1. DOI: https://doi.org/10.1038/s41467-018-06013-7.

Oudin, L., V. Andréassian, J. Lerat, and C. Michel (2008). "Has land cover a significant impact on mean annual streamflow? An international assessment using 1508 catchments". *Journal of Hydrology* 357.3, 303–316. DOI: https://doi.org/10.1016/j.jhydrol.2008.05.021.

Padrón, R. S., L. Gudmundsson, P. Greve, and S. I. Seneviratne (2017). "Large-Scale Controls of the Surface Water Balance Over Land: Insights From a Systematic Review and Meta-Analysis". *Water Resources Research* 53.11, 9659–9678. DOI: https://doi.org/10.1002/2017WR021215.

Park, J., J. Baik, and M. Choi (2017). "Satellite-based crop coefficient and evapotranspiration using surface soil moisture and vegetation indices in Northeast Asia". *Catena* 156, 305–314. DOI: https://doi.org/10.1016/j.catena.2017.04.013.

Pastorello, G., C. Trotta, E. Canfora, H. Chu, D. Christianson, Y.-W. Cheah, C. Poindexter, J. Chen, A. Elbashandy, M. Humphrey, P. Isaac, D. Polidori, A. Ribeca, C. van Ingen, L. Zhang, B. Amiro, C. Ammann, M. A. Arain, J. Ardö, T. Arkebauer, S. K. Arndt, N. Arriga, M. Aubinet, M. Aurela, D. Baldocchi, A. Barr, E. Beamesderfer, L. B. Marchesini, O. Bergeron, J. Beringer, C. Bernhofer, D. Berveiller, D. Billesbach, T. A. Black, P. D. Blanken, G. Bohrer, J. Boike, P. V. Bolstad, D. Bonal, J.-M. Bonnefond, D. R. Bowling, R. Bracho, J. Brodeur, C. Brümmer, N. Buchmann, B. Burban, S. P. Burns, P. Buysse, P. Cale, M. Cavagna, P. Cellier, S. Chen, I. Chini, T. R. Christensen, J. Cleverly, A. Collalti, C. Consalvo, B. D. Cook, D. Cook, C. Coursolle, E. Cremonese, P. S. Curtis, E. D'Andrea, H. da Rocha, X. Dai, K. J. Davis, B. De Cinti, A. de Grandcourt, A. De Ligne, R. C. De Oliveira, N. Delpierre, A. R. Desai, C. M. Di Bella, P. di Tommasi, H. Dolman, F. Domingo, G. Dong, S. Dore, P. Duce, E. Dufrêne, A. Dunn, J. Dušek,

D. Eamus, U. Eichelmann, H. A. M. ElKhidir, W. Eugster, C. M. Ewenz, B. Ewers, D. Famulari, S. Fares, I. Feigenwinter, A. Feitz, R. Fensholt, G. Filippa, M. Fischer, J. Frank, M. Galvagno, M. Gharun, D. Gianelle, B. Gielen, et al. (2020). "The FLUXNET2015 dataset and the ONEFlux processing pipeline for eddy covariance data". *Scientific Data* 7.1, 225. DOI: https://doi.org/10.1038/s41597-020-0534-3.

Perugini, L., L. Caporaso, S. Marconi, A. Cescatti, B. Quesada, N. De Noblet-Ducoudré, J. I. House, and A. Arneth (2017). "Biophysical effects on temperature and precipitation due to land cover change". *Environmental Research Letters* 12.5, 053002. DOI: https://doi.org/10.1088/1748-9326/aa6b3f.

Peters, W., A. Bastos, P. Ciais, and A. Vermeulen (2020). "A historical, geographical and ecological perspective on the 2018 European summer drought". *Philos Trans R Soc Lond B Biol Sci* 375.1810, 20190505. DOI: https://doi.org/10.1098/rstb.2019.0505.

Pfister, L., N. Martínez-Carreras, C. Hissler, J. Klaus, G. E. Carrer, M. K. Stewart, and J. J. McDonnell (2017). "Bedrock geology controls on catchment storage, mixing, and release: A comparative analysis of 16 nested catchments". *Hydrological Processes* 31.10, 1828–1845. DOI: https://doi.org/10.1002/hyp.11134.

Piao, S., P. Friedlingstein, P. Ciais, N. de Noblet-Ducoudré, D. Labat, and S. Zaehle (2007). "Changes in climate and land use have a larger direct impact than rising CO¡sub¿2¡/sub¿ on global river runoff trends". *Proceedings of the National Academy of Sciences* 104.39, 15242–15247. DOI: https://doi.org/10.1073/pnas.0707213104.

Pranindita, A., A. J. Teuling, I. Fetzer, and L. Wang-Erlandsson (2021a). *The role of forests in securing water for agriculture globally*. Conference Paper. DOI: https://doi.org/10.5194/egusphere-egu21-15766.

Pranindita, A., L. Wang-Erlandsson, I. Fetzer, and A. J. Teuling (2021b). "Moisture recycling and the potential role of forests as moisture source during European heatwaves". *Climate Dynamics*. DOI: https://doi.org/10.1007/s00382-021-05921-7.

Prentice, I. C., W. Cramer, S. P. Harrison, R. Leemans, R. A. Monserud, and A. M. Solomon (1992). "Special Paper: A Global Biome Model Based on Plant Physiology and Dominance, Soil Properties and Climate". *Journal of Biogeography* 19.2, 117–134. DOI: https://doi.org/10.2307/2845499.

Priestley, C. H. B. and R. J. Taylor (1972). "On the Assessment of Surface Heat Flux and Evaporation Using Large-Scale Parameters". *Monthly Weather Review* 100.2, 81–92. DOI: https://doi.org/10.1175/1520-0493(1972)100<0081:otaosh>2.3.co;2.

Rahman, A. F., J. A. Gamon, D. A. Fuentes, D. A. Roberts, and D. Prentiss (2001). "Modeling spatially distributed ecosystem flux of boreal forest using hyperspectral indices from AVIRIS imagery". *Journal of Geophysical Research: Atmospheres* 106.D24, 33579–33591. DOI: https://doi.org/10.1029/2001JD900157.

Ramonet, M., P. Ciais, F. Apadula, J. Bartyzel, A. Bastos, P. Bergamaschi, P. E. Blanc, D. Brunner, L. Caracciolo di Torchiarolo, F. Calzolari, H. Chen, L. Chmura, A. Colomb, S.

Conil, P. Cristofanelli, E. Cuevas, R. Curcoll, M. Delmotte, A. di Sarra, L. Emmenegger, G. Forster, A. Frumau, C. Gerbig, F. Gheusi, S. Hammer, L. Haszpra, J. Hatakka, L. Hazan, M. Heliasz, S. Henne, A. Hensen, O. Hermansen, P. Keronen, R. Kivi, K. Komínková, D. Kubistin, O. Laurent, T. Laurila, J. V. Lavric, I. Lehner, K. E. J. Lehtinen, A. Leskinen, M. Leuenberger, I. Levin, M. Lindauer, M. Lopez, C. L. Myhre, I. Mammarella, G. Manca, A. Manning, M. V. Marek, P. Marklund, D. Martin, F. Meinhardt, N. Mihalopoulos, M. Mölder, J. A. Morgui, J. Necki, S. O'Doherty, C. O'Dowd, M. Ottosson, C. Philippon, S. Piacentino, J. M. Pichon, C. Plass-Duelmer, A. Resovsky, L. Rivier, X. Rodó, M. K. Sha, H. A. Scheeren, D. Sferlazzo, T. G. Spain, K. M. Stanley, M. Steinbacher, P. Trisolino, A. Vermeulen, G. Vítková, D. Weyrauch, I. Xueref-Remy, K. Yala, and C. Yver Kwok (2020). "The fingerprint of the summer 2018 drought in Europe on ground-based atmospheric CO¡sub¿2¡/sub¿ measurements". *Philosophical Transactions of the Royal Society B: Biological Sciences* 375.1810, 20190513. DOI: https://doi.org/10.1098/rstb.2019.0513.

Rebmann, C. and ICOS ETC (2020). *Drought-2018 ecosystem eddy covariance flux product from Hohes Holz*. DOI: https://doi.org/10.18160/J1YB-YEHC.

Reichstein, M., E. Falge, D. Baldocchi, D. Papale, M. Aubinet, P. Berbigier, C. Bernhofer, N. Buchmann, T. Gilmanov, A. Granier, T. Grünwald, K. Havránková, H. Ilvesniemi, D. Janous, A. Knohl, T. Laurila, A. Lohila, D. Loustau, G. Matteucci, T. Meyers, F. Miglietta, J.-M. Ourcival, J. Pumpanen, S. Rambal, E. Rotenberg, M. Sanz, J. Tenhunen, G. Seufert, F. Vaccari, T. Vesala, D. Yakir, and R. Valentini (2005). "On the separation of net ecosystem exchange into assimilation and ecosystem respiration: review and improved algorithm". *Global Change Biology* 11.9, 1424–1439. DOI: https://doi.org/10.1111/j.1365-2486.2005.001002.x.

Renner, M., S. Hassler, T. Blume, M. Weiler, A. Hildebrandt, M. Guderle, S. Schymanski, and A. Kleidon (2016). "Dominant controls of transpiration along a hillslope transect inferred from ecohydrological measurements and thermodynamic limits". *Hydrology and Earth System Sciences* 20, 2063–2083. DOI: https://doi.org/10.5194/hess-20-2063-20.

Reyes-Acosta, J. L. and M. W. Lubczynski (2013). "Mapping dry-season tree transpiration of an oak woodland at the catchment scale, using object-attributes derived from satellite imagery and sap flow measurements". *Agricultural and Forest Meteorology* 174-175, 184–201. DOI: https://doi.org/10.1016/j.agrformet.2013.02.012.

Reyes-González, A., J. Kjaersgaard, T. Trooien, C. Hay, and L. Ahiablame (2018). "Estimation of crop evapotranspiration using satellite remote sensing-based vegetation index". *Advances in Meteorology* 2018. DOI: https://doi.org/10.1155/2018/4525021.

Roderick, M., P. Greve, and G. Farquhar (2015). "On the assessment of aridity with changes in atmospheric CO2". *Water Resources Research* 51.7, 5450–5463. DOI: https://doi.org/10.1002/2015WR017031.

Roebroek, C. T. J., L. A. Melsen, A. J. Hoek van Dijke, Y. Fan, and A. J. Teuling (2020). "Global distribution of hydrologic controls on forest growth". *Hydrol. Earth Syst. Sci.* 24.9, 4625–4639. DOI: https://doi.org/10.5194/hess-24-4625-2020.

Rosenzweig, C., D. Karoly, M. Vicarelli, P. Neofotis, Q. Wu, G. Casassa, A. Menzel, T. L. Root, N. Estrella, B. Seguin, P. Tryjanowski, C. Liu, S. Rawlins, and A. Imeson (2008). "Attributing physical and biological impacts to anthropogenic climate change". *Nature* 453.7193, 353–357. DOI: https://doi.org/10.1038/nature06937.

Ryan, M. G., N. Phillips, and B. J. Bond (2006). "The hydraulic limitation hypothesis revisited". *Plant, Cell & Environment* 29.3, 367–381. DOI: https://doi.org/10.1111/j.1365-3040.2005.01478.x.

Schenk, H. J. and R. B. Jackson (2002). "THE GLOBAL BIOGEOGRAPHY OF ROOTS". *Ecological Monographs* 72.3, 311–328. DOI: https://doi.org/10.1890/0012-9615(2002)072[0311:TGBOR]2.0.CO;2.

Schlesinger, W. and S. Jasechko (2014). "Transpiration in the global water cycle". *Agricultural and Forest Meteorology* 189-190, 115–117. DOI: https://doi.org/10.1016/j.agrformet.2014.01.011.

Schmitt, M., M. Bahn, G. Wohlfahrt, U. Tappeiner, and A. Cernusca (2010). "Land use affects the net ecosystem CO2 exchange and its components in mountain grasslands". *Biogeosciences* 7.8, 2297–2309. DOI: https://doi.org/10.5194/bg-7-2297-2010.

Schuldt, B., A. Buras, M. Arend, Y. Vitasse, C. Beierkuhnlein, A. Damm, M. Gharun, T. E. E. Grams, M. Hauck, P. Hajek, H. Hartmann, E. Hiltbrunner, G. Hoch, M. Holloway-Phillips, C. Körner, E. Larysch, T. Lübbe, D. B. Nelson, A. Rammig, A. Rigling, L. Rose, N. K. Ruehr, K. Schumann, F. Weiser, C. Werner, T. Wohlgemuth, C. S. Zang, and A. Kahmen (2020). "A first assessment of the impact of the extreme 2018 summer drought on Central European forests". *Basic and Applied Ecology* 45, 86–103. DOI: https://doi.org/10.1016/j.baae.2020.04.003.

Seijger, C., D. Kleinschmit, D. Schmidt-Vogt, M. Mehmood-Ul-Hassan, and C. Martius (2021). "Water and sectoral policies in agriculture–forest frontiers: An expanded interdisciplinary research approach". *Ambio* 50, 2311–2321. DOI: https://doi.org/10.1007/s13280-021-01555-5.

Sellers, P. J., R. E. Dickinson, D. Randall, A. Betts, F. G. Hall, J. Berry, G. Collatz, A. Denning, H. Mooney, C. Nobre, N. Sato, C. Field, and A. Henderson-Sellers (1997). "Modeling the Exchanges of energy, water and carbon between continents and the atmosphere". *Science* 275, 502–509. DOI: https://doi.org/10.1126/science.275.5299.502.

Sellers, P. (1985). "Canopy reflectance, photosynthesis and transpiration". *International Journal of Remote Sensing* 6.8, 1335–1372. DOI: https://doi.org/10.1080/01431168508948283.

Seneviratne, S. I., I. Lehner, J. Gurtz, A. J. Teuling, H. Lang, U. Moser, D. Grebner, L. Menzel, K. Schroff, T. Vitvar, and M. Zappa (2012). "Swiss prealpine Rietholzbach research catchment and lysimeter: 32 year time series and 2003 drought event". *Water Resources Research* 48.6. DOI: https://doi.org/10.1029/2011WR011749.

Senf, C. and R. Seidl (2021). "Persistent impacts of the 2018 drought on forest disturbance regimes in Europe". *Biogeosciences* 18.18, 5223–5230. DOI: https://doi.org/10.5194/bg-18-5223-2021.

Senf, C., A. Buras, C. S. Zang, A. Rammig, and R. Seidl (2020). "Excess forest mortality is consistently linked to drought across Europe". *Nature Communications* 11.1, 6200. DOI: https://doi.org/10.1038/s41467-020-19924-1.

Shabanov, N. V., H. Dong, Y. Wenze, B. Tan, Y. Knyazikhin, R. B. Myneni, D. E. Ahl, S. T. Gower, A. R. Huete, L. E. O. C. Aragao, and Y. E. Shimabukuro (2005). "Analysis and optimization of the MODIS leaf area index algorithm retrievals over broadleaf forests". *IEEE Transactions on Geoscience and Remote Sensing* 43.8, 1855–1865. DOI: https://doi.org/10.1109/TGRS.2005.852477.

Shao, J., X. Zhou, Y. Luo, B. Li, M. Aurela, D. Billesbach, P. D. Blanken, R. Bracho, J. Chen, M. Fischer, Y. Fu, L. Gu, S. Han, Y. He, T. Kolb, Y. Li, Z. Nagy, S. Niu, W. C. Oechel, K. Pinter, P. Shi, A. Suyker, M. Torn, A. Varlagin, H. Wang, J. Yan, G. Yu, and J. Zhang (2015). "Biotic and climatic controls on interannual variability in carbon fluxes across terrestrial ecosystems". *Agricultural and Forest Meteorology* 205, 11–22. DOI: https://doi.org/10.1016/j.agrformet.2015.02.007.

Shaw, T. A. (2019). "Mechanisms of Future Predicted Changes in the Zonal Mean Mid-Latitude Circulation". *Current Climate Change Reports* 5.4, 345–357. DOI: https://doi.org/10.1007/s40641-019-00145-8.

Sheil, D. and D. Murdiyarso (2009). "How Forests Attract Rain: An Examination of a New Hypothesis". *BioScience* 59.4, 341–347. DOI: https://doi.org/10.1525/bio.2009.59.4.12.

Si, Y., M. Schlerf, R. Zurita-Milla, A. Skidmore, and T. Wang (2012). "Mapping spatio-temporal variation of grassland quantity and quality using MERIS data and the PROSAIL model". *Remote Sensing of Environment* 121, 415–425. DOI: https://doi.org/10.1016/j.rse.2012.02.011.

Smith, D. M. and S. J. Allen (1996). "Measurement of sap flow in plant stems". *Journal of Experimental Botany* 47.305, 1833–1844.

Smith, N. E., L. M. J. Kooijmans, G. Koren, E. van Schaik, A. M. van der Woude, N. Wanders, M. Ramonet, I. Xueref-Remy, L. Siebicke, G. Manca, C. Brümmer, I. T. Baker, K. D. Haynes, I. T. Luijkx, and W. Peters (2020). "Spring enhancement and summer reduction in carbon uptake during the 2018 drought in northwestern Europe". *Philosophical Transactions of the Royal Society B: Biological Sciences* 375.1810, 20190509. DOI: https://doi.org/10.1098/rstb.2019.0509.

Sobrado, M. A. (1994). "Leaf age effects on photosynthetic rate, transpiration rate and nitrogen content in a tropical dry forest". *Physiologia Plantarum* 90.1, 210–215. DOI: https://doi.org/10.1111/j.1399-3054.1994.tb02213.x.

Spracklen, D., J. Baker, L. Garcia-Carreras, and J. Marsham (2018). "The Effects of Tropical Vegetation on Rainfall". *Annual Review of Environment and Resources* 43.1, 193–218. DOI: https://doi.org/10.1146/annurev-environ-102017-030136.

Stanke, C., M. Kerac, C. Prudhomme, J. Medlock, and V. Murray (2013). "Health Effects of Drought: A Systematic Review of the Evidence". *PLoS Currents* JUNE. DOI: https://doi.org/10.1371/currents.dis.7a2cee9e980f91ad7697b570bcc4b004.

Stuyfzand, P. J. (1984). "Effecten van vegetatie en luchtverontreiniging op de grondwaterkwaliteit in kalkrijke duinen bij Castricum : lysimeterwaarnemingen." *H twee O : tijdschrift voor watervoorziening en afvalwaterbehandeling* 17.8, 152–159.

Su, Z. (2002). "The Surface Energy Balance System (SEBS) for estimation of turbulent heat fluxes". *Hydrology and Earth System Sciences* 6.1, 85–99. DOI: https://doi.org/10.5194/hess-6-85-2002.

Sun, G., G. Zhou, Z. Zhang, X. Wei, S. G. McNulty, and J. M. Vose (2006). "Potential water yield reduction due to forestation across China". *Journal of Hydrology* 328.3, 548–558. DOI: https://doi.org/10.1016/j.jhydrol.2005.12.013.

Sun, X., B. P. Wilcox, and C. B. Zou (2019). "Evapotranspiration partitioning in dryland ecosystems: A global meta-analysis of in situ studies". *Journal of Hydrology* 576, 123–136. DOI: https://doi.org/10.1016/j.jhydrol.2019.06.022.

Swann, A. L. S., M. M. Laguë, E. S. Garcia, J. P. Field, D. D. Breshears, D. J. P. Moore, S. R. Saleska, S. C. Stark, J. C. Villegas, D. J. Law, and D. M. Minor (2018). "Continental-scale consequences of tree die-offs in North America: identifying where forest loss matters most". *Environmental Research Letters* 13.5, 055014. DOI: https://doi.org/10.1088/1748-9326/aaba0f.

Szilagyi, J. (2000). "Can a vegetation index derived from remote sensing be indicative of areal transpiration?" *Ecological Modelling* 127.1, 65–79. DOI: https://doi.org/10.1016/S0304-3800(99)00200-8.

Team, D. 2. and I. E. T. Centre (2020). "Drought-2018 ecosystem eddy covariance flux product for 52 stations in FLUXNET-Archive format". DOI: https://doi.org/10.18160/YVR0-4898.

Teuling, A. J., E. A. G. de Badts, F. A. Jansen, R. Fuchs, J. Buitink, A. J. Hoek van Dijke, and S. M. Sterling (2019). "Climate change, reforestation/afforestation, and urbanization impacts on evapotranspiration and streamflow in Europe". *Hydrol. Earth Syst. Sci.* 23.9, 3631–3652. DOI: https://doi.org/10.5194/hess-23-3631-2019.

Teuling, A. J., M. Hirschi, A. Ohmura, M. Wild, M. Reichstein, P. Ciais, N. Buchmann, C. Ammann, L. Montagnani, A. D. Richardson, G. Wohlfahrt, and S. I. Seneviratne (2009).

"A regional perspective on trends in continental evaporation". *Geophysical Research Letters* 36.2. DOI: https://doi.org/10.1029/2008GL036584.

Teuling, A. J. (2018). "A Forest Evapotranspiration Paradox Investigated Using Lysimeter Data". *Vadose Zone Journal* 17.1, 170031. DOI: https://doi.org/10.2136/vzj2017.01.0031.

Teuling, A. J. and A. J. Hoek van Dijke (2020). "Forest age and water yield". *Nature* 578.7794, E16–E18. DOI: https://doi.org/10.1038/s41586-020-1941-5.

Teuling, A. J., S. I. Seneviratne, R. Stöckli, M. Reichstein, E. Moors, P. Ciais, S. Luyssaert, B. van den Hurk, C. Ammann, C. Bernhofer, E. Dellwik, D. Gianelle, B. Gielen, T. Grünwald, K. Klumpp, L. Montagnani, C. Moureaux, M. Sottocornola, and G. Wohlfahrt (2010). "Contrasting response of European forest and grassland energy exchange to heatwaves". *Nature Geoscience* 3.10, 722–727. DOI: https://doi.org/10.1038/ngeo950.

Trabucco, A. and R. Zomer (2018). *Global Aridity Index and Potential Evapo-Transpiration (ET0)*. Dataset. DOI: https://doi.org/10.6084/m9.figshare.7504448.v3.

Treml, V., J. Maek, J. Tumajer, M. Rydval, V. Čada, O. Ledvinka, and M. Svoboda (2022). "Trends in climatically driven extreme growth reductions of Picea abies and Pinus sylvestris in Central Europe". *Global Change Biology* 28.2, 557–570. DOI: https://doi.org/10.1111/gcb.15922.

Tuinenburg, O. A. and A. Staal (2020). "Tracking the global flows of atmospheric moisture and associated uncertainties". *Hydrol. Earth Syst. Sci.* 24, 2419–2435. DOI: https://doi.org/10.5194/hess-24-2419-2020.

Tuinenburg, O. A., J. J. E. Theeuwen, and A. Staal (2020a). *Global evaporation to precipitation flows obtained with Lagrangian atmospheric moisture tracking*. Dataset. DOI: https://doi.org/10.1594/PANGAEA.912710.

– (2020b). "High-resolution global atmospheric moisture connections from evaporation to precipitation." *Earth Syst. Sci. Data* 12, 3177–3188. DOI: https://doi.org/10.5194/essd-12-3177-2020.

Turner, D. P., W. D. Ritts, W. B. Cohen, S. T. Gower, M. Zhao, S. W. Running, S. C. Wofsy, S. Urbanski, A. L. Dunn, and J. W. Munger (2003). "Scaling Gross Primary Production (GPP) over boreal and deciduous forest landscapes in support of MODIS GPP product validation". *Remote Sensing of Environment* 88.3, 256–270. DOI: https://doi.org/10.1016/j.rse.2003.06.005.

Van Der Ent, R. J. and H. H. G. Savenije (2011). "Length and time scales of atmospheric moisture recycling". *Atmospheric Chemistry and Physics* 11.5, 1853–1863. DOI: https://doi.org/10.5194/acp-11-1853-2011.

Van der Hoeven, P. (2011). "Lysimeters Castricum : meetproject en datafiles". *Alterra-rapport 2053-1*.

Van Heerwaarden, C. C. and A. J. Teuling (2014). "Disentangling the response of forest and grassland energy exchange to heatwaves under idealized land–atmosphere coupling". *Biogeosciences* 11.21, 6159–6171. DOI: https://doi.org/10.5194/bg-11-6159-2014.

Vecchi, G. A., B. J. Soden, A. T. Wittenberg, I. M. Held, A. Leetmaa, and M. J. Harrison (2006). "Weakening of tropical Pacific atmospheric circulation due to anthropogenic forcing". *Nature* 441.7089, 73–76. DOI: https://doi.org/10.1038/nature04744.

Vicca, S., M. Balzarolo, I. Filella, A. Granier, M. Herbst, A. Knohl, B. Longdoz, M. Mund, Z. Nagy, K. Pintér, S. Rambal, J. Verbesselt, A. Verger, A. Zeileis, C. Zhang, and J. Peñuelas (2016). "Remotely-sensed detection of effects of extreme droughts on gross primary production". *Scientific Reports* 6.1, 28269. DOI: https://doi.org/10.1038/srep28269.

Vuichard, N. and D. Papale (2015). "Filling the gaps in meteorological continuous data measured at FLUXNET sites with ERA-Interim reanalysis". *Earth Syst. Sci. Data* 7.2, 157–171. DOI: https://doi.org/10.5194/essd-7-157-2015.

Wagle, P., X. Xiao, R. L. Scott, T. E. Kolb, D. R. Cook, N. Brunsell, D. D. Baldocchi, J. Basara, R. Matamala, Y. Zhou, and R. Bajgain (2015). "Biophysical controls on carbon and water vapor fluxes across a grassland climatic gradient in the United States". *Agricultural and Forest Meteorology* 214-215, 293–305. DOI: https://doi.org/10.1016/j.agrformet.2015.08.265.

Wang, L., S. Good, and K. Caylor (2014). "Global synthesis of vegetation control on evapotranspiration partitioning". *Geophysical Research Letters* 41, 6753–6757. DOI: https://doi.org/10.1002/2014GL061439..

Wang, Q., S. Adiku, J. Tenhunen, and A. Granier (2005). "On the relationship of NDVI with leaf area index in a deciduous forest site". *Remote Sensing of Environment* 94, 244–255.

Wang-Erlandsson, L., I. Fetzer, P. W. Keys, R. J. van der Ent, H. H. G. Savenije, and L. J. Gordon (2018). "Remote land use impacts on river flows through atmospheric teleconnections". *Hydrol. Earth Syst. Sci.* 22.8, 4311–4328. DOI: https://doi.org/10.5194/hess-22-4311-2018.

Waring, R. H. and J. J. Landsberg (2011). "Generalizing plant-water relations to landscapes". *Journal of Plant Ecology* 4.1-2, 101–113. DOI: https://doi.org/10.1093/jpe/rtq041.

Wehr, R. and S. R. Saleska (2021). "Calculating canopy stomatal conductance from eddy covariance measurements, in light of the energy budget closure problem". *Biogeosciences* 18.1, 13–24. DOI: https://doi.org/10.5194/bg-18-13-2021.

Wei, Z., K. Yoshimura, L. Wang, D. Miralles, S. Jasechko, and X. Lee (2017a). "Revisiting the contribution of transpiration to global terrestrial evapotranspiration". *Geophysical Research Letters* 44, 2792–2801. DOI: https://doi.org/10.1002/2016GL072235.

Wei, Z., K. Yoshimura, L. Wang, D. G. Miralles, S. Jasechko, and X. Lee (2017b). "Revisiting the contribution of transpiration to global terrestrial evapotranspiration". *Geophysical Research Letters* 44.6, 2792–2801. DOI: https://doi.org/10.1002/2016gl072235.

Wierik, S. A. te, E. L. H. Cammeraat, J. Gupta, and Y. A. Artzy-Randrup (2021). "Reviewing the Impact of Land Use and Land-Use Change on Moisture Recycling and Precipitation Patterns". *Water Resources Research* 57.7, e2020WR029234. DOI: https://doi.org/10.1029/2020WR029234.

Wild, M., D. Folini, C. Schär, N. Loeb, E. G. Dutton, and G. König-Langlo (2013). "The global energy balance from a surface perspective". *Climate Dynamics* 40.11, 3107–3134. DOI: https://doi.org/10.1007/s00382-012-1569-8.

Williams, C. A. and J. D. Albertson (2004). "Soil moisture controls on canopy-scale water and carbon fluxes in an African savanna". *Water Resources Research* 40.9. DOI: https://doi.org/10.1029/2004wr003208.

Williams, C. A., M. Reichstein, N. Buchmann, D. Baldocchi, C. Beer, C. Schwalm, G. Wohlfahrt, N. Hasler, C. Bernhofer, T. Foken, D. Papale, S. Schymanski, and K. Schaefer (2012). "Climate and vegetation controls on the surface water balance: Synthesis of evapotranspiration measured across a global network of flux towers". *Water Resources Research* 48.6. DOI: https://doi.org/10.1029/2011WR011586.

Williams, I. N., Y. Lu, L. M. Kueppers, W. J. Riley, S. C. Biraud, J. E. Bagley, and M. S. Torn (2016). "Land-atmosphere coupling and climate prediction over the U.S. Southern Great Plains". *Journal of Geophysical Research: Atmospheres* 121.20, 12.125–12.144. DOI: https://doi.org/10.1002/2016jd025223.

Williams, I. N. and M. S. Torn (2015). "Vegetation controls on surface heat flux partitioning, and land-atmosphere coupling". *Geophysical Research Letters* 42.21, 9416–9424. DOI: https://doi.org/10.1002/2015gl066305.

Winkler, K., R. Fuchs, M. Rounsevell, and M. Herold (2021). "Global land use changes are four times greater than previously estimated". *Nature Communications* 12.1. DOI: https://doi.org/10.1038/s41467-021-22702-2.

Wolf, S., W. Eugster, C. Ammann, M. Häni, S. Zielis, R. Hiller, J. Stieger, D. Imer, L. Merbold, and N. Buchmann (2013). "Contrasting response of grassland versus forest carbon and water fluxes to spring drought in Switzerland". *Environmental Research Letters* 8.3, 035007. DOI: https://doi.org/10.1088/1748-9326/8/3/035007.

Woodwell, G. M., R. H. Whittaker, W. A. Reiners, G. E. Likens, C. C. Delwiche, and D. B. Botkin (1978). "The Biota and the World Carbon Budget". *Science* 199.4325, 141–146. DOI: https://doi.org/10.1126/science.199.4325.141.

Wrede, S., F. Fenicia, N. Martínez-Carreras, J. Juilleret, C. Hissler, A. Krein, H. H. G. Savenije, S. Uhlenbrook, D. Kavetski, and L. Pfister (2015). "Towards more systematic

perceptual model development: a case study using 3 Luxembourgish catchments". *Hydrological Processes* 29.12, 2731–2750. DOI: https://doi.org/10.1002/hyp.10393.

Wu, D., X. Zhao, S. Liang, T. Zhou, K. Huang, B. Tang, and W. Zhao (2015). "Time-lag effects of global vegetation responses to climate change". *Global Change Biology* 21.9, 3520–3531. DOI: https://doi.org/10.1111/gcb.12945.

Xie, X., A. Li, H. Jin, J. Tan, C. Wang, G. Lei, Z. Zhang, J. Bian, and X. Nan (2019). "Assessment of five satellite-derived LAI datasets for GPP estimations through ecosystem models". *Science of the Total Environment* 690, 1120–1130. DOI: https://doi.org/10.1016/j.scitotenv.2019.06.516.

Xu, B., T. Park, K. Yan, C. Chen, Y. Zeng, W. Song, G. Yin, J. Li, Q. Liu, Y. Knyazikhin, and R. B. Myneni (2018). "Analysis of global LAI/FPAR products from VIIRS and MODIS sensors for spatio-temporal consistency and uncertainty from 2012-2016". *Forests* 9.2. DOI: https://doi.org/10.3390/f9020073.

Xu, R., Y. Li, A. J. Teuling, L. Zhao, D. V. Spracklen, L. Garcia-Carreras, R. Meier, L. Chen, Y. Zheng, H. Lin, and B. Fu (2021). "Contrasting impacts of forests on cloud cover based on satellite observations". *Nature Communications* 13.1, 670. DOI: https://doi.org/10.1038/s41467-022-28161-7.

Xu, X., W. Liu, B. R. Scanlon, L. Zhang, and M. Pan (2013). "Local and global factors controlling water-energy balances within the Budyko framework". *Geophysical Research Letters* 40.23, 6123–6129. DOI: https://doi.org/10.1002/2013gl058324.

Yan, H., S. Q. Wang, D. Billesbach, W. Oechel, J. H. Zhang, T. Meyers, T. A. Martin, R. Matamala, D. Baldocchi, G. Bohrer, D. Dragoni, and R. Scott (2012). "Global estimation of evapotranspiration using a leaf area index-based surface energy and water balance model". *Remote Sensing of Environment* 124, 581–595. DOI: https://doi.org/10.1016/j.rse.2012.06.004.

Yan, K., T. Park, G. Yan, Z. Liu, B. Yang, C. Chen, R. R. Nemani, Y. Knyazikhin, and R. B. Myneni (2016). "Evaluation of MODIS LAI/FPAR product collection 6. Part 2: Validation and intercomparison". *Remote Sensing* 8.6. DOI: https://doi.org/10.3390/rs8060460.

Yang, D., W. Shao, P. J.-F. Yeh, H. Yang, S. Kanae, and T. Oki (2009). "Impact of vegetation coverage on regional water balance in the nonhumid regions of China". *Water Resources Research* 45.7. DOI: https://doi.org/10.1029/2008WR006948.

Yosef, G., R. Walko, R. Avisar, F. Tatarinov, E. Rotenberg, and D. Yakir (2018). "Large-scale semi-arid afforestation can enhance precipitation and carbon sequestration potential". *Scientific Reports* 8.1, 996. DOI: https://doi.org/10.1038/s41598-018-19265-6.

Yu, C. and D. Liu (2019). "Response in productivity of natural vegetation to drought in northeast China based on MODIS". *Shengtai Xuebao/ Acta Ecologica Sinica* 39.11, 3978–3990. DOI: https://doi.org/10.5846/stxb201803300655.

Zehe, E., U. Ehret, L. Pfister, T. Blume, B. Schröder, M. Westhoff, C. Jackisch, S. J. Schymanski, M. Weiler, K. Schulz, N. Allroggen, J. Tronicke, L. van Schaik, P. Dietrich, U. Scherer, J. Eccard, V. Wulfmeyer, and A. Kleidon (2014). "HESS Opinions: From response units to functional units: a thermodynamic reinterpretation of the HRU concept to link spatial organization and functioning of intermediate scale catchments". *Hydrol. Earth Syst. Sci.* 18.11, 4635–4655. DOI: https://doi.org/10.5194/hess-18-4635-2014.

Zha, T., A. G. Barr, G. van der Kamp, T. A. Black, J. H. McCaughey, and L. B. Flanagan (2010). "Interannual variation of evapotranspiration from forest and grassland ecosystems in western canada in relation to drought". *Agricultural and Forest Meteorology* 150.11, 1476–1484. DOI: https://doi.org/10.1016/j.agrformet.2010.08.003.

Zhang, K., J. S. Kimball, Q. Mu, L. A. Jones, S. J. Goetz, and S. W. Running (2009). "Satellite based analysis of northern ET trends and associated changes in the regional water balance from 1983 to 2005". *Journal of Hydrology* 379.1, 92–110. DOI: https://doi.org/10.1016/j.jhydrol.2009.09.047.

Zhang, L., W. R. Dawes, and G. R. Walker (2001). "Response of mean annual evapotranspiration to vegetation changes at catchment scale". *Water Resources Research* 37.3, 701–708. DOI: https://doi.org/10.1029/2000wr900325.

Zhang, L., K. Hickel, W. R. Dawes, F. H. S. Chiew, A. W. Western, and P. R. Briggs (2004). "A rational function approach for estimating mean annual evapotranspiration". *Water Resources Research* 40.2, W02502. DOI: https://doi.org/10.1029/2003wr002710.

Zheng, G. and L. Moskal (2009). "Retrieving Leaf Area Index (LAI) Using Remote Sensing: Theories, Methods and Sensors". *Sensors* 9.4, 2719–2745. DOI: https://doi.org/10.3390/s90402719.

Zhou, S., B. Yu, Y. Huang, and G. Wang (2015). "The complementary relationship and generation of the Budyko functions". *Geophysical Research Letters* 42.6, 1781–1790. DOI: https://doi.org/10.1002/2015GL063511.

Zhu, W., S. Jia, and A. Lv (2017). "A Universal Ts-VI Triangle Method for the Continuous Retrieval of Evaporative Fraction From MODIS Products". *Journal of Geophysical Research: Atmospheres* 122.19, 10.206–10.227. DOI: https://doi.org/10.1002/2017JD026964.

Zhu, Z., S. Piao, R. B. Myneni, M. Huang, Z. Zeng, J. G. Canadell, P. Ciais, S. Sitch, P. Friedlingstein, A. Arneth, C. Cao, L. Cheng, E. Kato, C. Koven, Y. Li, X. Lian, Y. Liu, R. Liu, J. Mao, Y. Pan, S. Peng, J. Peñuelas, B. Poulter, T. A. M. Pugh, B. D. Stocker, N. Viovy, X. Wang, Y. Wang, Z. Xiao, H. Yang, S. Zaehle, and N. Zeng (2016). "Greening of the Earth and its drivers". *Nature Climate Change* 6.8, 791–795. DOI: http://dx.doi.org/10.1038/nclimate3004.

Zimmermann, B. and H. Elsenbeer (2008). "Spatial and temporal variability of soil saturated hydraulic conductivity in gradients of disturbance". *Journal of Hydrology* 361.1, 78–95. DOI: https://doi.org/10.1016/j.jhydrol.2008.07.027.

Acknowledgements

Below I would like to thank some people that contributed to making my PhD years a very positive experience.

First of all, I would like to thank my supervisors. Kaniska, Miriam, Ryan, and Martin and Martin, thank you for giving me the opportunity to start this project with you and many thanks for providing inspiration and guidance during the past years. I very much appreciate it that you were open to ideas from my side and from each other, and that I received a lot of freedom in doing my work and spending time in all three research groups. Martin H, I appreciate your involvement in the project, your guidance on the process level, and that you were always available for questions or discussions. Ryan, thank you for the (ad hoc) meetings to discuss work and life, and without your "you could quickly check this, it should not take much longer than two days"-remarks I might not have considered some of the analyses present in the thesis today. Kaniska, thanks for your engagement in my work, for example during our Friday coffee breaks when you explained complex hydrological processes with metaphors. Miriam, I appreciated your very detailed feedback on my manuscripts and your active involvement in our research group. And Martin S, your focus on study objectives and hypotheses has taught me to be critical in the first phases of a study, something that I will benefit from for the rest of my academic career.

LIST, GRS, and HWM are amazing places to work. I would like to thank all my colleagues for welcoming me, and making me feel like a group-member, despite my frequent travels between the groups. Laurent and colleagues, thank you for setting up the DTU and for organising the meetings and retreat. LIST PhDs, thank you for the good company during lunches and after works in the park or Coyote bar. GRS, you are an an incredibly heartwarming environment. I love the three times daily coffee breaks and experienced that happiness and scientific growth increase with the number of coffee breaks. And a special thanks to the GRS band, I love your funny lyrics and performances. HWM, and specifically those that were ´Young and Hot´, you always made me feel welcome and accepted as a group member, despite the fact that I was around less often. Many thanks! Besides my direct colleagues, I had the opportunity to learn from and be inspired by several co-authors, (anonymous) reviewers, and great students. Thank you for sharing

data, for providing valuable suggestions and useful feedback on my manuscripts, and for providing new insight into very interesting research topics.

A special thanks to my paranymphs Daniela and Tessa. Thanks for being my first point of contact for serious updates and colleague gossip after I returned from a trip. Daniela, you were an amazing office mate from day one, and it was an honour to be your paranymph. Tessa, I was very fortunate to have you as my ENVISION-HWM buddy, "sitting in the same little barge" and I enjoyed our coffee walks. There are many other colleagues, but particularly Alvaro and Mo, that I would like to thank for the personal talks, inspiration, and for being such attentive people.

I would like to thank my friends that make every-day life so much fun. Acacie-A and -B: why again did we travel by vacuum cleaner? I look forward to many more years of crazy ideas, tea, and (road)trips together. The Eetclub, I enjoyed academically and personally growing up together, and above all our weekend-trips and vacations. Inge, Brechtje, and Erica, we met long before I moved to Wageningen, and I am grateful that we are still friends! Goeie Vraag, thank you for the nice rowing outings, sometimes even round the clock. Voorwaarts Van Vliet, thank you for the good company on Friday evenings and that I could sometimes join the 0-km-team. Minke and Matijs, and Moniek and Arjan, thanks for the stelletjes-spelletjes evenings, I always enjoy our relaxed get-togethers. "Your home is bigger than your house" is the motto of our great co-housing community ´t Punt. Dear CW neighbours, I am very happy that you are always available to help out, and that we make many good memories together.

Last, I would like to thank my family and family in law for their support. Caroline, Gilbert, and Marleen, many thanks that you are always there for me. I enjoy our nearly daily funny or serious chats on Whatsapp and in real life. You know me very well and I am very fortunate that you are always available to help me out when needed. Thomas, we met on my very first day as a student and we have been through many adventures since then. Thank you for your ecologist´s view on my work and thanks for supporting me in working and living abroad! Joris, thank you for all the funny moments, and the many kisses and hugs that you give me. Benjamin, our time together was too short, but I am thankful that we met.

About the author

Anne Jet Hoek van Dijke was born on 1 January 1992 in Rotterdam, the Netherlands. She attended the Wolfert Dalton high school in Rotterdam, and spent most of her free time playing music and juggling or being upside down at the local youth circus 'Rotjeknor'. Around the age of 14, Anne thought that she was the most happy person on Earth.

Following her interest in the environment, vegetarian food, and alternative people, Anne moved to Wageningen in 2010 for her bachelors in Soil, Water, Atmosphere. She had a broad interested and picked her free choice courses in geology, ecohydrology, Geo-Information Science and Remote sensing, and followed one course in paleoclimatology-paleoecology at the Utrecht University. In 2012, standing with her feet in a Finnish peat bog, she realised that the interaction between soil, water, and vegetation is what interested her most. Anne continued with her masters in Earth and Environment at Wageningen University. During an exchange semester in Stockholm she followed courses in glaciology, paleoglaciology, and Quaternary dating methods. For her minor thesis, she modelled how drainage and climate change impacted tree encroachment in two Canadian peatbogs. For her major thesis, she stayed at the beautiful field stations of Tarfala and Abisko in Northern Sweden, where she studied the so-called ´non-sorted circles´, another landscape feature formed by the interaction of water, soil, and vegetation. She conducted her internship at the Louis Bolk Institute, and studied the effect of long-term (organic and non-organic) fertilization treatments on crop growth. Anne completed her master studies in 2016.

After completing her MSc studies, Anne started her PhD research within the Hydro-CSI project, a joint project of the Luxembourg Institute of Science and Technology and several European universities. As one of 14 PhD candidates, Anne studied the interaction between vegetation characteristics and evaporation. Anne herself was affiliated with two research groups at Wageningen University and on a regular basis, she commuted between Belval and Wageningen.

After the submission of her PhD, Anne has started a PostDoc at the Max Planck Institute for Biogeochemistry in Jena, Germany. She was welcomed in the Hydrology-Bioshpere-Climate Interactions group. Her current research focuses on the drought legacy effects on streamflow, using LSTM models. She looks forward to the coming years of exciting research.

Peer-reviewed Journal Publications

Hoek van Dijke, A. J., M. Herold, K. Mallick, I. Benedict, M. Machwitz, M. Schlerf, A. Pranindita, J. J. E. Theeuwen, J.-F. Bastin, and A. J. Teuling (2022). "Shifts in regional water availability due to global tree restoration". *Nature Geoscience* 15, 363–368. DOI: https://doi.org/10.1038/s41561-022-00935-0.

Hoek van Dijke, A. J., K. Mallick, M. Schlerf, M. Machwitz, M. Herold, and A. J. Teuling (2020). "Examining the link between vegetation leaf area and land–atmosphere exchange of water, energy, and carbon fluxes using FLUXNET data". *Biogeosciences* 17.17, 4443–4457. DOI: 10.5194/bg-17-4443-2020.

Hoek van Dijke, A. J. and Mallick, K., A. J. Teuling, M. Schlerf, M. Machwitz, S. K. Hassler, T. Blume, and M. Herold (2019). "Does the Normalized Difference Vegetation Index explain spatial and temporal variability in sap velocity in temperate forest ecosystems?" *Hydrol. Earth Syst. Sci.* 23.4, 2077–2091. DOI: 10.5194/hess-23-2077-2019.

Roebroek, C. T. J., L. A. Melsen, **Hoek van Dijke, A. J.**, Y. Fan, and A. J. Teuling (2020). "Global distribution of hydrologic controls on forest growth". *Hydrol. Earth Syst. Sci.* 24.9, 4625–4639. DOI: 10.5194/hess-24-4625-2020.

Teuling, A. J., E. A. G. de Badts, F. A. Jansen, R. Fuchs, J. Buitink, **Hoek van Dijke, A. J.**, and S. M. Sterling (2019). "Climate change, reforestation/afforestation, and urbanization impacts on evapotranspiration and streamflow in Europe". *Hydrol. Earth Syst. Sci.* 23.9, 3631–3652. DOI: https://doi.org/10.5194/hess-23-3631-2019.

Teuling, A. J. and **Hoek van Dijke, Anne J.** (2020). "Forest age and water yield". *Nature* 578.7794, E16–E18. DOI: https://doi.org/10.1038/s41586-020-1941-5.

Other Scientific Publications

Hoek van Dijke, A. J., I. Benedict, K. Mallick, M. Herold, M. Machwitz, M. Schlerf, and A. J. Teuling (2021). *The 'global tree restoration potential': a first estimation of the hydrological effects*. EGU21-7697, 19-30 April 2019, online. DOI: https://doi.org/10.5194/egusphere-egu21-7697.

Hoek van Dijke, A. J., Herold, K. M. Mallick, M. Schlerf, M. Machwitz, and A. J. Teuling (2019a). *Linking vegetation and surface energy balance across a range of climatic and ecohydrological conditions*. 2019AGUFM.H23P2127H, 9-13 December 2019.

Hoek van Dijke, A.J., A. J. Teuling, K. Mallick, M. Schlerf, M. Machwitz, S. Hassler, T. Blume, and M. Herold (2019b). *The link between sap velocity, transpiration and the NDVI in space and time*. EGU2019-3914, 8-12 April 2019.

PE&RC Training and Education Statement

With the training and education activities listed below the PhD candidate has complied with the requirements set by the C.T. de Wit Graduate School for Production Ecology and Resource Conservation (PE&RC) which comprises of a minimum total of 32 ECTS (= 22 weeks of activities)

Review of literature (4.5 ECTS)

- The link between vegetation functional traits and evapotranspiration

Writing of project proposal (4.5 ECTS)

- The link between vegetation functional traits and evapotranspiration at multiple spatial scales

Post-graduate courses (5.1 ECTS)

- Multivariate analysis; WUR-PE&RC (2017)
- Machine learning for spatial data; WUR-PE&RC (2018)
- Summer school ecosystem & land use change; KIT (2018)

Invited review of (unpublished) journal manuscript (2 ECTS)

- HESS: ground water depth evapotranspiration, and vegetation indices
- HESS: vegetation greening, climate change, streamflow

Competence strengthening / skills courses (4.6 ECTS)

- PhD competence assessment; WUR-WGS
- Project and Time Management; WUR-WGS
- PhD Workshop Carousel, two workshops; WUR-WGS

- Interpersonal communication for PhD candidates; WUR-WGS
- Ethics in Plant and Environmental Sciences; WUR-WGS
- Scientific writing; WUR-WGS

PE&RC Seminars and the PE&RC weekend (0.9 ECTS)

- PE&RC Symposium: drought, plant hydraulic traits and vegetation modelling
- PE&RC Midterm weekend (2019)

Discussion groups / local seminars / other scientific meetings (6 ECTS)

- Seminar series in water resources research; LIST (2017-2021)
- DTU Doctoral Training Unit; LIST (2017-2021)

International symposia, workshops and conferences (8.6 ECTS)

- LIST PhD day; poster presentation (2017)
- LIST PhD day; oral presentation (2018)
- EGU; poster presentation (2019)
- AGU; poster presentation (2019)
- EGU; online; oral presentation (2021)

Lecturing / supervision of practical's / tutorials (3 ECTS)

- Practicals Introduction Geo-information Science (2018, 2019)

Supervision of MSc students

- Hydrologic controls on forest growth
- Streamflow response to tree cover change
- Climate change, water extraction, and water scarcity
- Water costs of tree restoration

The research described in this thesis was financially supported by the Luxembourg National Research Fund (FNR) under the grant agreement Nr. PRIDE15/10623093/HYDRO-CSI.

Financial support from Wageningen University for printing this thesis is gratefully acknowledged.

Cover design by Maartje de Goede.

Printed by ProefschriftMaken.

This thesis has been printed on FSC-certified paper.